

s-process nucleosynthesis-nuclear physics and the classical model

This content has been downloaded from IOPscience. Please scroll down to see the full text.

1989 Rep. Prog. Phys. 52 945

(<http://iopscience.iop.org/0034-4885/52/8/002>)

View the [table of contents for this issue](#), or go to the [journal homepage](#) for more

Download details:

IP Address: 139.184.14.159

This content was downloaded on 18/08/2015 at 17:22

Please note that [terms and conditions apply](#).

s-process nucleosynthesis—nuclear physics and the classical model

F Käppeler, H Beer and K Wissak

Kernforschungszentrum Karlsruhe, Institut für Kernphysik, D-7500 Karlsruhe, Federal Republic of Germany

Abstract

Among the various processes responsible for the formation of the heavy elements in stars, the slow neutron capture process (s-process) is distinguished by the fact that it involves mostly stable isotopes. Therefore, the relevant nuclear physics data can be determined by experiments. With this rather reliable data basis, s-process nucleosynthesis offers an important testground of models for the late stages of stellar evolution, which are supposed to be the s-process site. The empirical counterpart for such models is the so-called classical s-process, a purely phenomenological picture, that is successfully used to derive the resulting abundances as well as information on the physical conditions during the s-process. The status of this classical approach is reviewed with emphasis on the implications for various stellar models of the s-process and in the light of results obtained by stellar spectroscopy. A brief account of the potential s-process chronometers is also presented.

This review was received in January 1989.

Contents

	Page
1. Introduction	947
2. s-process models	949
2.1. The classical s-process	949
2.2. Stellar models	952
3. The data base	955
3.1. Abundances	955
3.2. Neutron capture rates	960
3.3. Beta decay rates	972
4. Status of the classical s-process	977
4.1. The $\sigma N_s(A)$ curve	977
4.2. Neutron economy	986
4.3. r-process residuals	988
5. s-process branchings	989
5.1. General discussion	989
5.2. The physical conditions during the s-process	990
5.3. Branchings to rare nuclei	996
6. Comparison to stellar models and to astronomical observations	997
6.1. Stellar models	998
6.2. Astronomical observations	1000
7. Chronometers	1001
7.1. Short timescale	1002
7.2. Intermediate timescale	1003
7.3. Long timescale	1004
7.4. ^{176}Lu —cosmic clock or stellar thermometer?	1006
8. Summary	1008
Acknowledgments	1009
References	1009

1. Introduction

This review deals with stellar nucleosynthesis by slow neutron captures (the s-process). It concentrates on the classical model and tries to delineate the essential nuclear physics which is required for input as well as the main results which represent completely unbiased constraints for stellar models of the s-process.

The origin of the chemical elements in nature constitutes a fascinating problem of nuclear astrophysics. Among the various theories of element formation, stellar nucleosynthesis has become most successful and is now commonly accepted. It assumes that only hydrogen, helium and the rare light isotopes with $A < 12$ are produced in the big bang. These isotopes are stepwise converted to heavier nuclei by the energy-generating fusion reactions in stars. In successive stages of stellar evolution a sequence of burning processes converts H to He, He to C, and so on until the isotopes around iron are reached in Si burning. These are the most stable nuclei in nature, exhibiting the highest binding energies per nucleon, and their stability results in a large abundance maximum around $A = 56$. Beyond that point, fusion of charged particles quickly ceases to contribute to the observed abundances because of the increasing coulomb barriers and the decreasing binding energies per nucleon. Heavier nuclei can only be created by successive neutron capture reactions and beta decays.

Stellar nucleosynthesis was greatly stimulated by the comprehensive survey of Burbidge *et al* (1957) who formulated a consistent picture of element formation in stars. Meanwhile, three decades of intense research confirmed many of these classical ideas though on a considerably refined level. While the static burning situations seem to be fairly well understood, explosive burning still represents a great challenge for nuclear astrophysics. The s-process takes an ‘intermediate’ position: the classical approach allows for a successful description of the observed abundances and many other aspects with the assumption of a *steady* neutron flux. On the other hand, stellar s-process models indicate that the s-process may occur predominantly in a *dynamic* environment. This duality will be repeatedly dealt with in this article because it is the interplay between classical approach and observations on one side and stellar models on the other side, which will provide the clues for identifying the true mechanisms of the s-process.

The classical s-process as it was first outlined by Burbidge *et al* (1957) represents a purely phenomenological approach to neutron capture nucleosynthesis. The only assumption on the astrophysical scenario was that it should be associated with helium burning in the red-giant stage of stellar evolution in order to define the s-process temperature. Evidence for such a site came from the observation of Tc lines in the spectra of certain S stars (Merrill 1952), and from the fact that under these burning conditions (α, n)-reactions may provide an efficient neutron source. This empirical ansatz has two attractive features:

- (i) Practically all important features of the s-process, such as abundances, neutron economy and physical conditions, are described surprisingly well.
- (ii) By its empirical nature it is completely unbiased by any stellar model, thus yielding independent constraints for the more comprehensive treatment in terms of stellar evolution.

The recipe for the classical s-process is simply to expose a pre-existing distribution of seed abundances to a suited neutron irradiation. The associated neutron flux is assumed to be steady and low enough that the beta decay rates dominate over the neutron capture rates. Consequently, the neutron capture chain of the s-process follows the valley of beta stability. This is best illustrated at the section of the chart of nuclides sketched in figure 1. The inset of figure 1 shows the observed abundance distribution (see § 3.1) with a strong maximum around iron. Consequently, neutron capture nucleosynthesis of the heavy chemical elements starts from the iron group isotopes. Neutron captures on a slow timescale of the order 1 to 10 yr follow the thick solid line in the valley of beta stability; if an unstable nucleus is encountered, usually beta decay to the next higher element is much faster than neutron capture. The resulting abundances are, therefore, determined by the respective neutron capture cross sections. Isotopes with small cross sections act as bottle necks in the neutron capture chain and build up large abundances, whereas isotopes with large cross sections are more easily burnt and hence develop small abundances only. This explains naturally the sharp maxima in the inset of figure 1 as being due to the s-process. At these points, the s-process path encounters nuclei with magic neutron numbers $N = 50, 82, 126$, which all exhibit particularly small cross sections.

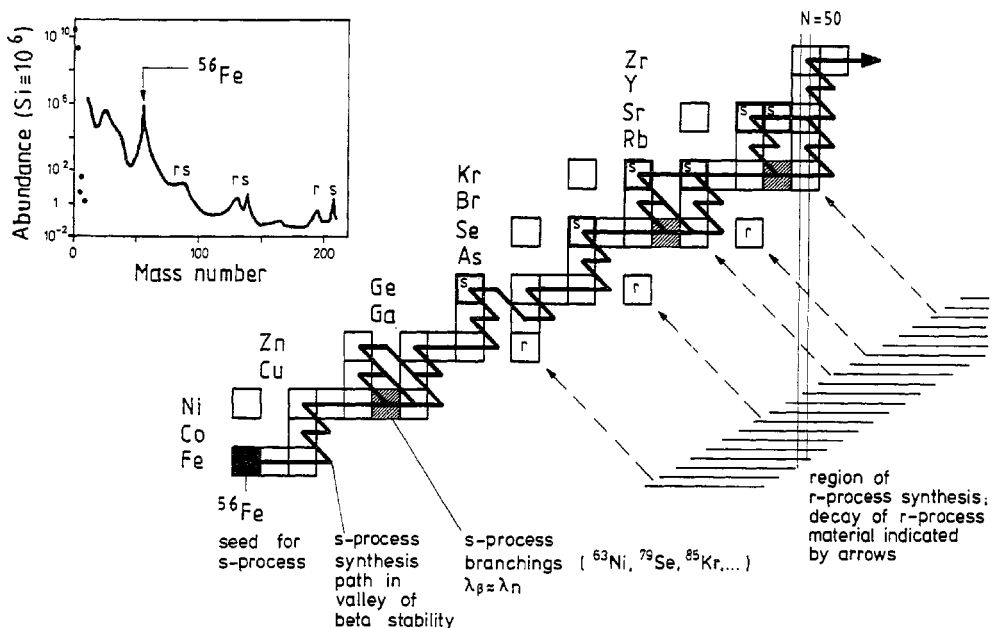


Figure 1. Section of the chart of nuclides for a discussion of the main features of neutron capture nucleosynthesis (see text).

Another important feature of the s-process is the branchings of the neutron capture chain—indicated by hatched boxes in figure 1—where the rates for beta decay and neutron capture are comparable. At these isotopes, e.g. at ^{63}Ni , ^{79}Se and ^{85}Kr , competition between neutron capture and beta decay leads to a branching of the synthesis path which is determined by the s-process neutron density and the respective beta half-life. Analysis of the abundance patterns in these branchings (§ 5) can provide for estimates of the neutron density, n_n , but also for the temperature, T_s , and even for the electron density during the s-process. The latter quantities manifest themselves through their influence on the beta decay rates of several branching isotopes. This

field was recently investigated in detail (§ 3.3). Branchings may also serve for investigating the conditions of a pulsed s-process.

In addition to the s-process at least two other mechanisms contributed to the observed abundances in the mass range $A > 70$. The neutron-poor isotopes are attributed to the so-called p-process, where p stands for proton capture and/or photo-disintegration. The related abundances are usually smaller by more than one magnitude compared to those built by the other two processes, and this may be one of the reasons why the p-process is still not well understood. However, p-process corrections to the s-only isotopes (§ 4.1) become increasingly important in view of the improved s-process treatment. Hence, a quantitative model for the p-process is badly needed. At present, p-process corrections are either neglected or somehow interpolated from the p-only nuclei. Already both approximations lead to uncertainties similar to those of the classical model, and may severely hamper further improvements.

The existence of the neutron-rich isotopes which cannot be reached by the s-process because of their short-lived neighbours calls for a rapid neutron capture process. This r-process is supposed to occur on a timescale of some hundred milliseconds, presumably during explosive stellar burning. The associated neutron densities of $\sim 10^{19} \text{ cm}^{-3}$ or more lead to a synthesis path close to the neutron drip line. This is indicated in figure 1 by the hatched area. The isotopic abundances produced in the r-process are determined by the beta decay times on the r-process path. As the half-lives are longest for nuclei with magic neutron numbers, these build up large abundances similar to the s-process, but at smaller mass number A (see figure 1). Therefore, the shift between the s- and r-process peaks in the abundance distribution marks the atomic numbers, Z , where the r-process path reached the magic neutron numbers. If the respective beta decay times are known from experiments or calculations, this information can be interpreted in terms of the prevailing r-process neutron densities and temperatures (Kratz *et al* 1988).

The isotopes created in the r-process are all short-lived and decay back to the valley of beta stability, so that most observed isotopes represent mixtures of abundance contributions from the s- and r-processes with contaminations from the p-process which are usually small. Fortunately, there are some 40 isotopes that can be attributed entirely to either process: in all cases where the beta decay chain ends at an r-only isotope that is not reached by the s-process because of its short-lived neighbour, e.g. at ^{80}Se and ^{82}Se , the respective isobars, ^{80}Kr and ^{82}Kr , are in turn shielded from the r-process. The abundances of this ensemble of s-only nuclei can therefore be used as a test for any s-process model.

The present work concentrates on the classical s-process; further information on related topics of nucleosynthesis may be found in the following references. Neutron capture nucleosynthesis: Mathews and Ward (1985); p-process: Rayet *et al* (1988); stellar neutron capture cross sections: Bao and Käppeler (1987); stellar weak-interaction rates: Takahashi and Yokoi (1987); solar abundances: Anders and Grevesse (1989); isotopic anomalies: Begemann (1980) abundances in stellar atmospheres: Lambert (1988); stellar models: Iben and Renzini (1983); nucleocosmochronology: Clayton (1984), Cowan *et al* (1987).

2. s-process models

2.1. The classical s-process

Under neutron irradiation the change in abundance of a particular isotope A can be

formally written as

$$dN_s(A)/dt = \lambda_n(A-1)N_s(A-1) - (\lambda_n(A) + \lambda_\beta(A))N_s(A). \quad (2.1)$$

The neutron capture rate, $\lambda_n = \Phi\sigma$, is proportional to the neutron capture cross section averaged over the stellar spectrum, σ , and to the neutron flux $\Phi = n_n v_T$, where n_n denotes the neutron density and $v_T = (2kT/m)^{1/2}$ the thermal neutron velocity, with m being the reduced mass. The beta decay rate $\lambda_\beta = \ln 2/t_{1/2}$ must be considered if isotope A is radioactive. Equation (2.1) defines a system of coupled differential equations comprising all isotopes on the s-process path. In the most general case the coefficients λ are not constant but depend on the (possibly dynamic) stellar environment. In the *classical* model the situation is simplified by two assumptions:

- (i) The s-process temperature, T_s , is constant, allowing for well defined cross sections. This is a good approximation because the neutron capture rates are almost independent of temperature: the neutron cross sections fall with $\sim 1/\sqrt{E_n}$ and this is compensated in the expression for λ_n by the thermal neutron velocity v_T .
- (ii) Radioactive nuclei on the synthesis path are either treated as stable ($\lambda_\beta \ll \lambda_n$) or as sufficiently short-lived that the capture chain continues with the daughter nucleus ($\lambda_\beta \gg \lambda_n$). In this way, λ_β is eliminated from equation (2.1). This assumption is justified for most unstable nuclei with the few exceptions of the s-process branchings; these have to be treated individually as shown below.

With these assumptions, equation (2.1) can be rewritten with time being replaced by the time-integrated neutron flux $\tau = \int \Phi dt$,

$$dN_s(A)/d\tau = \sigma(A-1)N_s(A-1) - \sigma(A)N_s(A). \quad (2.2)$$

Sufficiently long irradiation results in equilibrium between the production and destruction terms in equation (2.2), leading to a constant product, σN_s , of cross section and s-process abundance. Though this condition is not completely reached, the product σN_s —which is the characteristic quantity of the classical s-process—exhibits at least a smooth dependence on mass number.

Clayton *et al* (1961) showed that the observed abundances of the s-only isotopes cannot be reproduced by a single irradiation of an iron seed. A satisfactory solution was found by Seeger *et al* (1965) assuming an exponential distribution of neutron exposures, τ , of the form

$$\rho(\tau) = \frac{fN_{56}}{\tau_0} \exp(-\tau/\tau_0). \quad (2.3)$$

This ansatz even allows for a simple analytical solution of the system of equations (2.2):

$$\sigma(A)N_s(A) = \frac{fN_{56}}{\tau_0} \prod_{i=56}^A [1 + (\sigma(i)\tau_0)^{-1}]^{-1} \quad (2.4)$$

The product, $\sigma N_s(A)$, is completely determined by the cross sections, $\sigma(i)$, after the parameters f and τ_0 are fixed by a fit to the empirical σN_s values of the s-only isotopes. In this way, equation (2.4) yields the abundances produced by the s-process and, via the parameters f and τ_0 , information on the seed abundance and the neutron economy. A useful quantity in that respect is the number of neutrons captured per ^{56}Fe seed

nucleus (Clayton *et al* 1961)

$$n_c(A_{\text{seed}}) = \left(\sum_{A=A_{\text{seed}}}^{209} (A - A_{\text{seed}}) N_s(A) \right) / f N_\odot(^{56}\text{Fe}). \quad (2.5)$$

The total number of neutrons captured during the s-process is $\Sigma n_c(i)$, where i runs over all seeds (for a discussion see § 4.2).

When sufficiently detailed input data became available, it turned out that three different exponential distributions of neutron exposures are required for a complete description of the observed s-process abundances (Clayton and Rassbach 1967, Clayton and Ward 1974, Beer and Macklin 1985). The bulk of s-process material in the mass range $90 < A < 204$ is produced by what is called the *main* s-process component in the following. Below $A \sim 90$ this component fails to describe the steep increase of the σN_s curve towards the iron seed. Therefore, a *weak* component is added which is characterised by a smaller mean neutron exposure. Finally, a *strong* component is to be postulated in order to account for the abundance maximum at lead. These three components will be distinguished by adding indices 1, 2 and 3, respectively, to the parameters f and τ_0 . An exponential distribution for $\rho(\tau)$ appears to provide for an excellent fit of the main s-process component, but the weak component may better be described by single irradiations (Beer 1986, Beer and Macklin 1989). The strong component is only needed to explain a significant part of the ^{208}Pb abundance (Beer and Macklin 1985, Ratzel *et al* 1989).

Within the classical s-process model the description of the mass flow through the above-mentioned branchings requires the additional assumption that (iii) the s-process neutron flux is constant in time, and was formulated by Ward *et al* (1976). If we consider the branching at ^{79}Se in figure 2, the corresponding split of the σN_s curve to the neutron-rich side follows from

$$\sigma N(^{79}\text{Se}) = \zeta(^{79}\text{Se}) \sigma N(^{78}\text{Se}). \quad (2.6a)$$

The beta decay side of the branching is expressed by

$$\sigma N(^{79}\text{Br}) = \zeta(^{79}\text{Br}) [f(^{79}\text{Se})/(1-f(^{79}\text{Se}))] \sigma N(^{79}\text{Se}) \quad (2.6b)$$

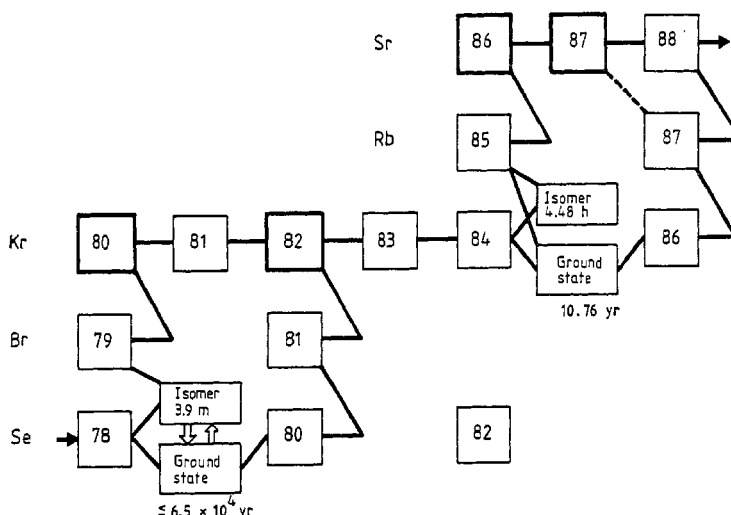


Figure 2. The s-process branchings at ^{79}Se and ^{85}Kr . The σN_s -values of the s-only isotopes imply almost equal branching ratios in both cases, suggesting a strong temperature dependence of the ^{79}Se half-life.

and the propagators in equations (2.6) are defined as

$$\zeta(^A Z) = [1 + (\tau_0 \sigma(^A Z))^{-1}]^{-1} \quad (2.7a)$$

$$\zeta'(^A Z) = [(f_n(^A Z))^{-1} + (\tau_0 \sigma(^A Z))^{-1}]^{-1} \quad (2.7b)$$

with the branching factor

$$f_\beta(^{79}\text{Se}) = \lambda_\beta(^{79}\text{Se}) (\lambda_\beta(^{79}\text{Se}) + \lambda_n(^{79}\text{Se}))^{-1}. \quad (2.8)$$

The s-process flow follows the two branches in the traditional way unless there is another branching point, as for example ^{80}Br , which decays to both ^{80}Kr and ^{80}Se . Finally, the two branches merge into the main s-process path at ^{82}Kr . Among the isotopes involved the s-only nuclei $^{80,82}\text{Kr}$ hold a key position as normalisation points for the ^{79}Se branching. Obviously, a fit of equations (2.6) to the empirical σN_s values of $^{80,82}\text{Kr}$ would yield λ_n via equation (2.8) and hence the neutron density, if the beta decay rate of ^{79}Se were not affected by temperature. As this is true in case of the ^{85}Kr branching, the neutron density thus obtained can be used to derive the effective stellar beta decay rate, λ_β , from the analysis of those branchings which exhibit a significant temperature dependence of the beta half-life, as for example at ^{79}Se .

Another aspect of the s-process branchings is the problem of a possible time-dependence of neutron density and temperature. A pulsed rather than a steady s-process was proposed by the conditions during helium shell burning which also provides for a natural explanation of the exponential form of the exposure distribution $\rho(\tau)$ (§ 2.2). An analytic solution of this problem within the classical model has been worked out by Ward *et al* (1978) for rectangular pulses, but a more realistic treatment requires numerical integration of equation (2.1) (Howard *et al* 1986, Beer and Macklin 1989).

It is evident from the above that each of the simplifying assumptions for the classical s-process bears immediate consequences for the s-process branchings. Systematic branching analyses are therefore capable of revealing many details of the s-process environment (§ 5).

2.2. Stellar models

Instead of a complete review of stellar s-process models (for recent references see Mathews and Ward (1985), Arnould (1986), Lambert (1988)) this section emphasises those models which are detailed enough to allow for quantitative comparisons with the results of the classical model as well as stellar observations (§ 6). From considerations concerning the classical model it was inferred that helium burning zones in red-giant stars are the most likely sites for the s-process.

2.2.1. Intermediate and low mass stars. The first assignment of a true stellar environment was achieved by the work of Weigert (1966) and of Schwarzschild and Härm (1967). These authors found that stars with masses $M < 9M_\odot$ (M_\odot = mass of sun) develop a convective helium burning shell during their AGB stage of evolution. This convection might reach outward far enough to mix hydrogen-rich material from the envelope into the He shell. There, neutrons could be produced by the reaction sequence $^{12}\text{C}(\text{p}, \gamma)^{13}\text{N}(\text{e}^+ \nu)^{13}\text{C}(\alpha, \text{n})^{16}\text{O}$. Helium burning in the convective shell occurs in rather short pulses which last for some years, followed by an interpulse period of several hundred years with hydrogen burning quiescently at the bottom of the envelope. If enough helium is replenished in that way, helium shell burning reignites and the next

pulse episode starts. The fact that the mass zones comprised of successive pulses overlap was shown by Ulrich (1973) to necessarily result in the exponential distribution of neutron exposures, $\rho(\tau)$, which was already found empirically by the classical model (Seeger *et al* 1965).

The pulsating helium shell model was further developed by Iben (1975a, b, 1976) who showed that mixing of protons into the helium shell is prohibited by an entropy barrier, but that the $^{22}\text{Ne}(\alpha, n)^{25}\text{Mg}$ reaction may be an alternative neutron source. This is illustrated in figure 3 which shows a very schematic sketch of the s-process operating in the helium burning shell of an AGB star. Note that the mass of the helium shell is greatly exaggerated; the true relations for a $7M_{\odot}$ star are such that the carbon-oxygen core has $M_c = 0.95 M_{\odot}$ followed by a very thin helium shell of $M_{\text{sh}} = 10^{-7} M_{\odot}$. All of the remaining mass is contained in the stellar envelope. With each pulse the helium shell grows outward leaving behind the ashes of the 3α reaction and comprising fresh material from the hydrogen burning region. Figure 4 illustrates this evolution for the 15th and 16th pulse of the $7M_{\odot}$ model star (Iben 1976). The positions of the convective envelope and the helium shell are shown in mass coordinates as a function of time. The shaded parts are the convective regions, i.e. the envelope and the helium shell during the pulses. As can be seen, the pulses last for about 12 yr with interpulse periods of ~ 3000 yr.

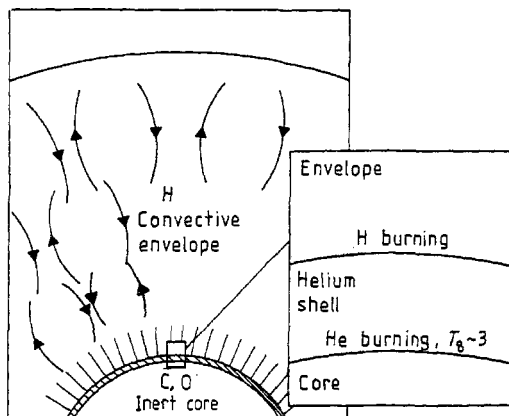


Figure 3. Schematic structure of a $7M_{\odot}$ mass star during shell burning. For illustration, the helium shell is greatly exaggerated. Helium shell burning occurs in pulses, which are triggered when the CNO cycle at the bottom of the envelope has produced a critical amount of helium.

Shortly after each pulse the envelope shrinks back and covers the upper part of the helium shell. In this way freshly s-processed material enters the envelope and ultimately reaches the stellar atmosphere. The next pulse already starts further out, powered by the helium which is produced by hydrogen burning via the CNO cycle in the interpulse period. The second most abundant product of the CNO cycle is ^{14}N to which almost all of the initial carbon, nitrogen and oxygen is converted. At the higher temperature of the helium shell the reaction sequence $^{14}\text{N}(\alpha, \gamma)^{18}\text{F}(e^+ \nu)^{18}\text{O}(\alpha, \gamma)^{22}\text{Ne}$ produces ^{22}Ne for the s-process to operate during the next helium shell flash via $^{22}\text{Ne}(\alpha, n)^{25}\text{Mg}$ reactions.

The fractional overlap of successive convective shells results in an exponential distribution of neutron exposures (Ulrich 1973): if $\Delta\tau$ is the neutron exposure per pulse, and if r denotes the overlap of the N th and the $(N-1)$ th convective shell, then

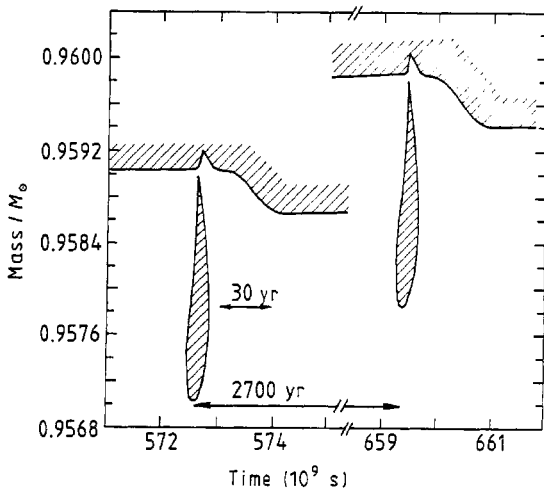


Figure 4. Position and size of the convective helium shell and of the convective stellar envelope for the 15th and 16th shell flash of a $7M_{\odot}$ mass star. Pulse duration is ~ 12 yr followed by interpulse periods of about 3000 yr. After each pulse, freshly processed material from the helium shell is taken up by the envelope and eventually transported to the stellar atmosphere. During the interpulse period the helium shell grows outward with new material from the CNO cycle being added. This fractional substitution of the helium shell results in an exponential distribution of neutron exposures in the s-process (see text).

the fraction of matter, $\rho(\tau)$, which experienced a total exposure $\tau = N\Delta\tau$ will be

$$\rho(\tau) = r^N = r^{(\tau/\Delta\tau)} \quad \text{or} \quad \rho(\tau) = \exp(\tau \ln(r)/\Delta\tau). \quad (2.9)$$

The parameter τ_0 from the classical model, equation (2.3), is hence related to the exposure per pulse, $\Delta\tau$, and the fractional overlap between pulses, r . According to Iben (1982), r depends on the core mass and decreases with increasing pulse number until a limiting value $r = 0.6 - 0.555(M_H - 0.6)$ is reached, M_H being the stellar mass up to the hydrogen burning shell. For the $7M_{\odot}$ mass star with $M_H = \sim 0.96$ one thus obtains $r = \sim 0.4$. During their AGB evolution, stars experience enough helium shell flashes to establish an exponential distribution $\rho(\tau)$.

Another feature of the s-process associated with helium shell burning is the correlation between the number of seed nuclei and the number of available neutrons. The abundance distribution of the light elements in population I stars being practically solar yields a fixed ratio $^{56}\text{Fe}/\Sigma\text{CNO} = 1/39$ (Anders and Ebihara 1982). Nearly all of the C, N and O is transformed to ^{14}N during the CNO cycle, so that ^{56}Fe and ^{14}N are mixed into the helium shell in the same ratio. This restricts the number of available neutrons per ^{56}Fe seed to < 39 , even if all of ^{14}N is used up for neutron production.

For stellar masses $< 3M_{\odot}$ the $^{22}\text{Ne}(\alpha, n)^{25}\text{Mg}$ reaction is not efficient enough for significant s-processing because the temperatures during the shell flash are too low. However, as stars in this mass range do show s-process enhancements, other mechanisms activating the $^{13}\text{C}(\alpha, n)^{16}\text{O}$ neutron source may become important, such as semiconvective mixing or diffusion (Iben and Renzini 1983). Therefore, low mass stars have received increased attention (Gallino *et al* 1988, Boothroyd and Sackmann 1988, Hollowell and Iben 1988, Gallino 1989), and it was found that low mass stars are indeed efficient sites for the main s-process component.

The advantage of the helium shell models is that they have been worked out in great detail, describing the relevant s-process conditions for a wide mass-range of AGB

stars, e.g. temperature and neutron density as a function of time. A critical discussion of these results will be given later in comparison with the classical model (§ 6).

2.2.2. Massive stars. Core helium burning in massive stars has been identified as another site for the s-process (Peters 1968). Towards the end of core helium burning in stars with $M > 10M_{\odot}$ temperatures become sufficiently high that a substantial neutron density can be established via the $^{22}\text{Ne}(\alpha, n)$ reaction. Recent calculations (Arnett and Thielemann 1985, Busso and Gallino 1985, Langer *et al* 1989) based on an improved stellar model and updated nuclear data confirm the earlier results of Lamb *et al* (1977) that significant s-process overproduction is obtained for $A < 90$. Arnett and Thielemann (1985) also found significant s-processing in that same mass region during hydrostatic carbon burning. For very massive stars Prantzos *et al* (1987) showed that the s-process yields are almost independent of stellar mass for $50 < M < 100M_{\odot}$. The abundances produced in all these scenarios appear to be compatible with the weak s-process component.

3. The data base

3.1. Abundances

The success of any theory of nucleosynthesis has to be measured by comparison with the abundance patterns observed in nature. The enormous efforts invested in abundance determinations cannot be adequately summarised in this review. Instead we will try to sketch the present status and to illustrate recent trends with a few examples of importance to the s-process. More detailed information may be found in the literature cited.

Our knowledge of abundances has been established essentially during the past five decades, based on the hypothesis that primitive meteorites might have preserved the original composition of the early solar system (Goldschmidt 1937). This idea has been confirmed by numerous measurements, and meteorite analyses now constitute the main source of information on solar abundances. Ten years earlier, the first quantitative abundance determinations were obtained from stellar spectra, in particular from that of the sun (Russell and Adams (1928); for a historic account see Unsöld (1979)). Analyses of stellar spectra yield—on average—surprisingly good agreement with solar values. This led people to think of generalising solar abundances to what were called ‘cosmic abundances’, assuming a homogeneous abundance distribution throughout our galaxy with the solar system being a representative sample. In the discussion about the site of nucleosynthesis, this homogeneity was considered to support the hypothesis of a cosmic event which created all matter in the universe. It was supposed that these element abundances were only marginally changed afterwards by stellar nuclear burning. However, significant improvements in observation techniques led to the discovery of numerous deviations from the composition of solar material, and the abundance patterns in objects like red giants, supernova remnants, interstellar matter etc are now considered as direct clues to stellar nucleosynthesis.

With respect to the s-process, it is clear from § 2 that the *isotopic* pattern derived from meteoritic samples provides for the most sensitive test of the classical model. On the other hand, the pronounced s-process enhancements in the surface abundances of red giants represent a direct link to stellar models and deserve therefore equal attention.

The status of the abundance information from various sources is briefly summarised below.

3.1.1. Meteoritic abundances. In the first compilation of Suess and Urey (1956) typical uncertainties were estimated to be not better than a factor of about 1.5. Subsequent compilations (Cameron 1973, Suess and Zeh 1973, Palme *et al* 1981, Cameron 1982, Anders and Ebihara 1982, Anders and Grevesse 1989) were based on continuously improved measurements and showed increasingly good agreement. In particular, the comprehensive work of Anders and collaborators confirmed earlier assumptions that the original composition of the solar system is best preserved in the relatively rare C1 carbonaceous chondrites. All other types of meteorites differ more or less from the C1 composition, especially with respect to volatile elements. These differences are readily ascribed to processing in the early solar nebula. From the variance of the available data obtained by different authors from different meteorites and with different techniques, it is found that the precision of solar abundances has reached the 5-10% level in the meantime.

More recent measurements, e.g. on rare earth elements in C1 chondrites (Patchett 1983, Beer *et al* 1984), have succeeded in improving the meteoritic abundance determinations for these elements to an accuracy of about 2%, and a similar precision has been reported for Fe and Cr. Figure 5 shows a set of Fe/Cr abundance ratios in carbonaceous chondrites (Palme 1985). Type 2 and type 3 chondrites define an Fe/Cr ratio which is about 3% lower than that observed in C1 chondrites, and it is not clear yet which of the two values represents the Fe/Cr ratio of the solar photosphere. The higher ratio in the C2 meteorite Nogoya reflects inhomogeneities in the Nogoya parent body due to extensive weathering, while the larger spread in the C3V chondrites is due to the larger grain size in these meteorites. The samples used for analysis were not big enough to obtain a reliable average. This problem is also evident from the variations in the Allende results. Nevertheless, the example of figure 5 demonstrates impressively the recent progress in solar abundance data, and this development provides great motivation to make an effort to improve the accuracy of neutron capture cross sections (§ 3.2).

In summary, meteoritic abundances are of twofold importance for s-process studies: they represent a complete abundance pattern for direct comparison with model calculations, and their (potential) precision allows or will allow sensitive tests of s-process models which afterwards can be applied to analyses of stellar abundances.

3.1.2. Solar spectrum. Compilations of solar abundances from the spectrum of the sun have been reported by Ross and Aller (1976), Holweger (1979) and Grevesse (1984). In general, somewhat larger uncertainties of 15 to 25% are reported for these data compared to meteoritic results. The difficulties in spectral analyses arise from uncertainties in the model atmosphere of the sun (deviations from local thermodynamic equilibrium, microturbulence, temperature inhomogeneities) as well as from uncertain atomic physics data (atomic transition probabilities, collision cross sections, line broadening parameters). For 38 elements of very different character the close correspondence of meteoritic and photospheric abundances is shown in figure 6 (Holweger 1984). Discrepancies between the two data sets are mainly due to depletion effects. In meteorites this holds for the volatile elements, especially for C, N and O. In all critical cases, the range of depletion from carbonaceous chondrites of type 1 towards types 2 and 3 is indicated by horizontal bars. In the sun, lithium is efficiently depleted, because this light element can undergo reactions with thermal protons in the convective zone. A similar comparison of meteoritic and solar abundances is given by Wasson (1985). A more puzzling discrepancy was noted for iron, where solar values exceed

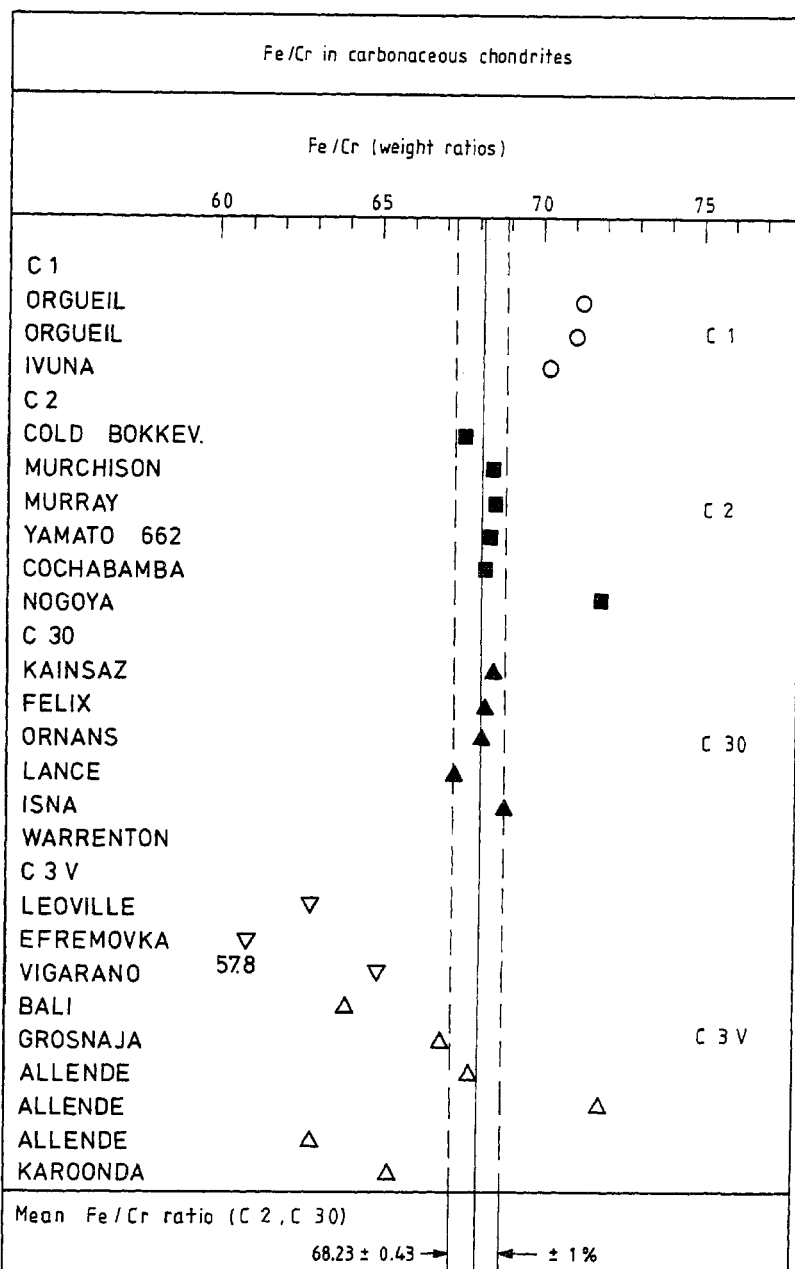


Figure 5. Recent precise measurements (black squares) of Fe/Cr ratios for a variety of meteorites showing remarkable consistency on the 1% level (Palme 1985).

the meteoritic abundances by ~40% (Grevesse 1987); possible reasons for this difference are currently being investigated (Anders and Grevesse 1989).

An example of a refined solar abundance determination is the work of Kwiatkowski *et al* (1984) on osmium. By using a greater variety of Os lines together with new and more accurate experimental transition probabilities, the osmium abundance in the solar photosphere ($N_{\text{Os}}^{\odot} = 0.77 \pm 20\%$) could be improved significantly, and is now in excellent agreement with the carbonaceous chondrite result ($N_{\text{Os}}^{\text{met}} = 0.717 \pm 9.8\%$,

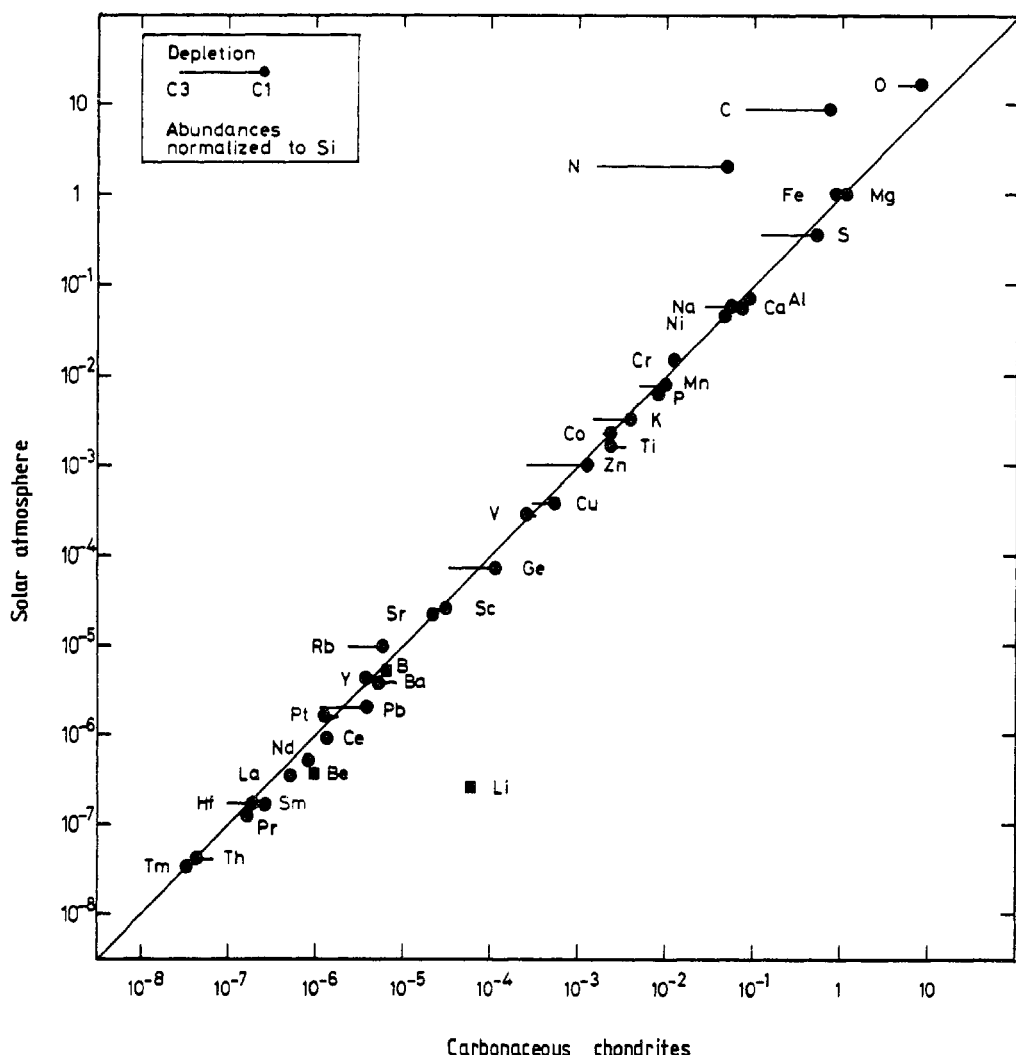


Figure 6. Comparison of elemental abundances in the sun with those in carbonaceous chondrites.

Anders and Ebihara (1982)). Note that all abundances quoted in this review correspond to the normalisation $N_{\text{Si}} = 10^6$. Solar and, in general, also stellar abundances represent *elemental* data as they are derived from atomic transitions. This feature has consequences for the interpretation of s-process patterns in red giant stars (§ 6).

3.1.3. Stellar spectra. The accurate new results for the solar photosphere appear most promising for the prospects of stellar abundances. The study of stellar spectra has, on average, confirmed the close relationship of abundance patterns in the sun, in main sequence stars similar to the sun and in interstellar matter. But, in addition, many deviating peculiarities were discovered reflecting galactic chemical evolution or ongoing nucleosynthesis. (For a comprehensive review see Trimble (1975).) Most important with respect to neutron capture reactions are the s-process enhancements in red giant stars.

A breakthrough for the idea of stellar nucleosynthesis was the discovery of technetium lines in the S star, R Andromedae, by Merrill in 1952 and in several other red

giants in the following years. As the longest-lived isotope of Tc has a half-life of four million years, it was immediately obvious that the observed technetium was produced in the stars themselves. By 1955, Cameron had explained quantitatively the production of Tc and other overabundant heavy elements in these stars in terms of a neutron capture process with neutrons released from the $^{13}\text{C}(\alpha, n)^{16}\text{O}$ reaction.

In his detailed review on abundances in evolved stars Baschek (1979) estimated a typical uncertainty for stellar abundance data of about three tenths of a decade. More recent observations claim uncertainties as small as 20% for favourable cases, and this does not appear to be a limit yet. Among the many publications the work of Tomkin and Lambert (1983) deserves a special mention as a nice example of a relatively complete set of abundances in the red giant HR774. Figure 7 shows how well these data can be reproduced by the classical s-process model (Käppeler (1986a); see also § 6).

It has to be noted at this point that analyses of stellar spectra do not yield data for a number of elements (As, Se, Kr, Te, Xe, I, Ta) either because these are rare or because their lines are masked by more abundant species.

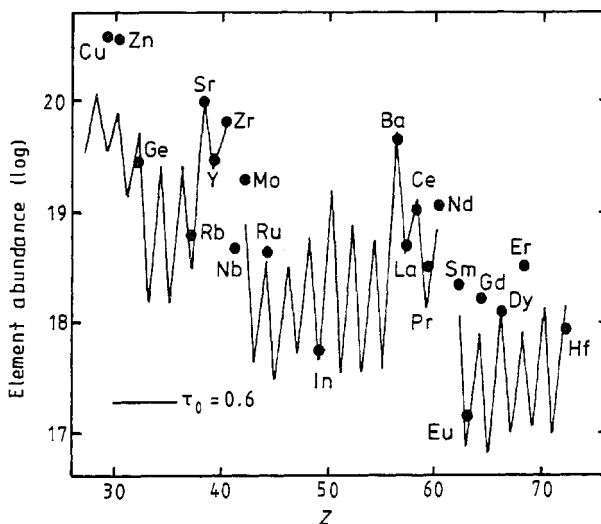


Figure 7. Observed s-process enhancements in HR774 fitted with the classical model (full curve). From Tomkin and Lambert (1983).

3.1.4. Cosmic rays. Galactic cosmic rays are an important independent channel of abundance information as they constitute the only accessible sample of matter from outside the solar system. This sample is rather young since the measured lifetime from source to observer is about 10^7 yr (Wiedenbeck and Greiner 1980), and it is also complete, containing all elements from hydrogen to the actinides. Cosmic rays have been extensively analysed in the past 15–20 yr with an impressive progress in detection techniques. Isotopes up to $Z \sim 28$ can be completely resolved, and at higher masses this is limited by decreasing yields rather than by detector resolution. Spacecraft experiments may significantly improve the exposure factors of present balloon flights so that isotopic abundances may also be expected in the mass region $Z > 28$.

Although cosmic-ray abundances can be measured with a precision of less than 10%, it is not easy to obtain a simple representation because the yields differ for different energy ranges. Modulations are due to interactions with interstellar matter

or within the solar system, involving spallation reactions, energy loss by ionisation, radioactive decay, etc. A cautious interpretation (Simpson 1983, Meyer 1985) suggests a mixture of aged r-process material and interstellar matter as the main component of cosmic-ray abundances. For a quantitative discussion in terms of neutron capture nucleosynthesis, the presently available data are not detailed enough. This holds in particular for the isotopic abundances in the range $Z > 28$.

3.2. Neutron capture rates

3.2.1. Laboratory cross-section measurements. As the s-process capture path follows the valley of beta stability, the neutron capture cross sections of most of the involved nuclei can be measured experimentally. Figure 8 illustrates the signature of a neutron capture event. The highly excited compound system decays promptly to the ground state of the product nucleus by emission of a gamma-ray cascade of total energy $E_{\gamma}^{\text{tot}} = (B_n + E_n)$ with B_n being the neutron separation energy and E_n the kinetic energy of the captured neutron. If the product nucleus is unstable the capture event can also be determined via its decay. The experimental techniques for neutron capture measurements will be briefly sketched in this section to outline their current status and possible improvements. In view of the role of reliable neutron capture rates as the main input data for the s-process this is an important point.

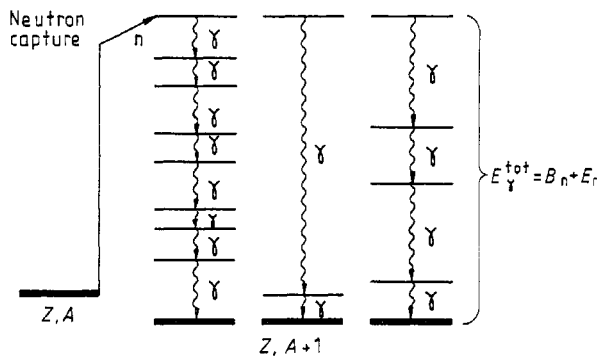


Figure 8. Characteristic features of a neutron capture event.

Differential methods. This term denotes those methods which yield the capture cross section as a function of neutron energy, $\sigma(E_n)$. In the energy range of interest for the s-process $1 < E_n < 200$ keV, this is achieved by the use of a pulsed neutron flux in combination with the time-of-flight (TOF) technique. The essential features of the respective methods are good time resolution, high efficiency for detecting the prompt gamma-ray cascade independent of its multiplicity and low sensitivity to scattered neutrons. The second point is important because the gamma-ray cascade is completely determined by statistics for practically all isotopes on the s-process path. (There are very few exceptions, where valence or direct capture dominates over the compound nucleus mechanism.) The many possible transitions in the decay of the compound nucleus lead to a smooth capture gamma-ray spectrum without prominent, isolated peaks which might be used for identification of capture events by high resolution spectroscopy, e.g. with Ge detectors. As neutron scattering is, in general, about ten times more likely than capture, detector systems for neutron capture studies should

be insensitive to scattered neutrons to avoid backgrounds, which are very difficult to distinguish from true events.

In principle, the best technique would be to sum up all gamma rays in the cascade to obtain a signal proportional to E_{γ}^{tot} . An ideal detector covering the entire solid angle of 4π with 100% efficiency and good energy resolution would then yield a spectrum of capture events as indicated in figure 9(a). This was first approximated by means of large liquid scintillator tanks of 300–3000 l volume, but these detectors are far from being ideal: the efficiency is limited to $\sim 70\%$, the large volume results in a significant cosmic ray background and the energy resolution is poor. Moreover, these detectors are sensitive to neutrons scattered in the sample, which are thermalised in the scintillator and subsequently captured in hydrogen. The resulting 2.2 MeV gamma-ray line is overwhelming the spectra, as sketched in figure 9(b), and has to be suppressed electronically. The corresponding correction for events falling below that threshold must be determined by extrapolation of the spectrum to zero pulse height. This procedure is affected by large systematic uncertainties of 5–8% thus limiting the overall accuracy to $\sim 10\%$ (Chrien 1975).

In order to circumvent the background problems with scintillator tanks, an alternative detector was developed by Moxon and Rae (1963). This very simple set-up is shown in figure 10(a). It consists of a graphite disc acting as a converter of gamma rays into electrons, followed by a thin plastic scintillator and a photomultiplier. The idea was to obtain a detector efficiency proportional to gamma-ray energy: electrons from low-energy gamma rays can reach the scintillator only from a thin layer of the converter, whereas high-energy gamma rays produce electrons energetic enough to penetrate the entire converter. As the efficiency of this Moxon-Rae detector is small

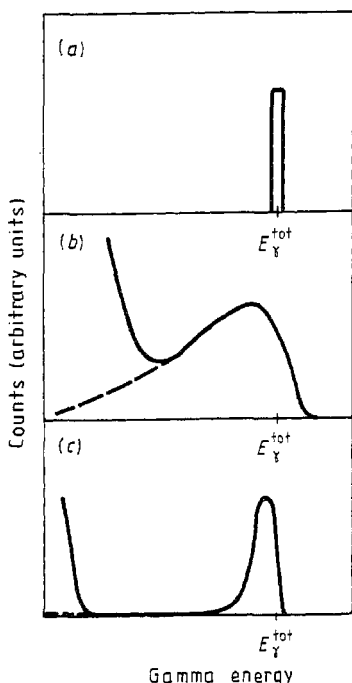


Figure 9. (a) Spectrum of capture events recorded with an ideal 4π detector. (b) Typical spectrum taken with a liquid scintillator tank. The peak around E_{γ}^{tot} is broadened and obscured by an intense background. (c) Expected spectrum for a 4π detector of BaF_2 .

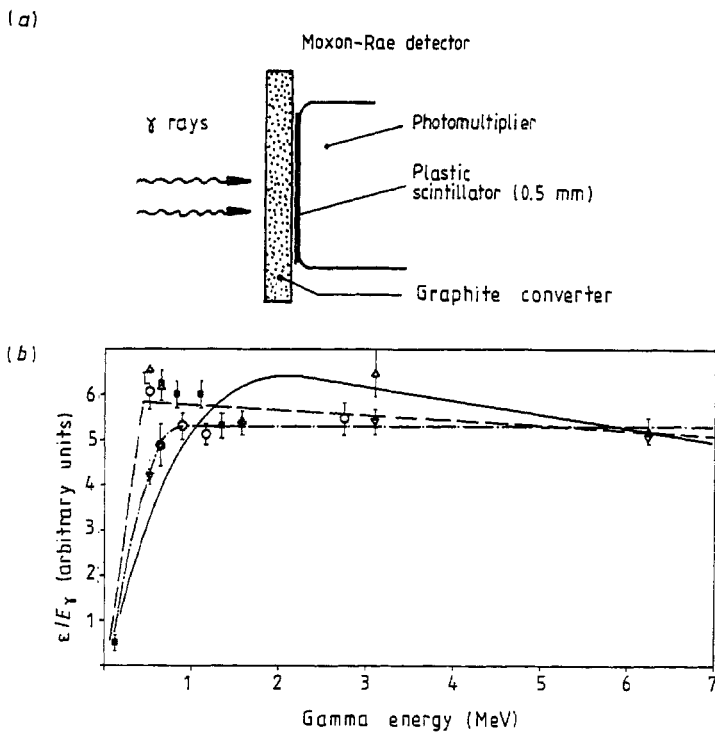


Figure 10. (a) Schematics of a Moxon-Rae detector. (b) Efficiency of a Moxon-Rae detector versus gamma-ray energy (Wissak and Käppeler 1981). Graphite converter: —, calculated; ---, experimental. Bi-C converter, - · -, experimental.

($\leq 1\%$), at most one gamma ray is detected per event, and the cascade efficiency

$$\varepsilon_{\text{casc}} = \sum_{i=1}^m \varepsilon_i(E_{\gamma i}) = \sum k \frac{m}{E_{\gamma i}} = k E_{\gamma}^{\text{tot}} \quad (3.1)$$

is in good approximation independent of the multiplicity and only determined by the total energy, E_{γ}^{tot} (Chrien 1975). With the set-up of figure 10(a) the proportionality between gamma-ray energy and efficiency is almost fulfilled as shown in figure 10(b) except for very low energies, where the efficiency drops steeply. This can be a significant advantage for the investigation of radioactive targets because low-energy gamma rays from the natural decay are automatically suppressed. This has been demonstrated with several examples by Wissak and Käppeler (1983 and references therein). These authors also studied the systematic uncertainties of the Moxon-Rae measurements in great detail and found that accuracies of typically 5% can be achieved (Reffo *et al* 1982, 1983).

A generalisation of the Moxon-Rae detector was developed by Macklin and Gibbons (1967). In this approach the converter in figure 10(a) is eliminated and the scintillator thickness is increased to ~ 10 cm. Even then, the volume of ~ 1 l is small enough that the ordinary organic scintillator can be replaced by the corresponding deuterated compound to avoid the problem of hydrogen capture. This so-called total-energy detector offers a much better efficiency per cascade of $\sim 20\%$, but no longer has an efficiency proportional to the gamma-ray energy. As was shown experimentally, the gamma-ray energy can be approximated by the observed pulse height, and a weighting function $W(E_{\gamma})$ can be applied to each event in order to restore the

relation $\varepsilon \sim E_\gamma$, artificially (Macklin and Gibbons 1967). This type of detector was extensively used in capture measurements, mostly in Oak Ridge by Macklin and collaborators (see Winters and Macklin (1982) for an example) but also in many other laboratories (e.g. in Karlsruhe, Livermore, Geel and Tokyo). Similar to the Moxon-Rae detector one finds that inherent systematic uncertainties restrict the accuracy of this technique to $\sim 5\%$. This value seems to be a general limit for the differential techniques available at present, which have been optimised over more than a decade. Therefore, further improvements of neutron capture rates for the s-process can only be achieved by new techniques.

A new 4π detector. For a significant improvement of the differential techniques described above, one has to return to the idea of detecting in the total gamma-ray energy of the capture cascade (Käppeler *et al* 1983). Figure 9(a) shows the gamma-ray spectrum for the ideal detector with 100% efficiency. While an ideal detector is only roughly approximated by the liquid scintillator tank (figure 9(b)), the use of scintillation crystals appears more promising because of their much better energy resolution. The gamma-ray spectrum expected for a 4π arrangement of scintillation crystals is sketched in figure 9(c). Most of the events fall in a line corresponding to the sum energy of the entire gamma-ray cascade, and only a minor fraction appears at smaller energies, because part of the gamma rays may escape from the detector or are absorbed in the detector cannings or in the sample.

At present, BaF_2 exhibits the best scintillation properties for a detector of neutron capture rates. The scintillation light of BaF_2 contains an extremely fast component (decay time = 600 ps) which is emitted in the uv region at 220 nm (Laval *et al* 1983). Even with large crystals an excellent time resolution of ~ 400 ps can be obtained, while the energy resolution of BaF_2 is close to that of NaI (Wissak and Käppeler 1984).

Because the size of the available crystals is limited, a 4π detector must be composed of many elements. So far, two concepts for a 4π geometry have been pursued. A honeycomb structure of equally shaped hexagonal crystals arranged in axial symmetry offers the advantage of flexibility (Twin 1983). The arrangement can be changed by inclusion of more and more elements, all of the same shape. The second approach, a crystal-ball-type detector (Habs *et al* 1979) is based on a spherical arrangement of detector elements all covering the same solid angle with respect to the sample, thus facilitating multiplicity measurements. Such a detector for the accurate determination of neutron capture rates has now been completed at Karlsruhe (Wissak *et al* 1989). It is composed of 42 BaF_2 crystals, 12 pentagons and 30 hexagons forming a spherical shell of 15 cm thickness. A sketch of the set-up at the accelerator is given in figure 11. The openings of the detector for the neutron beam and sample changer together with the spacings between the detector elements reduce the 4π solid angle by less than 5%.

The response of such a 4π detector for monoenergetic gamma rays was investigated by Wissak *et al* (1984). With this information the efficiency for neutron capture events was calculated for three extreme examples (^{56}Fe , ^{197}Au and ^{241}Am) characterised by very different gamma-ray cascades with respect to total energy, E_γ^{tot} , and to multiplicity. Figure 12 presents the resulting efficiency per gamma-ray energy interval. One finds a total efficiency close to 95% for all cases if a realistic threshold of 2.5 MeV is used for background suppression. This is remarkable as it means that the difference in efficiency even for very different capture cascades is only $\sim 1\%$, leading to very small systematic uncertainties in the measurements. The high efficiency and the expected low backgrounds of this detector will allow for much shorter measuring times compared to present techniques. This, in turn, enables the careful experimental investigation of

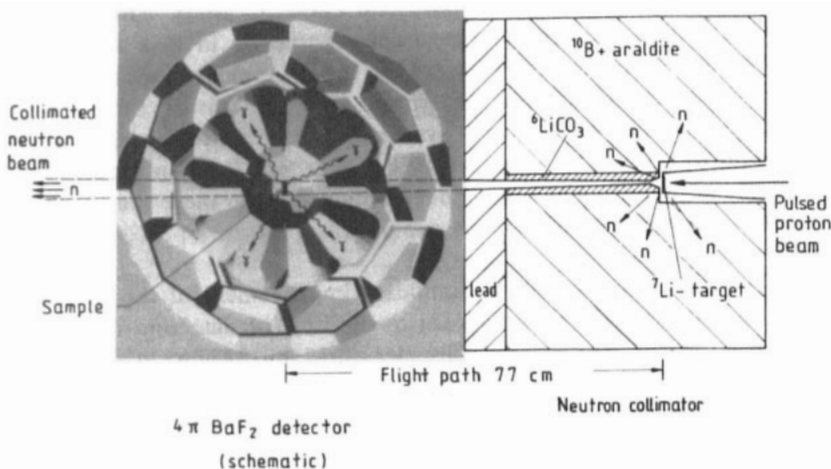


Figure 11. Schematic set-up of the Karlsruhe 4π detector at the accelerator. The detector consists of 12 pentagonal and 30 hexagonal BaF_2 crystals forming a spherical shell with 20 cm inner diameter and 15 cm thickness.

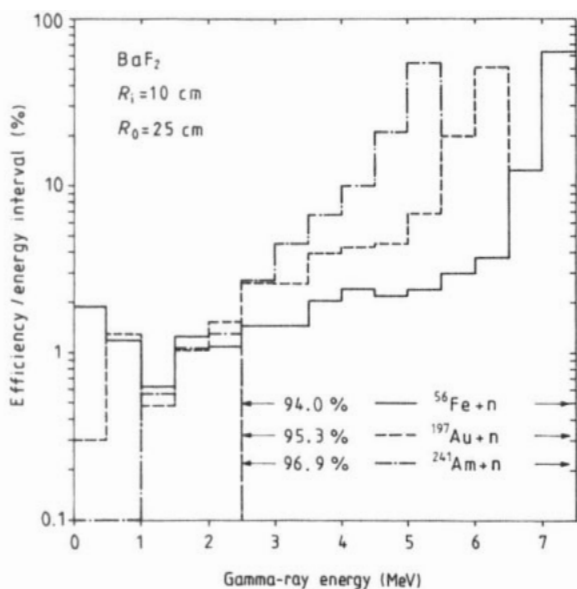


Figure 12. Calculated efficiency of the 4π detector for neutron capture cascades from ^{56}Fe , ^{197}Au and ^{241}Am . Note that for a threshold of 2.5 MeV one obtains the same efficiency of 95% for all three isotopes although these exhibit extremely different gamma-ray cascades.

remaining uncertainties which are related to the capture sample itself (neutron multiple scattering and self-shielding as well as gamma-ray self-attenuation). From the properties of the new detector and from the experience with present techniques an overall accuracy close to 1% can be expected for this new experimental method.

Activation technique. The potential of the activation technique in conjunction with the $^7\text{Li}(p, n)^7\text{Be}$ reaction for the determination of stellar capture rates was outlined by Beer and Käppeler (1980). An important point is the possibility of producing a

neutron energy spectrum very similar to the Maxwell-Boltzmann distribution during the s-process. This advantage adds to the well known features of the activation technique (i.e. selectivity, sensitivity and accuracy) resulting in a very successful method for neutron capture cross-section measurements. However, this method can only be applied if neutron capture leads to a radioactive isotope with a convenient half-life between a few seconds and about 400 days. On the other hand, it is the only means for measuring the partial capture cross sections for populating long-lived isomeric states which can decisively influence s-process branchings (§ 5).

The set-up during neutron irradiation is shown in figure 13(a). The energy of the incoming protons is chosen as 31 keV above the threshold of the $^7\text{Li}(\text{p}, \text{n})^7\text{Be}$ reaction.

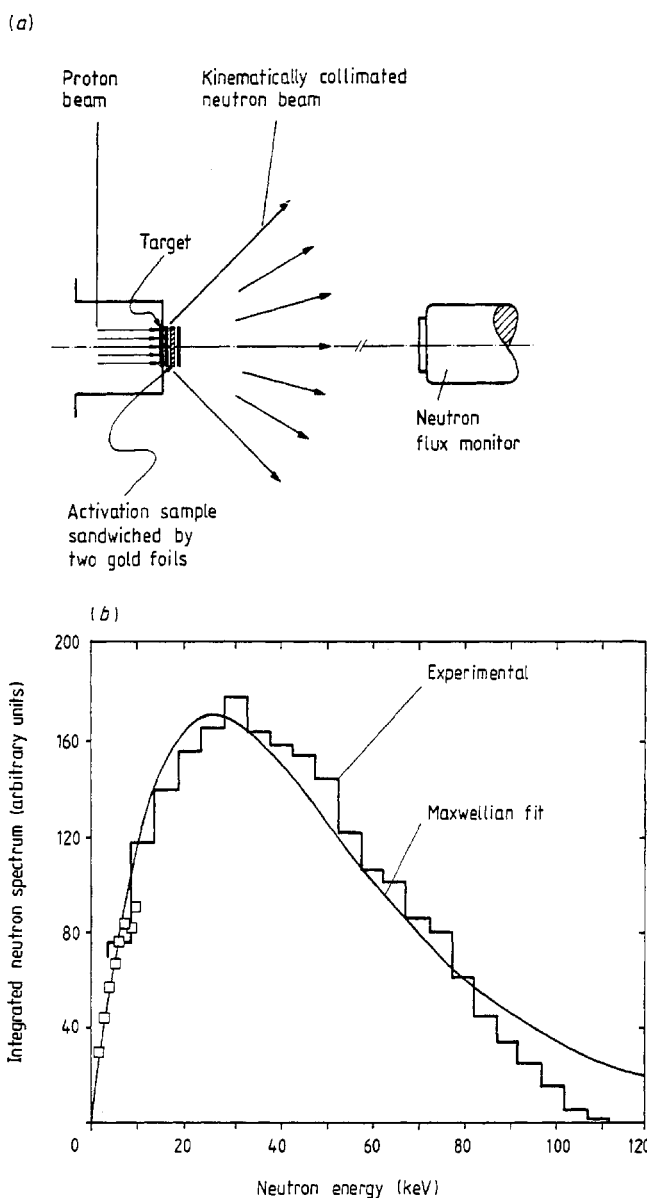


Figure 13. (a) Principle of the activation technique and (b) simulation of a Maxwellian energy spectrum ($kT = 25.0$ keV) via the $^7\text{Li}(\text{p}, \text{n})^7\text{Be}$ reaction. $E_p = 30$ keV above reaction threshold.

Then all neutrons are collimated by the reaction kinematics in a forward cone of 120° opening angle. The angle-integrated neutron spectrum imitates almost perfectly a Maxwell-Boltzmann distribution for a thermal energy of $kT = 25$ keV, as is illustrated in figure 13(b) (Ratynski and Käppeler 1988). With the same arrangement, a spectrum for $kT = 52$ keV can be produced via the $^3\text{H}(\text{p}, \text{n})^3\text{He}$ reaction (Käppeler *et al* 1987). This may be a useful complement, if the $kT = 25$ keV cross section has to be extrapolated to higher energies.

During the irradiation the samples are usually located very close to the neutron target and are sandwiched between two gold foils, which are used for determination of the neutron flux via the ^{197}Au as a cross section standard. A monitor at a distance of ~ 1 m from the neutron target records the time dependence of the neutron yield as the target degrades during the activation. From this time dependence the fraction of activated nuclei that decay during irradiation is calculated. The resulting correction can be significant if the half-lives of the investigated isotope and the gold reference are very different. After irradiation the activated samples are counted with high-resolution gamma or beta detectors as a function of time. This allows us to check whether the background in the activity measurement was properly subtracted, because only then are the correct half-lives reproduced.

The features of the activation technique are illustrated by the example of the very small cross section of the neutron magic isotope ^{48}Ca . Figure 14 shows the gamma-ray spectrum from a ^{48}Ca sample after irradiation with neutrons from the $^7\text{Li}(\text{p}, \text{n})^7\text{Be}$ reaction (Käppeler *et al* 1985). The sample consisted of a 43 mg CaCO_3 tablet (6 mm diameter, 82% ^{48}Ca) between two gold foils (15 mg each). The irradiation and counting

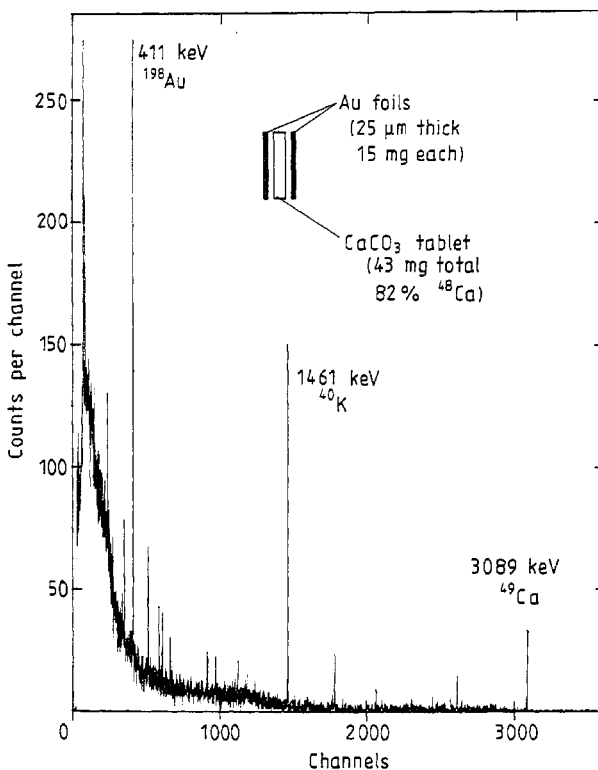


Figure 14. Example for the sensitivity of the activation technique: gamma-ray spectrum obtained for the difficult case of ^{48}Ca . The inset shows the activation sample.

times of 1000 s correspond roughly to two half-lives of ^{49}Ca . The spectrum exhibits the strong 411 keV line from ^{198}Au , the background line from ^{40}K and the 3089 keV line from ^{49}Ca . Although statistics are rather poor after one irradiation, it is obvious that backgrounds are almost negligible. This means that an accurate cross section ratio to ^{197}Au can be obtained by repeated irradiations. The good energy resolution in the gamma-ray spectrum allows identification of the gamma-ray transition in the particular isotope of interest, which makes the method selective: no highly enriched samples are required. The method is also very sensitive because of the low background: rather small sample amounts are sufficient and/or very small cross sections can be determined. For example, the ^{48}Ca cross section was found to be only 0.95 ± 0.09 mb.

Another important aspect of the activation technique is its suitability for very precise measurements. This has been demonstrated in conjunction with a recent improvement of the capture cross section of ^{197}Au (Ratynski and Käppeler 1988). As gold is often used as a cross-section standard, the sizeable spread in existing data called for an additional measurement with an independent method in order to avoid previous systematic uncertainties. The experiment was carried out with the activation technique by irradiating a gold sample in the kinematically collimated neutron cone (figure 13) such that all neutrons pass through the sample. Then the time-integrated neutron flux can be evaluated directly from the ^7Be activity of the neutron target. By systematic variation of the relevant experiment parameters the remaining uncertainties were carefully studied. In this way, the precision of the gold cross section could be improved to 1.5% (figure 15).

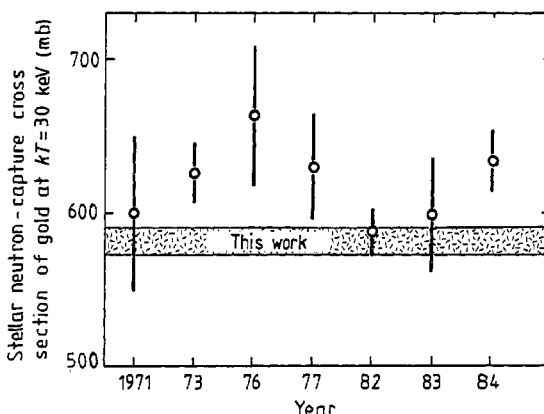


Figure 15. The capture cross section of ^{197}Au measured via the activation technique to $\pm 1.5\%$ (Ratynski and Käppeler 1988) compared to previous results.

The characteristic uncertainties of the activation technique are listed in table 1. While practically all effects can be defined with good accuracy, the spectroscopic information on the decay of the activated isotope (to be taken from literature) is often a limiting factor. In those cases it is advantageous to determine the induced sample activity via the beta-decay electrons, e.g. by the use of a 4π Si(Li) detector system (Ratzel *et al* 1989). In summary, the activation technique is indispensable for s-process investigations particularly because of its combination of high sensitivity and high accuracy.

Radioactive isotopes. Although the vast majority of nuclei involved in the s-process are stable, there are a number of radioactive isotopes which play a key role in the

Table 1. Systematic uncertainties of the activation technique.

Effect	Uncertainty (%)
Efficiency of activity measurement	1-2
Self absorption correction	<0.5-5
Sample mass	<1
Correction for decay during activation	<0.5
Relative intensity of detected radiation	0.5-10
Gold reference cross section	1.5

analysis of s-process branchings (§ 5). Cross-section measurements on these radioactive species in the laboratory will be extremely difficult in most cases because of the short half-lives of the order of 10 yr or less. The availability of sample material, sample handling and gamma-ray backgrounds from sample decay represent the main problems in this respect. Therefore, all existing measurements on radioactive isotopes of relevance to the s-process (Macklin 1982, 1985a,b) were carried out for the long-lived isotopes ^{99}Tc (2.1×10^5 yr), ^{107}Pd (6.5×10^6 yr) and ^{93}Zr (1.5×10^6 yr), respectively. These nuclei could be measured with a conventional set-up because of their low specific activity and the very soft gamma-radiation associated with their decay. Measurements on shorter-lived nuclei have been reported for a series of actinide isotopes by Wissak and Käppeler (1983). With a dedicated set-up these authors obtained a good signal-to-noise ratio even for the comparatively strong gamma-ray emitter ^{243}Am . By extrapolation from this example, some cases of interest to the s-process might be within the reach of conventional techniques.

An exciting new approach has become feasible, however, with the completion of the proton storage ring at the LAMPF accelerator in Los Alamos, which allows for such a high neutron flux that backgrounds from radioactive targets can be overridden about 1000 times better than at existing accelerators. In addition, this laboratory would also be capable of producing the required radioactive targets directly at the site (Bowman and Talbert 1985). A programme to systematically investigate the radioactive branching point isotopes at this facility would provide the information necessary to reveal the physical conditions during the s-process with good accuracy.

3.2.2. Model calculations. The calculation of cross sections represents an important complement to experimental studies for two reasons:

(i) Many of the radioactive species on the s-process path which constitute the important branching points (§ 5) are unaccessible to direct experiments at present. Hence, branching analyses depend heavily on reliable model calculations.

(ii) The typical s-process temperatures of 300–400 million degrees (corresponding to thermal energies of $kT \sim 30$ keV) are sufficient to establish thermal equilibrium between the low-lying nuclear states. This affects mostly the beta decay rates (§ 3.3) but also the stellar reaction rates. In general, the calculated laboratory and stellar neutron capture rates (Holmes *et al* 1976, Harris 1981) agree within $\sim 10\%$ because the population probabilities of excited states are usually small (Walter and Beer 1982). Nevertheless, such differences are significant when experimental rates with 1–2% precision become available. A famous example, where capture from excited states accounts for a large effect is the chronometric pair $^{187}\text{Re}/^{187}\text{Os}$ (§ 7).

Neutron capture rates for the s-process are usually calculated with the statistical model of nuclear reactions (Hauser and Feshbach 1952, Vogt 1969, Hodgson 1971).

This theory can be applied successfully only if two conditions are met: the level density in the compound nucleus at the interaction energy must be high enough so that many (>10) resonances contribute to the reaction rate and the energy of the incident particle must be sufficiently low that other than compound processes (direct or non-statistical reactions) are negligible. The second condition is practically always satisfied for s-process neutron energies, because non-statistical effects start to be important only above a few MeV. The first condition, however, is in question for all nuclei at or close to magic nucleon numbers, and must be considered individually.

By far the most calculations of stellar neutron capture rates are based on the Hauser-Feshbach formula. For the (n, γ) reaction the cross section is given by

$$\sigma = \frac{\pi \hbar^2}{(2J_I + 1)(2J_j + 1)} \sum_{j,\pi} (2J+1) \frac{T_f(J^\pi) T_d(J^\pi)}{T_{\text{tot}}(J^\pi)} W \quad (3.2)$$

where λ is the wavenumber of the incoming neutron, and J_I, J_j are the spins of the capturing state in the target nucleus and of the neutron, respectively. The transmission functions T_f and T_d describe the formation and decay of the compound nucleus. The summation runs over all states in the compound nucleus which can be reached by a combination of target and projectile spins I and j . The factor W accounts for width fluctuations.

The probability for formation of the compound nucleus T_f is calculated by means of the optical model. The corresponding parameters which characterise the potential well of the nucleus as felt by the incoming neutron, are the well depth, the radius and some information on the absorptive properties of the potential. Information on these parameters can be derived from a fit of total neutron cross sections, strength functions and scattering radii. Variation of the optical model parameters within reasonable limits does not affect the resulting cross section by more than about 10%; hence, this part of the cross section calculation is not as sensitive as the treatment of the exit channel.

The decay of the compound nucleus through the photon channel, i.e. the photon transmission function is calculated using the Brink-Axel hypothesis: If one assumes that dipole transitions dominate the photon channel, the photon transmission function can be expressed as

$$T_\gamma(J^\pi) = \sum_{\nu=0}^{\omega} (T_\gamma^\nu(\text{E1}) + T_\gamma^\nu(\text{M1})) + \int_{E_\omega}^{E_{\text{max}}} \int_{J', \pi'} (T_\gamma^\nu(\text{E1}) + T_\gamma^\nu(\text{M1})) \times \rho(E', J', \pi') dE' d\pi' dJ' \quad (3.3)$$

where the superscript ν indicates all excited states in the compound nucleus and E1, M1 are the electric and magnetic dipole transmission functions. The two terms in equation (3.3) account for transitions between discrete levels and transitions in and from the ‘continuum’ above the last known level at E_{max} . This continuum of levels is described by a level density $\rho(E)$. All transitions are subject to the appropriate dipole selection rules.

The dominant electric-dipole transitions can be described through the cross section for the inverse reaction. This means that the available information about the giant dipole resonance can be used to determine T_γ by extrapolation to the energy of the respective gamma transition in the decay of the compound nucleus. A global parameterisation for the calculation of T_γ is given e.g. by Holmes *et al* (1976) and Woosley *et al* (1978). More refined treatments have been reported by Reffo (1980) or Kopecky (1982).

Most important in the calculation of $\sigma_{n\gamma}$ are the probabilities for formation and decay of the compound nucleus, which depend sensitively on the number of accessible levels. Thus the level density ρ in the particular compound nucleus is the determining quantity in any cross-section calculation. Experimental information on the level density is available at low excitation energy from the known discrete levels (ground state up to about 1 MeV, e.g. Lederer and Shirley (1978)) and at the neutron separation energy from high-resolution neutron-resonance studies. In practical applications, a theoretical approach as for instance the back-shifted Fermi gas formula is parameterised and adjusted to the respective experimental values for ρ (Holmes *et al* 1976). Until this point, an accurate description of the level density throughout the periodic table could not be achieved, and cross-section calculations which relied on global parameter sets for ρ suffered from systematic uncertainties of typically 50%. Therefore, *local* parameter studies were carried out to account for shell and deformation effects on the level density (Reffo 1980, Reffo *et al* 1982, 1983), which used as much experimental information on discrete levels and neutron resonance schemes as were available. This method can be extended to all parameters in order to achieve a consistent set for a group of isotopes around the investigated sample, for which the relevant parameters can then be interpolated from the systematics.

The example of figure 16 shows the systematics in the mass region $145 < A < 155$, which was established to calculate the cross sections of radioactive $^{147,148}\text{Pm}$ (Winters *et al* 1986a). These nuclei belong to the important branching points on the s-process path (see § 5). One finds from figure 16 that the level density parameter a depends critically on the neutron number in the compound nucleus; beside a pronounced odd-even effect there is a clear discontinuity at $N = 89$, which would not be so evident in a global parameterisation. By sensitivity studies, starting from the scatter of the experimental values around the smooth systematics (e.g. all points in figure 16 except the interpolated stars for the Pm isotopes), an uncertainty of 20–25% was estimated for this calculational technique.

Whether the uncertainties of such calculations can be further reduced is difficult to judge at present. This problem deserves further investigation as better input data and more accurate experimental capture cross sections become available.

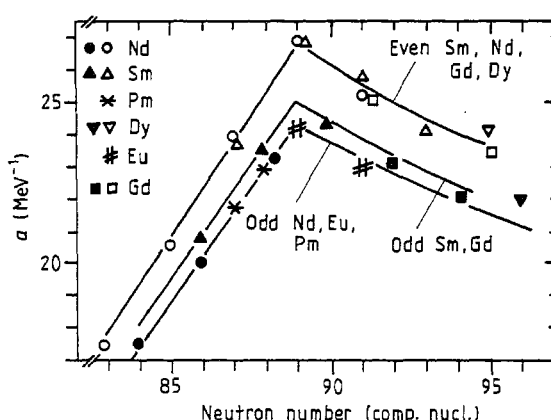


Figure 16. Systematics of the level density parameter a in the mass region $145 < A < 155$. Open and full symbols represent the level densities for even and odd target isotopes as derived from experimental information. Interpolated values for $^{147,148}\text{Pm}$ are denoted by stars.

3.2.3. Stellar neutron capture rates. As helium shell burning in red giant stars is commonly considered as the astrophysical site for the s-process, one deals with typical matter densities of $\sim 1000 \text{ g cm}^{-3}$, neutron densities of $\sim 10^8 \text{ cm}^{-3}$, and temperatures between 300 and 400 million degrees. In such an environment neutrons are in complete thermal equilibrium, exhibiting a Maxwell-Boltzmann spectrum

$$\Phi \sim \sqrt{E_n} \exp(-E_n/kT) \quad (3.4)$$

with thermal energies around $kT = 30 \text{ keV}$. The effective stellar capture cross section, $\langle\sigma\rangle$, is an average of the product of the differential cross section, $\sigma(E_n)$, and the relative velocity of neutron and target, v , over the thermal flux spectrum of equation (3.4). For astrophysical applications, $\langle\sigma\rangle$ is defined as

$$\langle\sigma\rangle = \frac{\langle\sigma v\rangle}{v_T} = \frac{2}{\sqrt{\pi}} \frac{\int_0^\infty \sigma(E_n) E_n \exp(-E_n/kT) dE_n}{\int_0^\infty E_n \exp(-E_n/kT) dE_n} \quad (3.5)$$

where E_n is the total kinetic energy in the centre-of-mass system (Clayton 1968). The factor $2/\sqrt{\pi}$ comes from the fact that the mean thermal velocity $v_T = \sqrt{(2kT/m)}$ with m being the reduced mass was used for normalisation instead of the average velocity. The definition of $\langle\sigma\rangle$ implies that the stellar neutron capture rate, λ_n , is rather insensitive to temperature because most differential cross sections $\sigma(E_n)$ scale with $1/v$. Therefore, s-process calculations are usually performed for a *standard* thermal energy of 30 keV.

It was noted recently that the stellar neutron spectrum may not be completely thermalised but may exhibit a small epithermal component, depending on the Q -value of the neutron-producing reaction (Petrov and Shlyakhter 1988). This component is certainly too small to affect the stellar neutron capture cross sections, but it may well cause an enhancement of (n, p) or (n, α) rates due to the rather sharp thresholds in these cross sections. Whether this effect can be verified by a typical signature in the observed abundances is still open at present.

Neutron capture rates. Previous compilations of experimental neutron capture cross sections for the s-process (Allen *et al* 1971, Conrad 1976, Newman 1978) have recently been extended and updated (Bao and Käppeler 1987, Beer *et al* 1989a). The present status is briefly summarised in table 2, and numerical values are included in table 4 (below). Though the majority of all required cross sections is determined experimentally, the respective uncertainties are often much larger than the 5 to 10% range of present techniques. Further measurements will have to concentrate on improving the accuracy, especially for the s-only isotopes, and on tackling the problem of radioactive nuclei.

In making the step from the laboratory to stellar capture rates it is not sufficient to determine the proper average over the stellar neutron spectrum. In addition, neutron capture in excited states and competition of superelastic scattering (by which the neutron de-excites a nucleus and gains in energy) must be considered as well. Model

Table 2. Maxwellian-averaged neutron capture cross sections at $kT = 30 \text{ keV}$.

Classification	Remarks
Stable isotopes on or near s-process path	~ 240 cross sections; only 22 not yet measured, but only 40% with uncertainties better than 8%
Stable s-only isotopes or isotopes with minor r-process contributions	~ 40 cross sections; all measured except for $^{128,130}\text{Xe}$ and ^{192}Pt ; in 9 cases still uncertainties between 12 and 20%: ^{87}Rb , ^{89}Y , ^{96}Mo , ^{110}Cd , ^{116}Sn , $^{122,124}\text{Te}$, $^{134,136}\text{Ba}$
Radioactive isotopes	50 cross sections, only 6 measured so far

calculations indicate that the stellar cross sections differ by less than 5% from the laboratory values in most cases (Harris 1981, Holmes *et al* 1976); but there are important s-only isotopes, where this difference is estimated to reach the 10–20% level, e.g. ^{154}Gd , ^{160}Dy , ^{170}Yb and ^{176}Hf , as well as the osmium isotopes 186 and 187 which are decisive for the chronometric pair $^{187}\text{Re}/^{187}\text{Os}$. Such corrections are already significant for the present $\sigma N(A)$ curve (Käppeler 1989), which is considered to be accurate to about 10%. As the model calculations available differ from each other by that same percentage, further efforts to refine the classical s-process model have therefore to improve on that aspect. As far as dynamic s-process models are concerned, superelastic scattering has been shown to be an important effect (Petrov and Shlyakhter 1984). For neutron densities $>10^{10} \text{ cm}^{-3}$ it is expected to influence the observed abundances significantly. As Ward and Fowler (1980) have pointed out, the stellar capture rates can become complex functions of the physical conditions during the s-process, when the population of excited states does not reach thermal equilibrium (see also § 3.3).

Other neutron-induced reactions. For a number of isotopes in the mass range $A < 90$, the (n, α) and (n, p) cross sections become significant and may well exceed that for neutron capture, leading to another type of s-process branchings. Important examples are the radioactive nuclei ^{35}Cl , ^{40}K and ^{41}Ca which all affect the abundances of the potential chronometric pair $^{40}\text{K}/^{40}\text{Ar}$ (Beer and Penzhorn 1987). Another example for an important (n, p) reaction is that on ^{26}Al , which is not related to the s-process, but determines the ^{26}Al abundance in explosive nuclear burning (Trautvetter *et al* 1986).

3.3. Beta decay rates

Branchings in the s-process path are determined by the competition between neutron capture and β decay. The branching ratio can be expressed by equation (2.8) in terms of the neutron capture rate, $\lambda_n = n_n \sigma v_T$, and the beta decay rate, $\lambda_\beta = \ln 2 / t_{1/2}$, of the respective branch-point isotope. The beta decay rate stands for all possible decay processes: β^- decay, electron capture or β^+ decay. For each s-process branching it has to be checked whether λ_n or λ_β could be affected by temperature. As was noted in § 3.2.3, neutron capture rates depend only slightly on temperature. In contrast, beta decay rates may undergo dramatic changes at typical s-process temperatures, either through beta decays from excited states or through atomic effects in the highly ionised, dense stellar plasma. As nuclear matrix elements remain unchanged, the stellar beta decay rates can be calculated from pure phase space arguments (Bahcall 1961), at least for the important allowed and first non-unique forbidden transitions.

How aggravatingly s-process temperatures may affect beta decay rates can be illustrated by the example of the branchings at ^{79}Se and ^{85}Kr . Figure 2 shows the s-process flow through the mass region $75 < A < 90$. The branchings manifest themselves by different σN -values of the respective s-only isotopes, i.e. $^{80,82}\text{Kr}$ and $^{86,88}\text{Sr}$. (Formally, ^{88}Sr is not a pure s-process isotope but the abundance contribution from the r-process is only about 20%; Walter *et al* (1986a).) While the σN -ratios of $^{80,82}\text{Kr}$ yield a good measure for the branching factor at ^{79}Se , the ^{85}Kr branching is more complicated due to the short-lived isomeric state in ^{85}Kr and due to the neutron shell closure at $N = 50$. About 57% of all neutron captures populate the isomer ^{85m}Kr , which then decays promptly (compared to the neutron capture timescale) with 79% probability to ^{85}Rb . In other words, only 54% of the s-process flow proceeds through the long-lived ground state of ^{85}Kr . Furthermore, the σN -values of $^{86,88}\text{Sr}$ have to be corrected for the effect of the small cross sections at $N = 50$, which cause a significant

step in the σN curve. The observation that the resulting branching ratios, both for ^{79}Se and ^{85}Kr , are almost equal seems to be in conflict with the fact that the terrestrial beta decay rates of ^{79}Se and ^{85}Kr differ by roughly four orders of magnitude.

This puzzle is resolved if beta decay from thermally populated excited states is taken into account. The ground-state decay of ^{79}Se is first unique forbidden, but allowed decays are possible from the isomeric state at 95.7 keV as well as from the states at 128 and 137.1 keV. These states are populated to 1.0, 0.4 and 1.2% at $kT = 30$ keV, and dominate the stellar beta decay rate of ^{79}Se completely:

$$\lambda_{\beta}^* = \sum_i \left(p_i \sum_j \lambda_{\beta ij} \right). \quad (3.6)$$

The index i runs over all excited states with population probabilities, p_i , and λ_{ij} is the decay rate from state i in the unstable nucleus to level j in the daughter nucleus. In thermal equilibrium the p_i are given by a Boltzmann distribution

$$p_i = (2J_i + 1) \exp(-E_i/kT) / \sum_m (2J_m + 1) \exp(-E_m/kT), \quad (3.7)$$

the sum in the denominator being the nuclear partition function. Population probabilities of excited states in radioactive nuclei of relevance for s-process studies have been published in tabular form by Walter and Beer (1982).

Apart from the beta decay of excited states, stellar decay rates are also influenced by atomic effects via the high degree of ionisation in the hot stellar plasma. Under such conditions electrons can also be emitted into unoccupied atomic orbits, thus adding the respective binding energy to the decay energy. This effect is always important when the decay energy is comparable to or smaller than the K-shell binding energy. The relevant nuclear parameter in this case is the decay energy itself, which is not always sufficiently well known as in the important example of the chronometric pair $^{205}\text{Tl}/^{205}\text{Pb}$ (Yokoi *et al* 1985). Even in the case of ^{79}Se , where the beta decay energy is about 20 times larger than the K-shell ionisation energy, bound-state decay contributes $\sim 25\%$ to the stellar rate (Conrad 1976, Takahashi and Yokoi 1987).

One of the major uncertainties in the stellar beta decay rates is due to the $\log ft$ values for transitions from excited states, which have been estimated by comparison with known analogous transitions in neighbouring isotopes. Experimental $\log ft$ values can hardly be expected for these states, because gamma decay by far dominates over beta transitions. ^{79}Se represents an important exception, as the stellar beta decay rate is determined by the isomeric state at 96 keV which has a half-life of 3.9 m (figure 17). At $kT = 30$ keV this isomer is populated to $\sim 1\%$, and its decay represents the only significant term in equation (3.6). The 10% uncertainty of the estimated $\log ft = 5.0$, however, results in an uncertainty of the stellar decay rate of a factor of three.

The rather long half-life of 3.9 m for the gamma decay to the ground state enabled a successful measurement of the beta decay branching ratio (Klay and Käppeler 1988). The 96 keV isomer was produced by activation in the high flux reactor of the Institut Laue-Langevin in Grenoble, using a sample of highly enriched ^{78}Se implanted into a thin, ultrapure graphite disc. The subsequent decay was investigated by using a Mini-Orange beta spectrometer with a low-energy cut-off near 100 keV for suppression of conversion electrons. With the experimental $\log ft$ value the temperature dependence of the ^{79}Se half-life was recalculated with the formalism of Takahashi and Yokoi (1983). Figure 17 compares this result with previous work using different estimates for the $\log ft$ value (Takahashi and Yokoi 1987, Conrad 1976, Cosner and Truran

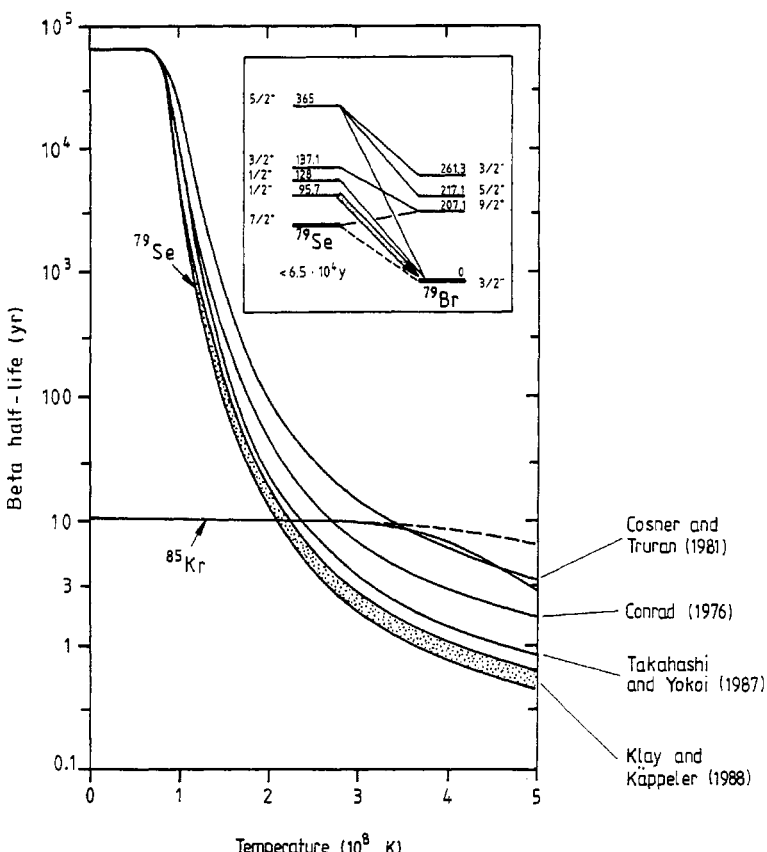


Figure 17. The beta decay half-lives of ^{79}Se and ^{85}Kr as a function of temperature in units of $T_8 = 10^8$ K. The decay of ^{79}Se is dramatically enhanced for $T_8 > 1$ due to decay from excited states.

1981). One finds that the decay rate is constant for $T < 10^8$ K but drops quickly to the order of a few years when the first excited states start to be thermally populated. Note that the calculated curves were uncertain by a factor of three due to the estimated 10% uncertainty in the $\log ft$ value.

For comparison, figure 17 also contains the beta decay rate of ^{85}Kr , which appears to be insensitive to temperature, at least under helium burning conditions, because the first excited states in this nucleus occur at 305 and 1107 keV (Yokoi and Takahashi 1985). This curve should be taken as a lower limit as it was calculated using the beta decay rate ($t_{1/2} = 4.5$ h) as the effective destruction rate of the isomer instead of the smaller equilibration rate by which the isomer is fed from the ground state (Ward and Fowler 1980; broken curve).

A summary of thermal effects on stellar beta decay rates is given in table 3 (Conrad 1976). Most important is beta decay from excited states including the possible back decay from excited states in the daughter nucleus as in the example of ^{79}Se . Bound-state beta decay is important for small decay energies below $Q_\beta < 300$ keV, where the electron binding energy has a significant impact. Quantitative treatment of bound-state beta decay requires knowledge of the degree of ionisation, i.e. a model of the stellar plasma. Such a model is also needed to calculate the stellar electron capture rates as these depend critically on the electron density at the nuclear surface. At typical s-process

Table 3. Thermal effects on beta decay rates under typical s-process conditions ($kT = 30 \text{ keV}$, $n_e = 10^{27} \text{ cm}^{-3}$).

Effect	Comment
1. β^- decay through excited states	Involves excited states below 200 keV; experimental decay rates very scarce
2. Bound state β^- decay	Significant for $E_\beta < 300 \text{ keV}$
3. Hindrance of electron capture due to high degree of ionisation	Typical factor 10?
4. Electron capture from continuum	Significant for $E_\beta < 30 \text{ keV}$
5. Weakening of screening corrections due to high degree of ionisation	Affects low-energy β^+ decays
6. Change of competing internal conversion rates due to high degree of ionisation	Applies for small transition energies and high multiplicity (isomers)
7. Other effects	Negligible for the s-process; see text

densities, electron concentrations are of the order of 10^{27} cm^{-3} , which means that electron capture from the continuum is no longer negligible, especially at decay energies below 30 keV. Another consequence of the high degree of ionisation is that the Fermi function is no longer modified by screening from the atomic electron cloud; this is important for low-energy β^+ decays.

Finally, minor effects are mentioned in entry 7 of table 3 which are not significant for the s-process but may become important at higher temperatures (photon-induced beta decay; Shaw *et al* (1965)), or at higher densities (Fermi statistics, reduction of electron phase space in a degenerate environment, neutronization of matter; Conrad (1976), Fuller *et al* (1982)).

Global calculations of beta decay rates for the s-process have been published by Newman (1973), and by Cosner and Truran (1981) using schematic assignments of unknown $\log ft$ values for transitions from excited states and neglecting bound-state decays. The work of Conrad (1976) included a simplified model for bound-state decay and $\log ft$ values derived from similar transitions in neighbouring nuclei. A thorough and comprehensive investigation was then carried out by Takahashi and Yokoi (1983) with due consideration of ionic states in the stellar plasma, transition probabilities and decay energetics in a wide domain of possible temperatures (10^6 – 10^9 K) and densities (10^{-4} – 10^4 g cm^{-3}). An important outcome of this work was that bound-state decay—which was neglected in some previous calculations—is of great importance to s-process analyses. Remarkable examples are ^{163}Dy , a terrestrially stable isotope which becomes unstable at high temperature (§ 5.2.2), and ^{187}Re , which was considered as a cosmochronometer until it was found that its decay is affected by temperature (§ 7).

These improved beta decay rates for the s-process are tabulated in numerical form for all relevant isotopes along the s-process path (Yokoi and Takahashi 1985, Takahashi and Yokoi 1987). Figure 18 is adopted from this work and illustrates impressively the influence of bound-state β^- decays. It shows the ratio between the rates of bound-state decay and continuum decay for allowed and non-unique first forbidden transitions versus Q_n , the neutral atomic mass difference between the initial and final nucleus. For small values of Q_n the rates are completely dominated by bound-state decay. As expected, this effect exhibits a strong Z dependence. Consequently, Yokoi and Takahashi noted severe discrepancies to earlier calculations, where bound-state decay was not considered (Newman 1973, Cosner and Truran 1981).

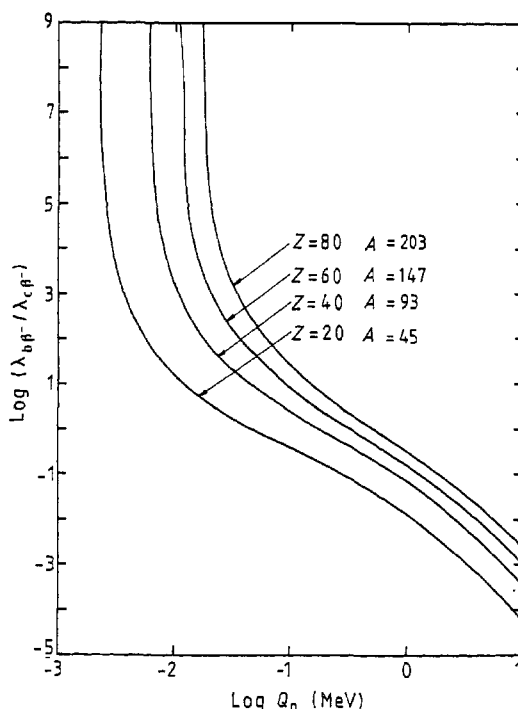


Figure 18. Ratio of bound-state β^- decay rate and continuum β^- decay rate versus Q_n , the neutral atomic mass difference between the initial and final nucleus (Yokoi and Takahashi 1985) for allowed and non-unique first forbidden transition.

For the study of s-process branchings it is sometimes also important to consider the timescale for reaching stationary conditions. This is of special importance in connection with long-lived isomeric states. These states are characterised by quantum numbers which are very different from those of the ground state, so that direct gamma-ray transitions are hindered by selection rules. During the s-process isomers can be populated by neutron capture or beta decay.

In principle, nuclei in the isomeric state must be treated as a separate species in parallel to the nuclei in the ground state. This concerns the effective capture cross sections (§ 3.2) as well as the stellar decay rates. However, separate treatment of the isomer and the ground state is only valid if the initial population of the isomeric state remains unchanged under s-process conditions. This needs to be verified in each case, as isomeric states may well be thermalised at high temperatures through transitions via mediating states at higher excitation energy (Ward 1977, Ward and Fowler 1980).

There are examples where the level spacing is too large for a mediating state to occur within the available thermal energy, e.g. in ^{121}Sn . Such isotopes fall under the category of *unthermalised* cases for which the equilibration time is much longer than the time required to capture a neutron. Consequently, the isomer and the ground state have to be treated separately (Ward 1977). In most cases, thermal equilibrium is rapidly achieved, as the equilibration time for a particular state is

$$\tau_{\text{eq}} = (\lambda \uparrow + \lambda \downarrow)^{-1} \quad (3.8)$$

where $\lambda \uparrow$ and $\lambda \downarrow$ denote the upward and downward transition rates. The downward rate is the sum of the natural decay rate plus the rate for stimulated emission, while the upward rate equals the downward rate times the Boltzmann factor. In any case,

the equilibration time is shorter than the natural half-life of a state. Therefore, the majority of all isotopes involved in the s-process are in *complete* thermal equilibrium, a situation which is convenient to calculate (Takahashi and Yokoi 1987).

Between these extremes one finds those isotopes which are only *partially* thermalised because the equilibration timescale is comparable to the timescale for neutron capture and/or changes in the astrophysical conditions. These cases are difficult to handle as the quantitative verification requires knowledge of the mediating transitions that provide the link between the ground state and the isomer. In view of the complicated structure of these nuclei, experimental transition rates are usually not available, and even level schemes are often incomplete. Under stellar conditions, terrestrial decay rates can additionally be modified by suppression of internal conversions, and inelastic collisions in the hot stellar plasma (Shaw and Clayton 1967, Ward 1981). An example for such a partially thermalised isomer is possibly ^{176}Lu , which is discussed in § 7.4.

The influence of temperature on alpha decay rates was also investigated (Perrone and Clayton 1971) with the result that these rates are affected relatively little under s-process conditions. Weak interaction rates for more extreme density and temperature regimes, e.g. conditions during stellar collapse, have been tabulated by Fuller *et al* (1982).

In summary, it is to be emphasised that the understanding of many details in the s-process depends on the reliability of relevant stellar beta decay rates. Further improvement of these rates mainly represents a theoretical challenge, but information from the experimental side remains an essential complement. Only then can the signatures in the observed abundance patterns be deciphered in terms of the s-process neutron density and temperature. This aspect will be discussed in detail in § 5.

4. Status of the classical s-process

4.1. The $\sigma N_s(A)$ curve

The credibility of the classical model is based on the successful reproduction of the empirical products of cross section times s-process abundance, σN_s , for the s-only isotopes. This property was the better confirmed the more reliable the relevant cross sections, and abundances were determined with time. A historic account of this observation is given by Mathews and Ward (1985). Figure 19 shows a comparison of the calculated σN_s curve obtained by Käppeler *et al* (1982) and a present fit together with the respective empirical σN_s products for those isotopes which are of pure s-process origin or which have only minor r-process contributions. The main component is plotted as a heavy full curve showing the contribution of the weak component explicitly. The present curve was determined with the code SPEED.CLAS (Beer 1985). The major improvement compared with the previous calculation is that now all significant s-process branchings are considered as indicated by the respective splits of the σN_s curve. Within error bars—which include the uncertainties from the abundances and from the cross sections as well—the empirical σN_s -values of all s-only nuclei are perfectly reproduced: a striking success of the classical model!

Differences between the two curves are due to improved abundances and cross sections as well:

(i) The abundance compilations of Anders and Ebihara (1982) and of Anders and Grevesse (1989) contain several changes with respect to that of Cameron (1982), which were important for the σN_s curve. For example, the Te abundance was lowered by

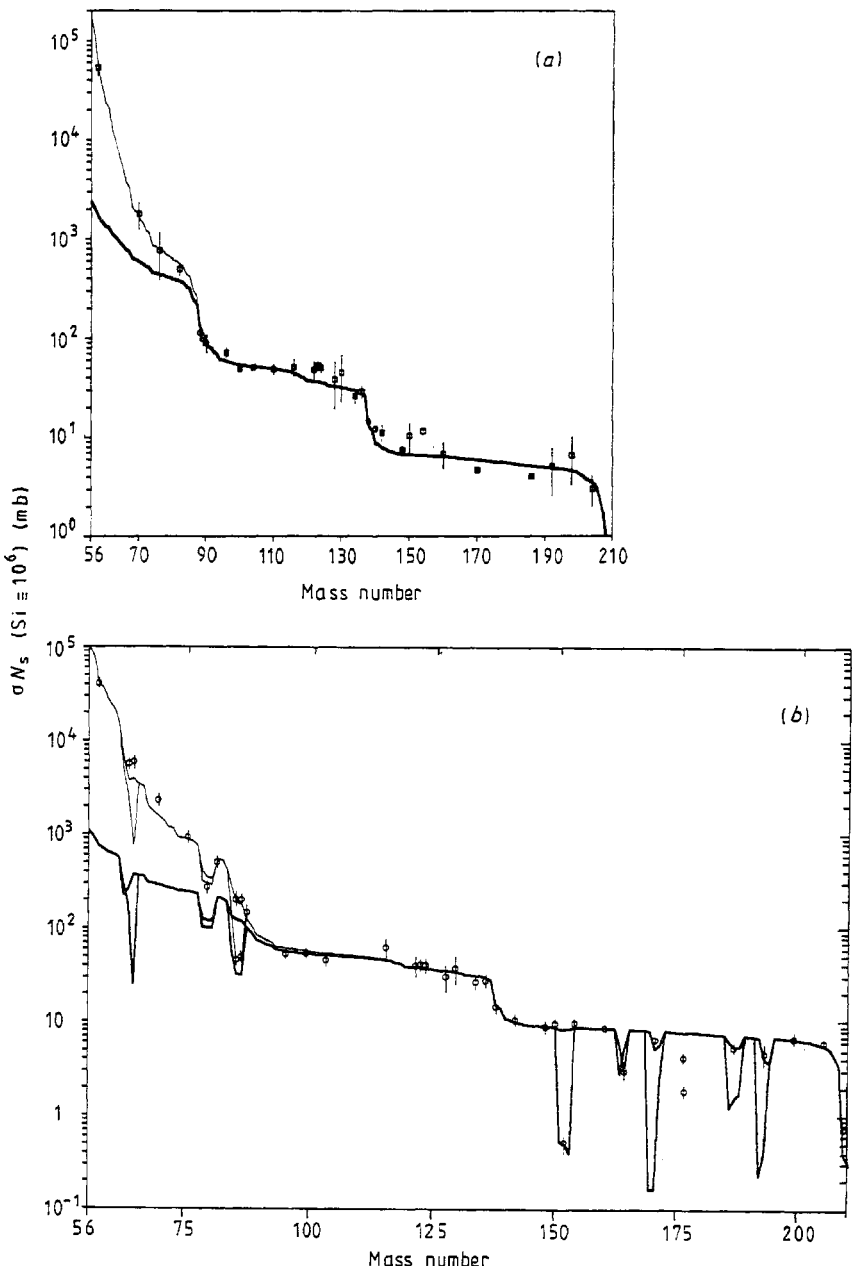


Figure 19. The characteristic product of cross section times s-process abundance versus mass number. We compare the status of this curve in 1982 (a) (with N_s from Cameron 1981) with the present situation (b) (N_s from Anders and Ebihara 1982). Symbols with error bars denote the empirical products of pure or almost pure s-isotopes.

25%, leading to good agreement of the $^{122,123,124}\text{Te}$ values with the model curve. Even more important was the revision of the rare-earth abundances. While the Gd abundance was lowered by 20%, most of the others were raised by $\sim 10\%$. These changes yielded an empirical σN_s -value of Gd, which is now consistent with the model curve, and reduced also the step in the σN curve at the magic neutron number 82. As a result, the ratio between seed abundance and integral s-process yield for the main component

has decreased, resulting in consequences for the neutron economy (§ 4.2). The abundances of volatile elements that had previously been determined by interpolation between neighbouring isotopes are now determined from the σN_s systematics, i.e. for Ar (Beer and Penzhorn 1987), Kr (Walter *et al* 1986a), Xe (Beer *et al* 1983) and Hg (Beer and Macklin 1985).

(ii) The set of neutron capture cross sections was also considerably improved during the last years (Bao and Käppeler 1987). Prominent examples are the s-nuclei ^{70}Ge , $^{128,130}\text{Xe}$, ^{142}Nd , $^{148,150}\text{Sm}$, ^{160}Dy , ^{198}Hg and ^{204}Pb , where the cross sections have been either measured for the first time or reinvestigated with considerably reduced uncertainties.

With all this new information, the reliability of the empirical σN_s products could be greatly enhanced, the combined uncertainties in cross section and abundance now reaching $\sim 10\%$ for many of these isotopes. Consequently, it is fair to say that the present σN_s curve is also accurate to $\pm 10\%$ because it does reproduce all these normalisation points within their uncertainties. Hence, the classical model allows for a consistent description of the observed s-process abundances including the various branchings (§ 5). This result is somewhat surprising at first sight, because it means that the classical model cannot be as wrong as could be expected from the very schematic assumptions of that approach. On the other hand, this result implies that the true nature of the s-process may still be hidden behind the present uncertainties. As these are mostly due to the nuclear physics involved, experimentalists are challenged to further improve the relevant input data.

However, at the present level two corrections to the empirical σN_s values can already no longer be neglected: the stellar enhancement of neutron capture rates as well as the p-process contributions to the observed s-abundances. It has been mentioned in § 3.2.3 that thermally populated excited states may exhibit very different capture cross sections, and this effect has the more impact on the total rate the higher the population probabilities are, i.e. the higher the temperature is. Being negligible for thermal energies below ~ 20 keV, these corrections can be of the order of 10% at $kT = 30$ keV. Among the s-only isotopes there are a few examples which are sensitive to this enhancement, but the present uncertainties are just at the limit for it to become manifest: the empirical σN_s -values of ^{160}Dy or ^{170}Yb need to be increased by 3 to 5% at the currently estimated s-process temperature of 2.5×10^8 K. (The only exception showing a much stronger temperature dependence is ^{187}Os , but this case must be considered separately; see § 7.) Principally, the stellar enhancement of the neutron capture rates of a variety of isotopes constitutes a potential thermometer for the s-process in addition to those represented by s-process branchings (§ 5). Though a quantitative estimate cannot be derived at present, it is at least possible to consider $kT = 30$ keV as an upper limit for the thermal energy characteristic of the s-process; any higher temperature would lead to stellar enhancement factors larger than the 10% uncertainty of the present σN_s curve.

It is certainly plausible that the p-process is not restricted to the relatively few isotopes that are not accounted for by neutron capture reactions, but that it also contributes to the s-abundances. At present, the corresponding corrections are either neglected or somehow interpolated from the p-only nuclei. Both approximations lead to uncertainties similar to those discussed above; hence, the future development of a quantitative model for the p-process is much needed.

The results of figure 19 are presented in numerical form in table 4. The cross sections quoted in column 3 are based on the compilation of Bao and Käppeler (1987),

Table 4. σN_s values from the classical model compared to empirical σN_\odot products of s-only nuclei corrected for p-process contributions; r-process residuals and r-only abundances are listed in the last two columns. The numerical values of this table correspond to figures 19 and 20. Note that the r-residuals in the mass range $A < 90$ are slightly different if the single flux solution for the weak s-process component is adopted (σN_s -values in brackets).

Mass number	Element	p-correction		σN_\odot		σN_s		$N_{\odot,r}$		$N_r = N_\odot - N_s$ (Si = 10 ⁶)
		to s-only abundance	(%)	s-only nuclei (mb, Si = 10 ⁶)	main component (mb, Si = 10 ⁶)	all components (mb, Si = 10 ⁶)	r-only nuclei (Si = 10 ⁶)			
56	Fe	14.0 ± 0.7		1097	104 859 (3561)					
57	Fe	44.7 ± 4.5		946	80 840 (3968)					
58	Fe	15.6 ± 1.6		40 720 ± 4220	765	46 323 (7720)				
59	Co	43.3 ± 4.3			705	36 463 (8662)				
60	Ni	34.9 ± 1.7		638	25 549 (8792)					
61	Ni	92.9 ± 9.0		614	21 860 (9063)					
62	Ni	43.4 ± 4.9		566	16 332 (9311)					
63	Ni	30		224	6 864 (5693)					
64	Cu	70.9 ± 10.6		298	4 647 (3410)					
64	Ni	11.8 ± 1.3		261	3 798 (4533)					
64	Zn	70.2 ± 5.9		176	2 580 (1944)					
65	Cu	60.5 ± 5.7		375	3 942 (5363)					
65	Zn	148.5		25	763 (444)					
66	Zn	39.5 ± 3.4		366	3 461 (4675)					
67	Zn	182 ± 18		358	3 207 (4426)					
68	Zn	21.9 ± 2.7		307	1 951 (2692)					
69	Ga	161 ± 7		300	1 793 (2466)					
70	Ge	105.4 ± 6.2	9.7	2 305 ± 256	290	1 581 (2121)	7.81 ± 0.79 (70Zn)			
71	Ge	138 ± 9		283	1 437 (1894)					
72	Ge	65		268	1 191 (1489)					
73	Ge	324		265	1 144 (1410)					
74	Ge	60 ± 8		249	944 (1072)					
75	As	636 ± 39		248	926 (1042)					
76	Se	186 ± 23	9.7	940 ± 130	243	866 (945)	9.20 ± 0.95 (76Ge)			
77	Se	504			241	846 (910)				
78	Se	102		233		755 (765)				
79	Se	249 ± 57		104		412 (537)				
79	Br	702 ± 46		127		316 (242)				

80	Se	46.6 ± 2.6	15.0	270 ± 45	102	$347 (383)$	24.3 ± 1.99
80	Kr	287 ± 14			120	$293 (225)$	
81	Br	702 ± 46			101	$336 (361)$	4.64 ± 1.11
81	Kr	77.9			119	$289 (222)$	
82	Kr	89.1 ± 6.8	3.0	495 ± 88	212	$553 (449)$	3.75 ± 0.47
83	Kr	267 ± 16.0			209	$531 (422)$	18.00 ± 2.45
84	Kr	40.0 ± 4.6			191	$423 (245)$	
85	Kr	76 ± 19			55.3	$126 (69.1)$	
85	Rb	397 ± 20			132	$274 (168)$	2.79 ± 0.47
86	Kr	5.2 ± 0.4			32.4	$49.3 (40.6)$	<0.93
86	Sr	90 ± 4.0	5.6	199 ± 19	123	$190 (140)$	
87	Rb	20.6 ± 2.0			31.8	$45.6 (31.7)$	
87	Sr	123.4 ± 8.0		201 ± 21	119	$178 (126)$	0.10 ± 0.22
88	Sr	7.3 ± 0.6		142 ± 17	100	$124 (101)$	2.55 ± 2.84
89	Y	32.0 ± 3.4		148 ± 20	90.0	107	1.31 ± 0.50
90	Zr	18.7 ± 1.1		103 ± 15	75.2	84.7	0.99 ± 0.77
91	Zr	68.5 ± 9.1			71.4	79.3	0.04 ± 0.21
92	Zr	57.1 ± 6.9			67.1	73.6	0.54 ± 0.28
93	Nb	309 ± 17			65.0	70.8	0.11 ± 0.12
94	Zr	37.7 ± 5.7			59.2	63.6	0.17 ± 0.34
95	Mo	333 ± 14			58.6	62.9	0.213 ± 0.024
96	Mo	128 ± 9			53.9	57.0	$0.300 \pm 0.039 (^{96}\text{Zr})$
97	Mo	387 ± 16			56.4	60.2	0.087 ± 0.015
98	Mo	113.1 ± 8.0			54.6	58.1	0.093 ± 0.051
99	Tc	893 ± 57			5.27	5.55	0.172 ± 0.014
99	Ru	1063			49.2	52.3	
100	Ru	235 ± 15		55.1 ± 4.6	53.6	56.8	$0.2422 \pm 0.013 (^{100}\text{Mo})$
101	Ru	113.8 ± 46			53.4	56.5	0.266 ± 0.017
102	Ru	212 ± 13			52.5	55.4	0.327 ± 0.036
103	Rh	996 ± 80			52.3	55.2	0.289 ± 0.028
104	Pd	330 ± 33	9.0	46.0 ± 5.8	51.7	54.5	$0.348 \pm 0.019 (^{104}\text{Ru})$
105	Pd	1369 ± 69			51.6	54.3	0.269 ± 0.024
106	Pd	288 ± 29			50.9	53.5	0.193 ± 0.035
107	Ag	913 ± 27			50.8	53.3	0.239 ± 0.026
108	Pd	232 ± 23			50.0	52.4	0.145 ± 0.037
109	Ag	890 ± 26			49.8	52.1	0.196 ± 0.024

Table 4. (continued)

Mass number	Element	p-correction to s-only abundance (%)		σN_{\odot}		σN_s		$N_{\odot,r} = N_{\odot} - N_s$ (Si = 10 ⁶)
		$\sigma \pm \Delta\sigma$ (mb)	(%)	s-only nuclei (mb, Si = 10 ⁶)	main component (mb, Si = 10 ⁶)	all components (mb, Si = 10 ⁶)	r-only nuclei (Si = 10 ⁶)	
110	Cd	289 ± 34	7.0	53.5 ± 7.2	49.2	51.4	0.164 ± 0.013 (110Pd)	0.162 ± 0.014
111	Cd	1214 ± 143		49.0	51.2			0.184 ± 0.037
112	Cd	254 ± 34		48.3	50.4			0.134 ± 0.014
113	Cd	831 ± 91		48.1	50.1			0.170 ± 0.056
114	Cd	171 ± 29		47.1	49.0			0.119 ± 0.013
115	In	849 ± 85.0		46.9	48.7			
116	Sn	114 ± 22	2.6	62.9 ± 13.3	45.5	47.0	0.119 ± 0.008 (116Cd)	
117	Sn	459 ± 88		45.1	46.6			0.194 ± 0.034
118	Sn	72.0 ± 13.7		42.9	44.2			0.315 ± 0.145
119	Sn	282 ± 54		42.4	43.6			0.175 ± 0.043
120	Sn	44.5 ± 8.0		39.1	40.0			0.341 ± 0.199
121	Sb	845 ± 114		39.0	39.8			0.155 ± 0.037
122	Te	337 ± 69	3.6	40.0 ± 9.4	38.5	39.4	0.174 ± 0.016 (122Sn)	
123	Te	939 ± 57		41.3 ± 5.6	38.4	39.2	0.150 ± 0.027 (123Sb)	
124	Te	185 ± 24	2.0	41.0 ± 7.2	37.6	38.4	0.215 ± 0.020 (124Sn)	
125	Te	507 ± 50		37.4	38.1			0.269 ± 0.042
126	Te	91.4 ± 13.7		35.9	36.6			0.518 ± 0.126
127	I	725 ± 34		35.7	36.4			0.850 ± 0.189
128	Xe	284 ± 67		35.3	35.9			
129	Xe	537 ± 127		35.0	35.6			1.314 ± 0.277
130	Xe	175 ± 48		37.9 ± 12.9	34.3	34.9	1.690 ± 0.203 (120Te)	0.995 ± 0.218
131	Xe	397 ± 99		34.0	34.5			0.829 ± 0.268
132	Xe	65.7 ± 4.3		32.2	32.7			0.316 ± 0.023
133	Cs	581 ± 24		31.9	32.3			0.482 ± 0.097 (134Xe)
134	Ba	252 ± 40	4.2	27.0 ± 4.5	31.0	31.4		0.242 ± 0.017
135	Ba	522 ± 90		30.7	31.1			
136	Ba	78.8 ± 11.4	1.3	28.2 ± 4.3	29.9	30.3	0.391 ± 0.078 (136Xe)	28.6
137	Ba	65.1 ± 11.4						0.074 ± 0.082

138	Ba	4.4 ± 0.3	15.5 \pm 1.6	15.4	15.6	<0.29
139	La	42.5 ± 3.0		14.2	14.3	0.111 ± 0.035
140	Ce	12.3 ± 0.6		10.9	11.0	0.131 ± 0.075
141	Pr	136 ± 17		10.6	10.8	0.095 ± 0.016
142	Nd	51.7 ± 4.3	9.3	10.7 \pm 1.2	9.92	10.0
143	Nd	273 ± 10		9.79	9.91	$0.129 \pm 0.007\ (^{142}\text{Ce})$
144	Nd	123 ± 6.3		9.51	9.63	0.121 ± 0.015
145	Nd	554 ± 114		9.45	9.56	0.0521 ± 0.0060
146	Nd	179 ± 46		9.26	9.37	0.092 ± 0.017
147	Sm	1448 ± 114		2.65	2.77	0.0331 ± 0.0030
148	Sm	300 ± 13	1.1	9.0 \pm 0.8	9.12	$0.0477 \pm 0.0033\ (^{148}\text{Nd})$
149	Sm	1638 ± 66		9.10	9.21	0.0316 ± 0.0028
150	Sm	504 ± 25	1.7	9.8 \pm 0.9	9.03	$0.0468 \pm 0.0033\ (^{150}\text{Nd})$
151	Sm	2207		8.49	8.59	
151	Eu	4988 ± 200		0.53	0.54	0.0426 ± 0.0038
152	Sm	451 ± 25		8.44	8.55	0.0523 ± 0.0054
152	Gd	1125 ± 70	33.0	0.50 ± 0.04	0.50	0.51
153	Eu	3620 ± 362		8.54	8.65	
153	Gd	3152		0.40	0.41	0.0481 ± 0.0042
154	Gd	1503 ± 116	5.0	9.9 \pm 0.9	8.92	$0.0605 \pm 0.0045\ (^{154}\text{Sm})$
155	Gd	3198 ± 320		8.91	9.02	0.0462 ± 0.0023
156	Gd	730 ± 73		8.86	8.98	0.0559 ± 0.0035
157	Gd	1757 ± 176		8.84	8.96	0.0469 ± 0.0025
158	Gd	244 ± 22		8.71	8.83	0.0460 ± 0.0052
159	Tb	2056 ± 114		8.70	8.81	0.0546 ± 0.0071
160	Dy	941 ± 41	2.4	8.7 ± 0.5	8.66	$0.0722 \pm 0.0034\ (^{160}\text{Gd})$
161	Dy	2461 ± 74		8.65	8.78	
162	Dy	540 ± 57		8.59	8.77	0.0746 ± 0.0035
163	Dy	1294 ± 44		2.85	2.97	0.0888 ± 0.0050
163	Ho	2937		5.72	5.83	0.0982 ± 0.0005
164	Dy	306 ± 24		5.44	5.56	0.0977 ± 0.0056
164	Er	846 ± 69	9.0	3.34 ± 0.31	3.05	3.16
165	Ho	1505 ± 75		8.47	8.58	
166	Er	694 ± 70		8.42	8.54	0.0722 ± 0.0041
167	Er	1757 ± 176		8.40	8.52	0.0530 ± 0.0027
168	Er	417 ± 50		8.33	8.45	0.0483 ± 0.0040

Table 4. (continued)

Mass number	Element	$\sigma \pm \Delta\sigma$ (mb)	p-correction to s-only abundance (%)		σN_{\odot} s-only nuclei (mb, Si = 10 ⁶)		main component (mb, Si = 10 ⁶)	all components (mb, Si = 10 ⁶)	$N_{\odot,r}$ r-only nuclei (Si = 10 ⁶)	$N_r = N_{\odot} - N_s$ (Si = 10 ⁶)
			σN_s	σN_s	σN_{\odot} s-only nuclei (mb, Si = 10 ⁶)	σN_{\odot} s-only nuclei (mb, Si = 10 ⁶)				
169	Er	696			0.17	0.28				
169	Tm	1289 ± 64			8.14	8.26				0.0320 ± 0.0025
170	Er	255 ± 38			0.17	0.28				
170	Tm	2581			2.80	2.81				
170	Yb	876 ± 27	4.3	6.61 ± 0.31	5.28	5.39				0.0376 ± 0.0017 (¹⁷⁰ Er)
171	Tm	1125			2.37	2.48				
171	Yb	1618 ± 59			5.82	5.94				
172	Yb	468 ± 39			8.12	8.24				
173	Yb	988 ± 82			8.09	8.21				
174	Yb	201 ± 18			7.95	8.07				
175	Lu	1364 ± 47			7.92	8.04				
176	Lu	1755 ± 68			3.50	3.55				
176	Hf	545 ± 24			4.39	4.46				
177	Hf	1560 ± 70			7.87	7.99				0.0241 ± 0.0020
178	Hf	371 ± 12			7.80	7.91				0.0215 ± 0.0030
179	Hf	1166 ± 35			7.77	7.89				0.0146 ± 0.0015
180	Hf	219 ± 6.2			7.64	7.76				0.0197 ± 0.0040
181	Ta	828 ± 46			7.61	7.72				0.0133 ± 0.0023
182	W	313 ± 9.0			7.52	7.64				0.0116 ± 0.0029
183	W	568 ± 17			7.47	7.59				0.0067 ± 0.0016
184	W	256 ± 8.0			7.37	7.48				0.0128 ± 0.0034
185	W	907			1.24	1.26				
185	Re	1749 ± 228			6.11	6.21				
186	W	201 ± 6.0			1.57	1.57				
186	Os	482 ± 18	1.1	5.48 ± 0.58	5.57	5.66				
187	Re	1793 ± 114			1.75	1.77				0.0333 ± 0.0041 (¹⁸⁷ Re)
187	Os	1013 ± 32			5.51	5.61				
188	Os	456 ± 17			7.20	7.32				0.0793 ± 0.0094
189	Os	1754 ± 53			7.19	7.30				0.1108 ± 0.0113

190	Os	337 ± 51	7.11	7.22	0.1676 ± 0.0188
191	Os	1245	0.23	0.23	
191	Ir	1536 ± 77	6.86	6.98	0.2413 ± 0.0155
192	Os	355 ± 51	0.40	0.40	
192	Ir	3837	2.53	2.57	
192	Pt	443 ± 150	4.12	4.19	
193	Ir	988 ± 49	3.27	3.29	$0.4084 \pm 0.0261 (^{193}\text{Ir})$
193	Pt	1738	3.74	3.81	
194	Pt	358	6.96	7.08	0.4312 ± 0.0451
195	Pt	1212	6.94	7.06	0.4572 ± 0.0463
196	Pt	200 ± 19	6.82	6.93	0.3123 ± 0.0349
197	Au	665 ± 10	6.78	6.89	0.1756 ± 0.0279
198	Hg	193 ± 17	6.65	6.77	$0.0986 \pm 0.0099 (^{198}\text{Pt})$
199	Hg	431 ± 27	6.59	6.71	0.0434 ± 0.0056
200	Hg	127 ± 13	6.41	6.53	0.0298 ± 0.0094
201	Hg	325 ± 17	6.34	6.45	0.0265 ± 0.0045
202	Hg	78.1 ± 6.3	6.05	6.17	0.0256 ± 0.0120
203	Tl	142 ± 9.1	5.80	5.91	0.0115 ± 0.0059
204	Pb	99.1 ± 6.1	5.50	5.61	$0.0204 \pm 0.0023 (^{204}\text{Hg})$
205	Tl	61.7 ± 4.6	3.66	3.71	0.0412 ± 0.0146
205	Pb	61.7 ± 13.7	1.71	1.76	
206	Pb	15.4 ± 0.8	4.58	5.02	0.2233 ± 0.0434
207	Pb	12.7 ± 0.8	3.55	3.98	0.2890 ± 0.0471
208	Pb	0.46 ± 0.04	0.40	0.73	0.1184 ± 0.1672
209	Bi	12.4 ± 1.23	0.31	0.63	0.0930 ± 0.0127

but are extrapolated to $kT = 23$ keV according to the s-process temperature derived from branching analyses; in a few significant cases, the cross sections were also corrected for stellar enhancement factors. Branchings are considered only if they are strong enough to stand out on figure 19; the weaker branchings do not affect the abundances significantly, but can be important for estimating neutron density and temperature (see for example the branchings at $A = 147,148$ and at ^{134}Cs , ^{154}Eu , (§ 5.2.1)). The branchings connected with the s-only isotopes ^{176}Lu , ^{176}Hf and ^{187}Os are complicated by long-lived radioactive decays. These decays are potential chronometers for the age of the s-process elements and will be discussed in some detail in § 7.

The weak and strong s-process components can alternatively be assumed to result from single neutron exposures. Such an assumption allows for a better reproduction of the s-only isotopes ^{70}Ge and ^{76}Se (Beer 1986, 1988, Beer and Macklin 1989); this is illustrated in table 4, where numerical σN_s -values for a single flux solution of the weak component are given in brackets in column 7. For possible stellar scenarios see § 6.

4.2. Neutron economy

The main difference between the σN_s curves in figure 19 comes from the revision of the rare-earth abundances by Anders and Ebihara (1982), giving rise to a much less pronounced step in the new σN_s curve at the magic neutron number 82. This corresponds to an increase of the mean neutron exposure, τ_0 , and to a decrease of the required seed abundance, f . A comparison with the results for the 1982 curve (Käppeler *et al* 1982; Almeida and Käppeler 1983) is given in table 5.

Given the perfect agreement between the empirical σN_s -values and the calculated curve, one can be rather confident about the present s-process abundances. This statement is additionally supported by the smoothness of the related r-process abun-

Table 5. Comparison of mean neutron exposure, τ_0 , and fractional seed abundance, f , with values based on abundance compilations prior to Anders and Ebihara (1982). For a discussion of the neutron balance condition for the $^{22}\text{Ne}(\alpha, n)$ source see the text.

	Käppeler <i>et al</i> (1982)	Present
Mean neutron exposure τ_0 (mb^{-1})		
Main component	0.24 ± 0.01	$(0.30 \pm 0.01) \left(\frac{kT(\text{keV})}{30} \right)^{1/2}$
Weak component	0.056 ± 0.005	$(0.068 \pm 0.007) \left(\frac{kT(\text{keV})}{30} \right)^{1/2}$
Strong component	—	7.0
Seed abundance, f (% of $N_{\odot}(^{56}\text{Fe})$)		
Main component	0.092 ± 0.015	0.043 ± 0.002
Weak component	2.7 ± 0.2	1.6
Strong component	—	1.2×10^{-4}
Total number of neutrons captured per ^{56}Fe seed nucleus, Σn_c (equation (4.1))		
Main component	13.0 ^a	15.1 ± 0.8
Weak component	—	2.8
Strong component	—	141.0

^a Almeida and Käppeler (1983).

dance distribution (§ 4.3). As the number of neutrons, n_c , consumed during the s-process by the various seed nuclei is directly linked to the abundances (equation (2.5)), the values of n_c are equally reliable. This is necessary but not sufficient for a discussion of the neutron balance. Knowledge of the neutron-producing reaction(s) and of the stellar environment is also needed. These conditions are uncertain for the weak and strong components, but are rather well defined for the main component by the model for helium shell burning in intermediate mass stars.

As discussed in § 2.2, there is a detailed model for the main component to be attributed to helium shell burning with the $^{22}\text{Ne}(\alpha, n)^{25}\text{Mg}$ reaction as the neutron source. For that case, no more than 39 neutrons are available per ^{56}Fe nucleus if C, N, O and Fe occur in the standard abundance ratios typical for population I stars. This condition was checked by Almeida and Käppeler (1983) via the neutron balance: number of neutrons produced = number of neutrons captured, i.e.

$$\begin{aligned} q(fN_{\odot}(\text{CNO})) &= \sum n_c(A_{\text{seed}}) + (1-q)n_c(^{22}\text{Ne}) + qn_c(^{25}\text{Mg}) \\ 39.0q &= 13.0 + (1-q)12.2 + 24.7q \end{aligned} \quad (4.1)$$

where q is the fraction of ^{22}Ne that undergoes an (α, n) reaction. On the right-hand side of equation (4.1) one has to consider all possible seeds. As the metallicity is assumed to be that for population I stars, all elements are expected to occur in their solar ratios. This means that the fraction $f = 0.043\%$ (table 5) that was obtained for the seed abundance of ^{56}Fe to reproduce the empirical values can also be used for the lighter elements. Though these do not contribute noticeably in the mass range above ^{56}Fe , they act to some extent as neutron poisons. Therefore, the sum over $n_c(A_{\text{seed}})$ in equation (4.1) runs from $A = 20$ to 56 . Extra terms are required for the abundant species ^{22}Ne and ^{25}Mg which take part in the (α, n) reaction and which therefore depend on q . The numbers in equation (4.1) follow from the s-process abundances derived from the σN_s curve of Käppeler *et al* (1982), yielding $q = 0.95$. The remaining 5% of ^{22}Ne were attributed to the competing (α, γ) reaction. As the reaction rate ratio $\lambda(\alpha, n)/\lambda(\alpha, \gamma)$ depends strongly on temperature, the result of the neutron balance condition could be used to estimate a lower limit of 3.3×10^8 K for the s-process temperature.

However, this nicely consistent picture no longer holds (Käppeler 1986b). With the larger τ_0 values of the revised σN_s curve, the number of neutrons captured per ^{56}Fe seed nucleus increased by $\sim 30\%$, which changes the neutron balance equation into

$$39.0q = 18.0 + (1-q)16.7 + 29.7q$$

leading to the physically unreasonable solution $q > 1$. The above neutron balance is based on the abundance compilation of Anders and Ebihara (1982); it also depends sensitively on the neutron capture rates of ^{22}Ne and ^{25}Mg . Even if these data were modified within the quoted uncertainties, however, one would still be left with $q > 1$. This result implies that the s-process during helium shell burning requires the C, N and O abundances to be enriched by about 40% relative to ^{56}Fe in order to re-establish $q = 0.95$, consistent with the prevailing temperature. In fact, an enrichment in C and O may result naturally from the helium burning zone itself: according to § 2.2, a fraction $r \sim 0.4$ of the material exposed to helium burning is mixed to the envelope after each pulse episode, thus adding freshly produced carbon and oxygen to the CNO cycle, which burns hydrogen during the quiescent interpulse phases. This feeding of the C and O abundances might explain the extra supply of s-process neutrons. A quantitative

treatment may ultimately tell something about the mixing mechanism between the helium shell and envelope, provided that the $^{22}\text{Ne}(\alpha, n)^{25}\text{Mg}$ reaction is the only neutron source for the main s-process component.

The neutron balance argument does not apply for scenarios with $^{13}\text{C}(\alpha, n)^{16}\text{O}$ as the main neutron-producing reaction, e.g. in low mass stars (Gallino *et al* 1988). In that case, the number of neutrons is determined by the number of protons mixed into the helium zone to yield ^{13}C , and therefore no longer correlated to the seed abundances.

4.3. r-process residuals

The improved s-process abundances from the updated σN_s curve can be used for a revision of the r-process residuals $N_r = N_\odot - N_s$. The resulting differences between solar and s-process abundances are plotted in figure 20 together with the ensemble of r-only isotopes. The refined s-process treatment and the more accurate solar abundances allow calculation of the uncertainties for the r-process residuals thus derived. These are reasonably small except near magic neutron numbers where large s-process abundances occur as a consequence of the small capture cross sections. These r-abundances are included in table 4. Some of the quoted r-only nuclei are corrected for minor s-process contributions if these did not exceed $\sim 5\%$.

First of all, it is most remarkable that the agreement between the calculated distribution of r-process yields and the r-only isotopes became considerably better with the improved s-process analysis, if compared with a previous study (Käppeler *et al* 1982). This convincingly supports the s-process abundances obtained with the classical

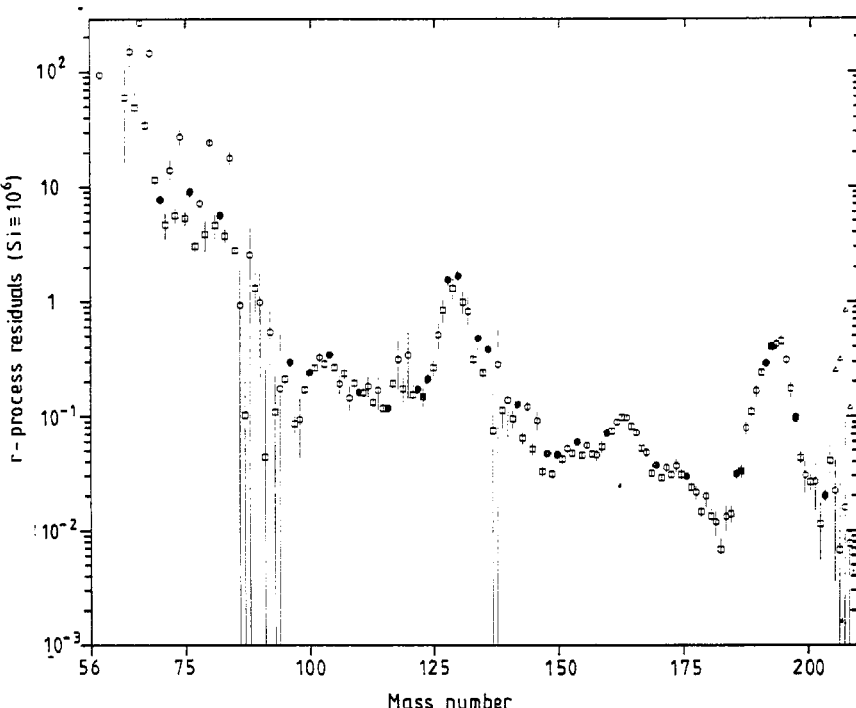


Figure 20. r-Process yields: the distribution of r-only isotopes (full points) and the abundances obtained by subtraction of s-process abundances from solar values (open symbols).

model, because it means that two independent pieces of information are perfectly matching. It also ensures that figure 20 represents the best information on the actual r-process abundances, and hence can be recommended as a reliable basis for model calculations of the r-process.

In particular, one finds that the abundance maxima around $A = 130$ and 195 appear well defined. They indicate those mass numbers where the r-process path reached the magic neutron shells $N = 82$ and 126 . Their position and shape are important to identify the 'waiting points' during the r-process. With this information and with the recently measured beta decay rates of some key isotopes, Kratz *et al* (1988) were able to show that (n, γ) - (γ, n) equilibrium was achieved during the r-process. The r-process abundance peak related to the magic neutron number 50 could be studied for the first time by the explicit treatment of the s-process branchings at $A = 79$ and 85 (Walter *et al* 1986a, b; § 5). It is not as outstanding as the other two and appears as a sharp step in the abundance distribution rather than as a peak. This could indicate that abundance contributions from other processes might have to be considered up to mass 80 . Currently, the related uncertainties are still too large for any definite conclusions. In this context, it is interesting to note the outstanding abundances at $A = 74$, 80 and 84 . A possible explanation via strong feeding of the respective r-process decay chains by beta-delayed neutron emission (Kratz *et al* 1988) appears doubtful, as the neighbouring abundances do not seem to be very depleted.

At the end of the distribution, the need for a strong s-process component becomes evident. The triangles at $A = 206$, 207 , 208 and 209 would be obtained, if the main component only were subtracted from the solar values; but by inclusion of the strong component one obtains the smooth r-process yields compatible with the general phenomenology and with the abundances of the long-lived actinides (Beer and Macklin 1985). The reduction of the lead abundance suggested by solar spectroscopy (Grevesse and Meyer 1985) would eliminate the need for a strong component (Ratzen *et al* 1989); however, a recent spectroscopic study (Youssef and Khalil 1989) confirmed the meteoritic lead abundance (Anders and Grevesse 1989), leaving the ^{208}Pb problem unsolved.

The distribution of figure 20 exhibits the smoothness expected for the r-process yields. Any initial abundance fluctuations due to odd-even effects in the beta decay rates on the r-process path are effectively smeared out due to beta-delayed neutron emission in the decay chains to the stability valley. Within uncertainties, there are no deviations from a smooth distribution, though some indications for an odd-even effect exist in the mass range $145 < A < 180$. The only significant deviation from the smooth distribution occurs at the tin isotopes 117 , 118 , 119 and 120 . In this case, one might suspect that the tin abundance of Anders and Ebihara (1982) is too high by 23%. This suspicion is based on the fact that the r-process abundances become smoothly distributed if the tin abundance is normalised by the σN -value of s-only ^{116}Sn (Beer *et al* 1989b).

5. s-process branchings

5.1. General discussion

As shown in §§ 2.1 and 3.3, s-process branchings can be analysed to yield estimates for neutron density and temperature during the s-process. The branching factor f_β

(equation (2.8)) can be expressed by the rates for neutron capture and beta decay

$$\lambda_n = n_n \sigma v_T \quad \text{and} \quad \lambda_\beta = \ln 2 / t_{1/2}(T) \quad (5.1)$$

of the branching point isotope. On the other hand, f_β can be derived from the classical model as outlined in § 2.1 by comparison of the empirical σN -value of the involved s-only isotope with the smooth $\sigma N(A)$ curve.

If the beta decay rate of the branching point isotope is known, equation (2.8) yields the stellar neutron capture rate and ultimately the neutron density during the s-process via equation (5.1). However, the beta decay rates of some of the branching point isotopes are affected by temperature as discussed in § 3.3. This means that all possible branchings need to be investigated systematically, starting with those cases which allow for an estimate of the neutron density. In a second step, this information can be used to derive the effective beta decay rates from the temperature-dependent branchings. With the tabulated temperature dependence of the relevant s-process isotopes of Takahashi and Yokoi (1987), these branchings can be interpreted as thermometers to estimate the s-process temperature.

The branching analyses represent an important test for the validity of the classical model. If the solutions for neutron density and temperature derived from as many branchings as possible are found to be consistent with each other, then the s-process was indeed smooth enough to justify the simple assumption of constant neutron density; otherwise, the abundance patterns of the various branchings should be determined by freeze-out effects, leading to inconsistent results in the classical approach. This would be important information in itself, and would allow the study of s-process dynamics.

Two classes of branchings can be distinguished: those which are characterised by a single s-only isotope partially bypassed by the s-process flow, and others where an additional s-only isotope of the same element occurs that experiences the total s-process flow. The advantage of the second class is that the branching factor can be derived via the well known cursive ratio of the s-only isotopes, while in the first case the uncertainty of the respective *elemental* abundance must be considered, which is usually much larger. Therefore, branchings with two s-only isotopes can be analysed more precisely, e.g. those at $A = 79$, $A = 147,148$ and $A = 151$.

As the classical model deals with three components, these have to be investigated separately. There are six to eight branchings that can be used to characterise the main component, but only two for the weak, and possibly two others for the strong component. Consequently, a systematic study has to start with the main component. With the results thus obtained, the contribution of the main component can be corrected in the mass regions $A < 90$ and $A > 205$ to derive the isotopic patterns representative for the weak and strong components. Branchings are not only sensitive to neutron density and temperature (§ 5.2.1), but to electron density and to a possible time dependence of the neutron density as well; these latter aspects will be discussed in §§ 5.2.2 and 5.2.3.

5.2. The physical conditions during the s-process

5.2.1. Neutron density and temperature. The first step in a systematic branching analysis is to investigate the main s-process component in the mass range $100 < A < 200$. By combination of the branchings at ^{151}Sm , ^{170}Yb and ^{185}W , Beer *et al* (1984) determined limits for neutron density and temperature characteristics of the main s-process component, as indicated by the full outline in figure 21. (In the following text, thermal energies, kT , are always given in keV, and temperatures, T_8 , in units of 10^8 K; conversion

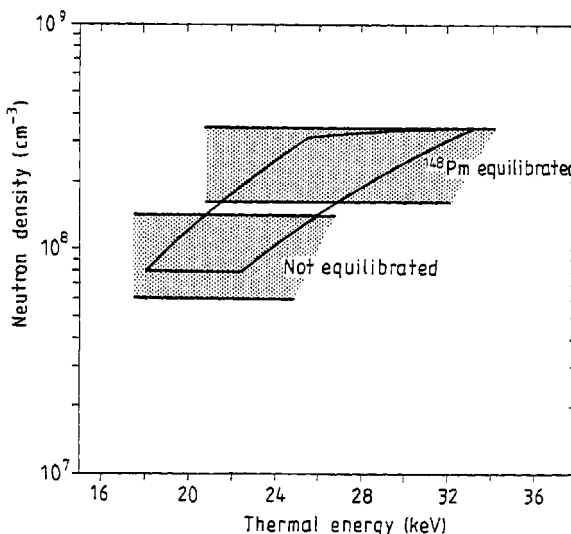


Figure 21. Allowed regions of neutron density and thermal energy for the main s-process component as obtained from analyses of various branchings. Note the ambiguity due to the problem of thermal equilibration in ^{148}Pm . —, Beer *et al* (1984); shaded areas, Winters *et al* (1986a).

between these quantities is provided by the relation $kT = 8.62 T_8$.) The allowed region in the neutron density–temperature plot of figure 21 could be reduced by inclusion of the branchings at $A = 147$ and 148 (Winters *et al* 1986a). However, the influence of temperature is ambiguous in this case, depending on whether the ground state and the 137 keV isomer in ^{148}Pm —which are about equally populated by neutron capture in ^{147}Pm —are thermally equilibrated on the beta decay timescale of a few days. This was a longstanding question, because the level scheme of ^{148}Pm was almost unknown: beside the ground state (5.4 d) and the isomer (41 d) only one additional level is reported at 76 keV. As direct transitions between the isomer and the other two states are too slow, equilibrium could only be achieved via mediating states at higher excitation. Such states are now reported by Lesko *et al* (1989), so that the high-temperature–high-neutron-density solution of figure 21 is confirmed.

In principle, the branchings at ^{134}Cs and ^{154}Eu could be used to derive additional lower limits for the s-process temperature. The beta-decay rates of these branch point nuclei and hence the branching factors depend strongly on temperature. This is shown in figure 22 (Käppeler 1988), where the shaded bands are calculated using two values for the neutron density (1.0×10^8 and $2.5 \times 10^8 \text{ cm}^{-3}$). Given the present cross section uncertainties, there is no evidence for an effective branching, neither for ^{134}Cs nor for ^{154}Eu ; instead, the related uncertainties can be used for estimating a lower limit for the respective branching ratios. In the case of ^{134}Cs only the 15% uncertainty of the cross-section ratio $\sigma(^{134}\text{Ba})/\sigma(^{136}\text{Ba})$ must be considered, but for ^{154}Eu the uncertainties of the cross section, the abundance and the σN curve (8, 5 and 10%) contribute. The upper limits for the branching factor thus obtained (indicated in figure 22) are not yet stringent enough to allow for a conclusion on the ^{148}Pm ambiguity, but seem to support the possibility of complete equilibration. If the allowed region in figure 21 can be further restricted by refined branching analyses, this would have consequences for the s-process neutron source: a low temperature would favour the $^{13}\text{C}(\alpha, n)^{16}\text{O}$ reaction, whereas the $^{22}\text{Ne}(\alpha, n)^{25}\text{Mg}$ reaction requires higher temperatures to operate.

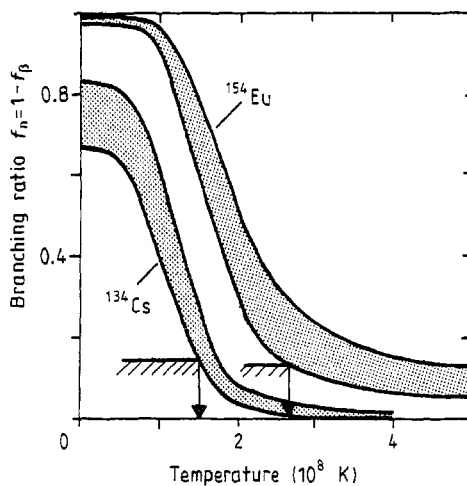


Figure 22. The branching factors of ¹³⁴Cs and ¹⁵⁴Eu plotted against temperature. Though no effective branchings are evident from s-process analyses, the respective uncertainties (shaded bars) are used to estimate lower limits for the s-process temperature.

Further efforts to identify the neutron source of the s-process should therefore concentrate on improving the stellar neutron capture and beta decay rates for the relevant isotopes in the various branchings, including

- (i) a confirmation of the level scheme of ¹⁴⁸Pm;
- (ii) measurements of the capture cross sections of the s-only nuclei to 1-2% accuracy to reliably define the branching factors;
- (iii) measurements of the capture cross sections of the unstable branching point isotopes as proposed by Bowman and Talbert (1985);
- (iv) more precise estimates for the log *ft* values of excited states.

Weak component. The two branchings to characterise the weak s-process component are those at ⁷⁹Se and ⁸⁵Kr. Figure 2 shows the s-process path in the mass region $75 < A < 90$ with the terrestrial half-lives indicated at the branch points. The fact that both branching ratios are about equal (Walter *et al* 1986a, b) implies that the beta decay rate of ⁷⁹Se must be greatly enhanced at s-process temperatures. As was shown in § 3.3, the temperature dependence of the ⁷⁹Se half-life is now well described by the experimental log *ft* value (Klay and Käppeler 1988), hence allowing for a more reliable analysis of the ⁷⁹Se thermometer. Figure 23 (Käppeler 1988) illustrates how the possible region for neutron density and temperature typical for the weak s-process component was reduced with the experimental log *ft* value compared to a previous estimate, the remaining uncertainty being dominated by cross-section uncertainties; an updated version of figure 23 yields slightly higher neutron densities for the weak component (Klay and Käppeler 1988). Note that this analysis is still based on the assumption that the decay of ¹⁴⁸Pm is not affected by temperature; but if the ground state and the isomer in ¹⁴⁸Pm are thermally equilibrated (Lesko *et al* 1989), then the region for the main component centres around $n_n = 2.5 \times 10^8 \text{ cm}^{-3}$ and $kT = 27 \text{ keV}$, while the region for the weak component will move to somewhat lower neutron densities; these results have recently been confirmed and updated (table 6; Toukan and Käppeler 1989, Käppeler *et al* 1989a, b, Beer *et al* 1989c).

Principally, the weak s-process component is difficult to analyse in terms of the classical model because of two problems:

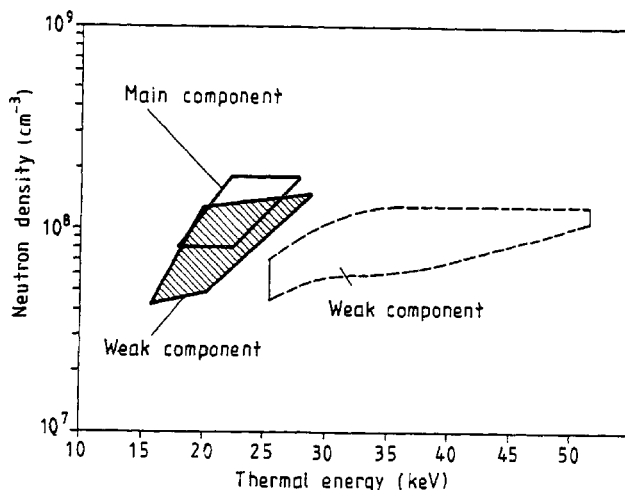


Figure 23. Allowed regions of neutron density and thermal energy for the two s-process components (Käppeler 1988); this analysis was still based on the assumption that the decay of ^{148}Pm was not affected by temperature. The new results of Lesko *et al* (1988) suggest that the region for the main component centres at $2.5 \times 10^8 \text{ cm}^{-3}$ and 27 keV.

(i) The use of an exponential distribution of neutron exposures is not as successful in reproducing the s-only isotopes as it is for the main component. Besides the tendency for underproducing ^{70}Ge and ^{76}Se , there is also a tendency for overproduction of the light Zr isotopes. Therefore, a single exposure solution was suggested (Beer 1986, Beer and Macklin 1989), which accounts for the observed abundances in the mass range $A > 65$ (see table 4).

(ii) The contribution of the weak component to the branchings at ^{79}Se and ^{85}Kr depends significantly on the type of the adopted neutron exposure. Analysis of these branchings is more complicated than outlined above, because the contributions from the main component depend critically on whether and how the main component is characterised by a pulsed s-process (see § 5.2.3). At present, the only conclusion can be the need to improve the input data for these analyses to better identify the possible deficiencies of the classical model.

Strong component. At the end of the s-process chain, the α -unstable isotopes $^{210,211}\text{Po}$ and ^{211}Bi cause a recycling of the neutron capture flow to $^{206,207}\text{Pb}$ as illustrated in figure 24. The analytic treatment (Clayton and Rassbach 1967, Ward and Clayton 1982, Beer and Macklin 1985) shows that this recycling is possibly influenced by two branchings, which depend strongly on the physical conditions. For the temperature and neutron-density regimes typical for the main and weak components, one finds that the α -decay of ^{210}Po dominates, and that the branchings at ^{210}Bi and ^{210}Po are almost negligible: the small capture rate of neutron-magic ^{210}Po prevents a significant production of ^{211}Po at neutron densities below $3 \times 10^9 \text{ cm}^{-3}$. Similarly, the production of ^{211}Bi is hampered because the long-lived isomer ^{210m}Bi is quickly destroyed in the stellar photon bath at temperatures higher than about $1.5 \times 10^8 \text{ K}$.

Whether the strong component took place under such conditions as to make these branchings efficient may possibly be deduced from the observed abundance ratio $^{206}\text{Pb}/^{207}\text{Pb}$. If the branchings were not significant, the only decay is that of ^{210}Po , leading to ^{206}Pb ; otherwise the decays from ^{211}Po and/or ^{211}Bi are feeding the ^{207}Pb abundance. A determination of the s-process abundances of $^{206,207}\text{Pb}$ is complicated,

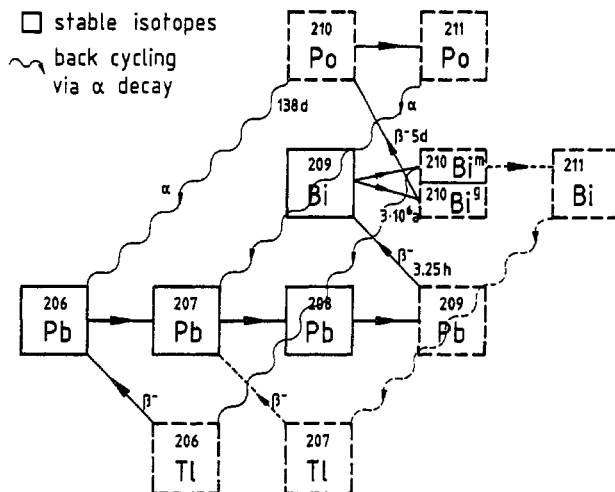


Figure 24. The s-process flow at the end of the neutron capture chain. Various possibilities for α recycling to $^{206,207}\text{Pb}$ are indicated, but are difficult to identify because of the different r-process contributions involved. For details see text.

however, because their separation from the respective r-process contributions has to consider not only the normal r-process yields, but also the radiogenic component from the decay of various trans-bismuth progenitors and of $^{235,238}\text{U}$. At present, this separation is still too uncertain (see error bars in figure 20 for $A > 205$) for any conclusion on the possible branchings characteristic for the strong component.

In a recent study of the s-process in the lead-bismuth region, Ratzel *et al* (1989) noted that the lower lead abundance from the solar photosphere (Grevesse and Meyer 1985) would question the need for a strong component; however, this possibility is superseded by the measurement of Youssef and Khalil (1989). In this context it would be important to reconsider the radiogenic ^{207}Pb lead abundance as a chronometer for the r-process as well as the question of whether the decay of ^{204}Tl was thermally enhanced as assumed previously, or whether spins and parities of the low-lying states were such as to make ^{204}Tl an effective branching point. This would be a necessary condition in order to reconcile a lower lead abundance with the $\sigma N(A)$ systematics of s-only ^{204}Pb .

5.2.2. Mass density. For the identification of the stellar s-process site the mass density is an important parameter. As described in § 3.2.3, the electron capture rates in the highly ionised stellar plasma are dominated by capture of continuum electrons, and hence depend on the electron density. The electron-to-baryon ratio being almost exactly 0.5 allows determination of the mass density, if a branching can be identified that is characterised by such a density-dependent electron capture rate. Yokoi and Takahashi (1981) have pointed out that terrestrially stable ^{163}Dy becomes unstable at s-process temperatures due to bound-state decays to ^{163}Ho . This isotope may either capture an electron (which means a decay back to ^{163}Dy) or it may capture a neutron. The latter possibility leads via ^{164}Ho to ^{164}Er , thus explaining the relatively large abundance of this isotope, which does not seem at first glance to belong to the s-process chain. The competition between electron and neutron capture on ^{163}Ho was studied in terms of an s-process branching by Beer *et al* (1985). In order to reproduce the observed ^{164}Er abundance (corrected for a possible p-process contribution, see table 4) these authors

derived an estimate for the electron density via the strong dependence of the half-lives of ^{163}Dy , ^{163}Ho and ^{164}Ho on that quantity (Takahashi and Yokoi 1987); the neutron density and temperature in this analysis were as inferred from the other branchings (§ 5.2.1). The result for the electron density, $0.8 \times 10^{27} < n_e < 4 \times 10^{27} \text{ cm}^{-3}$ is equivalent to mass densities between 2600 and 13 000 g cm^{-3} for the s-process site, in reasonable agreement with stellar models for helium shell burning in intermediate mass stars (Iben and Renzini 1983).

5.2.3. Limits for pulsed s-process scenarios. Stellar s-process scenarios based on helium shell burning in intermediate mass stars (§ 2.2) imply a pulsed s-process with pulses of a few years followed by quiescent intervals of several hundred years. According to Ward and Newman (1978) such a sequence should have affected some of the observed branchings. The unstable branch point isotope can decay during the interpulse period and has to build up again in the subsequent pulse before the neutron-deficient branch becomes operative. The criterion for whether a branching is sensitive to a pulsed s-process is that the total lifetime, $\tau = (\lambda_n + \lambda_\beta)^{-1}$, of the branch point isotope should be shorter than or comparable to the pulse duration, Δt . For $\Delta t \ll \tau$ the branching does not exist at all, whereas $\Delta t \gg \tau$ means that the pulsed s-process approaches the classical steady-state solution.

Of all observed branchings, the case of ^{151}Sm is best suited for deriving a lower limit of the pulse duration (Beer 1986, Beer and Macklin 1988). Under the physical conditions derived in the previous section, the lifetime of this branch point is determined by the neutron capture rate (via its large capture cross section). This means that the ^{151}Sm abundance is quickly rebuilt to its equilibrium value at the beginning of each pulse. In addition, this branching is well defined by the two s-only nuclei $^{152,154}\text{Gd}$. Figure 25 shows how the σN_s -values of the isotopes involved in that branching depend on the pulse duration Δt . The calculation assumes the interpulse periods to be long enough so that all the unstable ^{151}Sm and ^{153}Gd decays completely. Then one finds

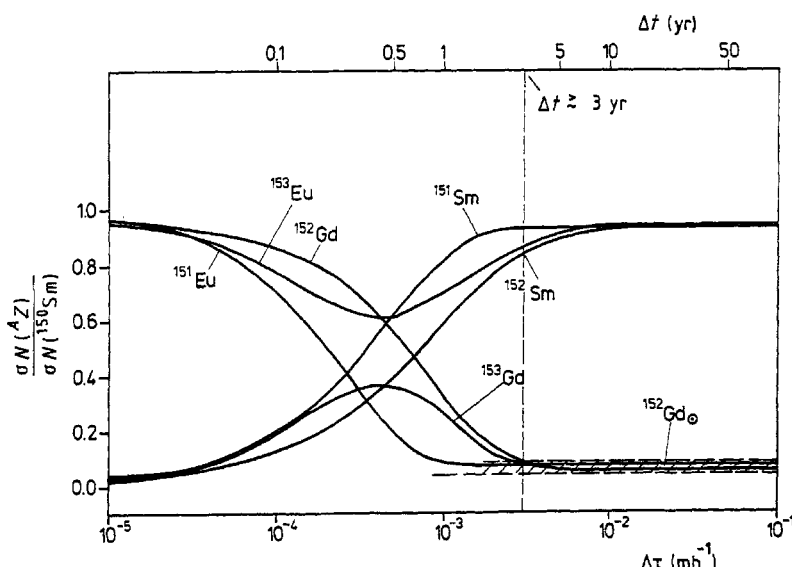


Figure 25. The σN_s -values of the isotopes in the ^{151}Sm branching as a function of the pulse duration during the s-process. The empirical value for the s-only isotope ^{152}Gd (hatched area) is reproduced for $\Delta t > 3 \text{ yr}$.

that the empirical σN_s -values of $^{152,154}\text{Gd}$ are correctly reproduced only if the pulse duration is longer than about 3 yr.

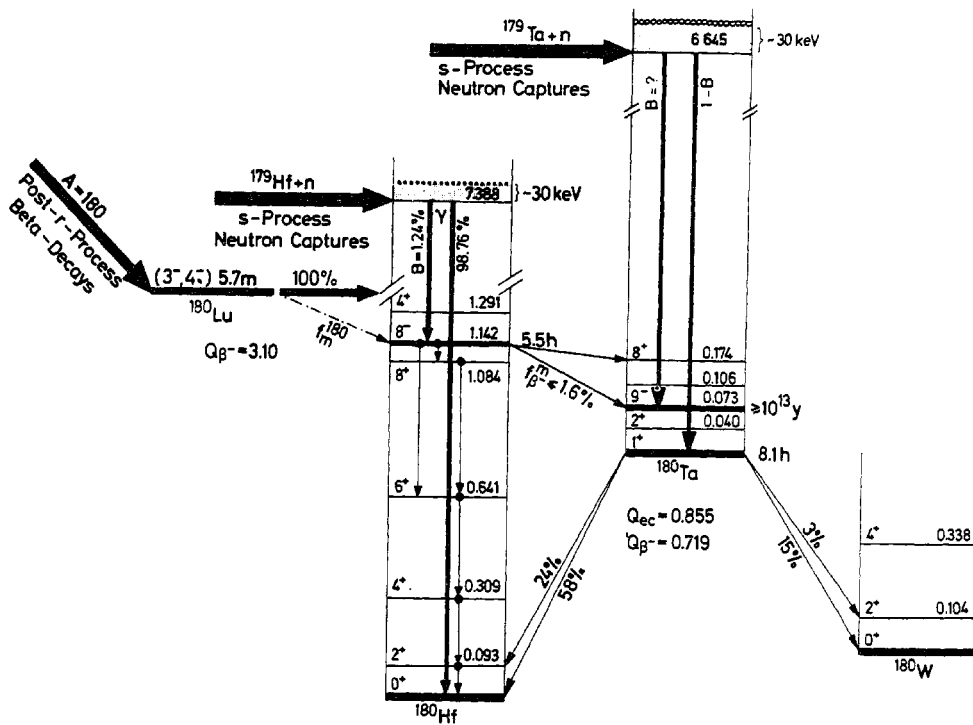
A similar study of the ^{85}Kr branching points to an upper limit for Δt of $\sim 10\text{--}15$ yr, because longer pulses would tend to cause an overproduction of ^{86}Kr (Beer and Macklin 1989). The difficulty of this analysis comes from the fact that the contribution of the weak component to the abundance pattern of the ^{85}Kr branching is strongly model-dependent, and that there is no reliable way to deduce the respective parameters, except via the branchings at ^{79}Se and ^{85}Kr as well. The situation in the mass region $A < 90$ therefore appears ambiguous. Another obvious branching for a test of the maximum pulse length is not in sight. The delicate balance between the influence of neutron density, temperature and pulse duration requires, however, significant improvements on the relevant input data for these branching analyses; otherwise, it will not be possible to separate true effects from ambiguities in the model or in the input values.

5.3. Branchings to rare nuclei: the case of ^{180}Ta

Isomeric states often play an important role in s-process branchings. This was demonstrated in §§ 3.3 and 5.2 for the examples ^{79m}Se , ^{147m}Pm and ^{210m}Bi , and in more detail by Ward (1977), Ward and Fowler (1980) and Beer and Käppeler (1982). A particularly interesting case is the problem of the ^{180}Ta abundance, which has received considerable attention during the past decade. The abundance of nature's rarest stable isotope ^{180}Ta does not fit into the general s-, r- and p-process systematics. There seem to be several competing possibilities to produce ^{180}Ta , all of which pose exciting questions for nuclear astrophysics. The various production mechanisms for ^{180}Ta are indicated in figure 26 by the heavy arrows. Following the normal s-process capture chain in the hafnium isotopes, Beer and Ward (1981) proposed a branching in the decay of ^{180}Hf to be responsible for the observed ^{180}Ta abundance. Beer and Macklin (1982) showed that under s-process conditions 1.24% of all neutron captures in ^{179}Hf populate the high-spin isomer in ^{180}Hf , which can beta decay by an allowed transition to the long-lived isomer in ^{180}Ta . With plausible estimates for the $\log ft$ value of that transition, it appeared as if all the ^{180}Ta could have been made in this way. Meanwhile, there exist two measurements of this $\log ft$ value (Barden 1985, Rauch 1987), which set a limit of 1.6% for this beta decay branch, thus restricting that particular s-process contribution to 22% of the observed ^{180}Ta abundance.

A second possibility for populating the high-spin isomer in ^{180}Hf was r-process beta decays in the $A = 180$ mass chain. If the beta decay of ^{180}Lu feeds into this isomer, then the ^{180}Ta production could have occurred in this way as well. Eschner *et al* (1984) reported a branching factor of 0.46% for this decay, in contradiction to another experiment (Kellogg and Norman 1986), which yielded $0.005 \pm 0.018\%$, compatible with zero. This discrepancy seemed to indicate the existence of an additional isomer in ^{180}Lu with a half-life of less than 300 s, which would have been detected only in the experiment of Eschner *et al* (1984). However, the existence of such an isomer can now be excluded, since neither Lesko *et al* (1986) nor Runte *et al* (1987) succeeded in finding gamma transitions related to this hypothetical isomer. Therefore, any r-process contribution to the ^{180}Ta abundance seems to be at least questionable.

An alternative route to ^{180}Ta has been proposed by Yokoi and Takahashi (1983), who found that ^{179}Hf becomes unstable under s-process conditions against beta decay from excited states. Accordingly, a finite $^{179}\text{Hf}/^{179}\text{Ta}$ ratio will develop during the s-process, which means that ^{180}Ta is now produced directly by neutron captures in



technetium lines in the spectra of certain S stars (Merrill 1952). As there are no stable Tc isotopes, and as the longest Tc half-life is much shorter than the age of red giants, this was direct evidence for ongoing s-processing in the interior of these stars. Various stellar models have been worked out in sufficient detail to allow for quantitative studies (§ 2.2). Comparison with results from the classical model shows, however, that there are still many open problems, and that both approaches have to be further improved to solve the quest for the stellar s-process.

6.1. Stellar models

The three s-process components outlined in § 2.1 may be attributed to various stellar sites. According to Truran and Iben (1977) these are

- (i) massive stars ($>15M_{\odot}$), which were shown to produce most of the abundances in the range $A < 90$ during core helium burning;
- (ii) intermediate mass stars ($2-8M_{\odot}$), which may synthesise the isotopes between $A = 90$ and 204 in their thermally unstable helium burning shell;
- (iii) stars of comparably low mass ($<1M_{\odot}$), which could produce the lead and bismuth abundances in core helium flashes.

This concept is still useful, but requires some modifications outlined below.

6.1.1. Weak component. Helium burning in the cores of massive stars has been identified as a possible s-process site by Peters (1968). Towards the end of core helium burning in stars of $10-25M_{\odot}$, temperatures become sufficiently high that a substantial neutron density can be established via the $^{22}\text{Ne}(\alpha, n)^{25}\text{Mg}$ reaction. Recent calculations (Arnett and Thielemann 1985, Busso and Gallino 1985, Prantzos *et al* 1987, Langer *et al* 1989) with an improved stellar model and with updated nuclear information confirm earlier results (Lamb *et al* 1977) reporting significant s-process production in the mass range $A < 90$. In all these models, ^{58}Fe is produced in similar abundance ratios compared to other s-process nuclei. The respective yields depend on the helium core masses such that in lighter cores ($<4M_{\odot}$) only isotopes near ^{56}Fe are significantly overproduced, while the overproduction is fairly constant in the mass range $60 < A < 80$ for larger helium cores (Arnett and Thielemann 1985). The ^{58}Fe abundance calculated by these models is obviously in contradiction to the results obtained if the weak component is described by a single neutron exposure in the classical s-process (§ 5).

Very massive stars ($M > \sim 50M_{\odot}$) are known to develop strong stellar winds, which efficiently remix the s-processed material into the interstellar medium. In this scenario, all s-only isotopes in the mass region $56 < A < 90$ are well reproduced if the respective contributions from the main component are considered (Prantzos *et al* 1987). The integral neutron dose derived from the stellar model also agrees reasonably well with the mean neutron exposure τ_0 obtained from the classical model. However, the results for neutron density and temperature are somewhat discrepant. The stellar models predict neutron densities around $\sim 10^7 \text{ cm}^{-3}$ and temperatures above $2.5 \times 10^8 \text{ K}$, while the classical model yields $n_n \sim 10^8 \text{ cm}^{-3}$ and somewhat lower temperatures. These problems do not originate from the simplifying assumptions of the classical model, but were identified by Prantzos *et al* (1987) to be the consequence of the abundances in the ^{79}Se branching. On the other hand, it was noted in § 5 that previous estimates of neutron density and temperature for the weak component have to be modified according to the changes for the main component. In addition, due consideration of a pulsed main component also affects the resulting neutron density and temperature

for the weak component. These changes may ultimately lead to better agreement between the classical s-process and the stellar models.

6.1.2. Main component. The first model that was able to predict s-process abundances was that of helium shell burning in intermediate mass stars (Weigert 1966, Schwarzschild and Härm 1967, Iben 1976, Iben and Renzini 1983). The operation of the $^{22}\text{Ne}(\alpha, n)^{25}\text{Mg}$ source in thermally pulsing stars was shown to produce the s-process abundances in the mass range $90 < A < 204$ in solar proportions (Truran and Iben 1977) as well as to be efficient enough to explain the abundance level of s-process nuclei in the galaxy (Iben and Truran 1978). However, it was argued that the high neutron densities associated with the pulsed model may lead to non-solar abundance ratios at s-process branchings (Despain 1980). This problem was quantified by Howard *et al* (1986) in a parametric study of the pulsed model for a range of core masses between $1-1.4 M_{\odot}$. In all these cases, poor fits of the empirical $\langle \sigma \rangle N_s$ values were obtained, because of the extremely rapid decay of the neutron density during the pulses. The resulting average neutron density is much too high to reproduce the branchings properly, even though the effects of this high neutron density are partly smoothed out during captures at the end of the pulse (Cosner *et al* 1980). As an alternative approach, Howard *et al* (1986) investigated a schematic model with pulses of constant neutron density and temperature. With this assumption, they arrived at conclusions very similar to the results of the classical model, e.g. neutron densities around 10^8 cm^{-3} , temperatures of $2.7 \times 10^8 \text{ K}$ and a mean neutron exposure of $\tau_0 = 0.26 \text{ mb}^{-1}$ (§§ 4 and 5).

The conditions typical of the pulsed model are compared to the results of the classical model in table 6, showing that the neutron density is significantly smaller in the latter case. The pulse duration predicted by the stellar model appears to be close to the lower limit derived from the classical approach, but is much shorter than $\Delta t \sim 450 \text{ yr}$ estimated by Howard *et al* (1986) from their schematic model pulses via the relation $\tau_0 = n_n v_T \Delta t$. For the stellar scenario, these 450 yr represent an upper limit, because they correspond to the accumulated exposure from several pulses: as the helium burning shell moves outward, only a fraction $(1-r) = \sim 70\%$ of processed matter is removed from the shell after each pulse (§ 2.2). Reasonably good agreement is obtained for the mean neutron exposure, at least for the core mass of $1.16 M_{\odot}$, for which the predicted $\tau_0 = 0.32 \text{ mb}^{-1}$ is very close to the result of the classical model ($\tau_0 = 0.30 (kT/30)^{1/2} \text{ mb}^{-1}$).

The above problems with the $^{22}\text{Ne}(\alpha, n)^{25}\text{Mg}$ source in intermediate mass stars and the fact that significant s-process enhancements are only observed in low mass, metal-poor AGB stars have increased the interest in these stars, particularly since Iben and

Table 6. The physical conditions during the s-process—results from the classical model compared to predictions of stellar models

Parameter	Main component	Helium shell burning ($2-8 M_{\odot}$; $M_{\text{core}} = 1.16 M_{\odot}$)	Weak component	Core helium burning ($> 10 M_{\odot}$)
Temperature (10^8 K)	2.8-3.9	1.6-3.7	1.8-3.0	> 2.5
Neutron density (10^8 cm^{-3})	2.3-4.5	1-5000	$<(0.8-1.9)$	~ 0.1
Matter density (10^3 g cm^{-3})	2.6-13	2-10		
Duration of pulse (yr)	> 3	3.2		

Renzini (1982, 1983) had shown that semiconvective mixing of protons into the helium burning shell could produce enough ^{13}C to make the $^{13}\text{C}(\alpha, \text{n})^{16}\text{O}$ reaction an efficient neutron source. This possible site for the s-process was investigated in a number of recent studies (Boothroyd and Sackmann 1988, Hollowell and Iben 1988, Gallino *et al* 1988). Again, first estimates yielded high neutron densities of 10^{11} to 10^{12} cm^{-3} (Iben and Renzini 1982, Malaney 1987, Picchio *et al* 1988) in contradiction to the classical model or to observations, which show little or no ^{96}Zr (Zook 1978). In reanalysing the pulse model of Iben (1982) with a large reaction network, Gallino *et al* (1988) obtained a strong reduction in neutron density to values below $3 \times 10^9 \text{ cm}^{-3}$, and hence a remarkably constant s-process overproduction in the entire mass range from $A = 90$ to 200.

In this model, there are two neutron bursts in each thermal pulse. The main burst is caused by the $^{13}\text{C}(\alpha, \text{n})^{16}\text{O}$ reaction at $\sim 1.5 \times 10^8 \text{ K}$, when a ^{13}C pocket left from the previous pulse is engulfed in the convective helium shell. A smaller burst follows at the end of the pulse via the $^{22}\text{Ne}(\alpha, \text{n})^{25}\text{Mg}$, when the temperature at the bottom of the shell rises sharply to $\sim 3 \times 10^8 \text{ K}$. In a way, this second burst adjusts the s-process thermometers (§ 5), which otherwise would reflect the lower temperature during the main burst.

6.1.3. Strong component. The idea that the core helium flash in stars of less than $1M_\odot$ could be responsible for the strong component (Truran and Iben 1977), has not been investigated quantitatively yet. To date it is not clear whether this core flash is a single event or whether it may occur repeatedly (Wood 1985). However, it is to be expected that neutrons are produced via the $^{13}\text{C}(\alpha, \text{n})^{16}\text{O}$ reaction, and that these flashes may be characterised by a sufficiently large neutron exposure to account for the observed lead and bismuth abundances. On the other hand, the reservations noted by Ratzel *et al* (1988) need first to be clarified before the strong component can be considered as established.

In summary, one finds that the present results from the classical s-process only allow for a rough comparison with stellar models, indicating a number of inconsistencies. Consequently, both the classical approach as well as comprehensive studies of s-process enhancements in AGB stars need to be improved in order to establish reliable constraints for stellar nucleosynthesis. Stellar models yield an increasingly quantitative picture of the s-process. The weak component seems to be well described by helium burning in massive stars, while the pulsed s-process associated with helium shell burning remains an attractive model for the main component. At present, low mass AGB stars appear as the most promising candidates for this s-process component.

6.2. Astronomical observations

Enhancements of s-process elements in stellar atmospheres have been found in two classes of red giants, in relatively cool stars of type MS and S with surface temperatures between 2000 and 3800 K, and in so-called barium stars with rather normal surface temperatures of 4000 to 5500 K. For many years, the s-enhancements in barium stars were not understood, because these stars have not yet reached the asymptotic giant branch (AGB stage), i.e. they were not expected to exhibit convective mixing of material from the deep interior to the surface. Detailed studies (McClure 1984, Böhm-Vitense *et al* 1984) revealed that barium stars are members of binary systems that have received

considerable mass overflow from the companion star during or after its AGB phase. This means that the s-abundances in barium stars are the products of the more evolved companion. Therefore, the MS and S giants can be considered as the only true, living examples of AGB stars with a pulsating helium shell, from where freshly produced s-process material is mixed at the surface.

Consequently, the MS and S giants are of greatest interest as their composition provides for the most direct access to the actual s-process. Though their low temperatures make them difficult to observe, recent investigations succeeded in deriving remarkably complete and accurate abundance patterns (e.g. Tomkin and Lambert 1983, Smith and Lambert 1986, 1988). As only elemental abundances can be derived spectroscopically, most aspects of the s-process cannot be resolved with as much detail as for solar material. Nevertheless, the abundances of typical s-elements, such as Sr, Y, Zr, Ba and Nd, can be used to determine the mean neutron exposures characteristic for these stellar abundance patterns. One finds the corresponding values for τ_0 to range between 0.15 and 0.5 mb⁻¹, compatible with the result obtained for the main component. Estimates for the neutron density can be derived from the Sr/Rb or Y/Rb ratios (Tomkin and Lambert 1983, Käppeler 1986a, Malaney and Lambert 1988, Beer and Macklin 1989) or from the isotopic abundances of Zr, which can be determined via molecular bands for sufficiently cool stars (Zook 1978, Malaney 1986, Smith 1988). These studies yield neutron densities around 10⁸ cm⁻³ similar to the result obtained with the classical model.

A discrepancy with respect to the s-process in the pulsed helium shell concerns the neutron source. So far, all observed Mg isotope ratios are close to solar and do not show any ²⁵Mg enhancements due to the ²²Ne(α , n)²⁵Mg reaction. Furthermore, estimates of the luminosities indicate that the available observations refer to low mass stars ($<2M_\odot$), whereas in more massive AGB stars s-process enhancements were not yet observed. Recent studies even consider the possibility that stars with $M > 3M_\odot$ may not reach the AGB stage because of excessive mass loss in stellar winds (Mould and Reid 1987); this result would totally question intermediate mass stars as a possible s-process site!

Though stellar observations of s-process enhancements are not yet sufficiently accurate or representative to allow for detailed conclusions, it is clear that this type of information is invaluable as it represents a direct link to actual s-processing. Further studies with improved accuracy and more complete abundance patterns promise to yield important constraints on stellar dredge-up mechanisms (§ 7), and on the systematics of the s-process as a function of stellar evolution.

7. Chronometers

The chronological aspect has fascinated many researchers since the beginning of quantitative studies of nucleosynthesis. A large number of publications have been devoted to interpreting the naturally occurring radioactive nuclei in terms of a cosmic timescale, either by studying the abundances of nuclei that are unstable but still alive, e.g. ¹⁷⁶Lu, ¹⁸⁷Re and the long-lived Th and U isotopes, or the abundances of the respective decay products. Instead of a thorough discussion, which would require a review of its own, this section is restricted to a selection of s-process chronometers ordered according to their timescales. Principally, any unstable isotope on the s-process

path may be considered as a potential chronometer, provided that it is not obscured by abundance contributions from the r-process, and that its decay had significant consequences for the isotopic abundance pattern observed today. The available chronometers relate to different phenomena, depending on their half-lives.

$t_{1/2} < 10^6$ years. This timescale is typical for the dynamics in helium shell burning, which is the likely scenario for the main component of the s-process; it concerns for example the duration of shell flashes and the time required for dredge-up of processed material to the stellar atmosphere.

$t_{1/2} \sim 10^6 - 10^8$ years. This timescale relates to the question of whether the formation of the solar system was triggered by a nearby supernova explosion. There is evidence from the discovery of isotopic anomalies in meteorites that the protosolar cloud was peppered by freshly synthesised material originating from such an event.

$t_{1/2} > 10^9$ years. This timescale is close to that for the age of the universe as deduced from the age of the oldest stars or from the red shift of distant galaxies, and it would be most important to complement these estimates with an age for the chemical elements.

With this classification, one example will be given for each epoch in the following subsections. More information can be found in the references cited.

7.1. Short timescale

An example of this type was presented in § 5.2.3, where it was shown that ^{151}Sm may be used as a clock for the duration of the helium shell flashes, which provide the natural explanation for the exponential distribution of neutron exposures characteristic of the main s-process component.

Another outstanding example is ^{99}Tc , which is produced in the s-process, and which was discovered in the atmospheres of S stars, a subclass of red giants (Merrill 1952). This observation provided an important argument in favour of stellar nucleosynthesis. As all Tc isotopes are unstable with half-lives much shorter than the age of these stars, they must have been produced within these stars. By improved observational techniques and atmospheric models, technetium abundances can be determined even quantitatively (Smith and Wallerstein 1983, Dominy and Wallerstein 1986, Smith and Lambert 1986, 1988). These direct observations were all the more exciting since it was found that the decay rate of ^{99}Tc is drastically enhanced at high temperature (Cosner and Truran 1981, Schatz 1983, Takahashi and Yokoi 1987): the half-life decreases from 2.1×10^5 yr at $T < 10^8$ K to a few years at $T \sim 3 \times 10^8$ K, the estimated temperature for the s-process (§ 5.2.1).

That ^{99}Tc survives and is observed at the surface therefore implies that it is quickly removed from the s-process site to cooler zones by efficient convective motions. Hence, the short lifetime of ^{99}Tc at s-process temperatures represents a clock for the dynamics of helium shell burning in these stars. As soon as ^{99}Tc has reached a zone with $T < 10^8$ K, it practically decays with its terrestrial half-life. This change in the timescale of the ^{99}Tc clock can be accounted for by means of ^{93}Zr ($t_{1/2} = 1.5 \times 10^6$ yr), a neighbouring unstable s-process nucleus with a half-life almost insensitive to temperature. While ^{93}Zr is not easily detected in astronomical observations due to the presence of the stable Zr isotopes, the decay can be followed via the daughter nucleus ^{93}Nb . As this is the only stable isotope of niobium, and as it is *not* produced in the s-process, its abundance is a sensitive indicator for the decay of ^{93}Zr . Note that with time ^{93}Nb increases in abundance and ^{99}Tc decreases.

This change of abundances during the transport of ^{99}Tc and $^{93}\text{Zr}/^{93}\text{Nb}$ from the helium burning zone to the surface and in the stellar atmosphere itself, was studied on the basis of existing stellar models (Mathews *et al* 1986, Takahashi *et al* 1986). It was found that the observed Tc and Nb abundances relative to each other as well as to their neighbouring elements Zr and Mo may indeed be considered as a clock for the lifetime of stars in the thermally pulsing third dredge-up phase. Further investigations of this possibility require more accurate and systematic field studies of AGB stars and improved stellar models that are able to reproduce the observed s-process abundances (§ 6).

7.2. Intermediate timescale

Isotopes with half-lives between $\sim 10^6$ and 10^8 yr are particularly interesting in connection with isotopic anomalies in meteorites. Whereas isotopic ratios are fairly constant in most materials or are at most modified by physical effects such as diffusion, very pronounced anomalous isotope patterns were discovered in small inclusions of certain meteorites. Some of these anomalies were shown to be the result of *in situ* decay of now-extinct radionuclides, e.g. ^{26}Al , ^{107}Pd , ^{129}I and ^{244}Pu . This means that these radionuclides were alive during the formation of solid bodies in the early solar system, and hence were synthesised shortly before. One possible explanation for their origin was to assume a local supernova, which triggered the collapse of the protosolar cloud and also produced these radionuclides. The resulting isotopic anomalies could therefore be analysed in terms of the different half-lives to establish a chronometry of the early solar system.

However, this interpretation is questioned by Clayton (1979), who pointed out that the anomalies need not be the result of a local event. Instead, presolar grains could have formed much earlier and could have been ingested by the protosolar cloud. Such a model, of course, would deny any chronological information with respect to the solar system, but would rather yield information on the timescale for condensation of supernova ejecta. For a detailed presentation of the field see the reviews by Clayton (1979), Begemann (1980), Wasserburg and Papanastassiou (1982), for example.

The s-process aspect of this problem may be interesting insofar as it depends on the stellar mass, and whether and how much of s-processed matter is released in a supernova; alternatively, s-process material could have been ejected in stellar winds during the red-giant phase prior to the supernova. Significant isotopic anomalies have been reported for xenon and krypton (Srinivasan and Anders 1978, Alaerts *et al* 1980, Ott *et al* 1988) and for neodymium (Lugmair *et al* 1983a, b) and were interpreted as being characteristic for s-process nucleosynthesis (Clayton 1978, 1979, 1983, Beer *et al* 1983, Mathews and Käppeler 1984, Walter *et al* 1986b). In this context, it would be important to identify an anomaly associated with an unstable s-process isotope, which could serve as an appropriate clock in order to test these ideas.

Yokoi *et al* (1985) have shown that ^{205}Pb would be such a case. This clock was long overlooked, because it was assumed that the decay of ^{205}Pb was strongly enhanced at stellar temperatures so that it could not be produced in significant amounts during the s-process. However, the small neutral atomic mass difference between ^{205}Pb and ^{205}Tl causes the latter isotope to become unstable in the ionised stellar plasma against bound-state decay (§ 3.3). Under certain conditions, the decay rate of ^{205}Tl can even exceed that of ^{205}Pb as shown in figure 27. Though ^{205}Tl is unstable only at temperatures above $\sim 1.5 \times 10^8$ K and therefore does not counterbalance the decay of ^{205}Pb in the

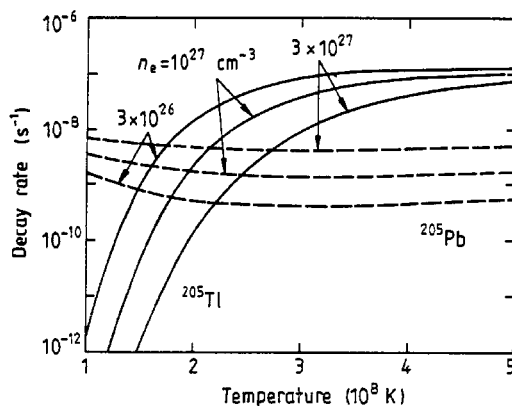


Figure 27. The stellar decay rates of ²⁰⁵Tl (full curves) and ²⁰⁵Pb (broken curves) versus temperature (Takahashi and Yokoi 1987). Note the strong dependence on electron density, n_e .

range $2 \times 10^6 < T < 1.5 \times 10^8$ K, Yokoi *et al* (1985) estimated that in intermediate mass stars enough ²⁰⁵Pb may survive the convective transport from the helium burning zone to sufficiently cool the outer layers. The resulting ²⁰⁵Pb/²⁰⁴Pb ratios were estimated to range between 10^{-5} and unity, so that one could expect isotopic anomalies in excess of those reported by Huey and Kohman (1972) who found an upper limit for the ²⁰⁵Pb/²⁰⁴Pb ratio of 9×10^{-5} at the time of solidification of the meteoritic material. A renewed search for extinct ²⁰⁵Pb seems therefore to be justified and possibly rewarding.

7.3. Long timescale

There are numerous attempts to derive an estimate of the age of our galaxy by interpretation of the observed long-lived radionuclides as chronometers for galactic nucleosynthesis. The main difficulty in these attempts originates from the fact that they have to be based on solar system material. This material is known to represent the result of element production and modification up to 4.6 Gyr ago. Since that time there has been free decay of the respective radionuclides; but what was before? Obviously, this question has two aspects:

- (i) What are the isotopic yields of the various nucleosynthetic processes, e.g. in the s- or r-process?
- (ii) What is the time dependence of galactic nucleosynthesis for each of these processes?

Both aspects are still affected by sizeable uncertainties with the consequence that the galactic timescale set by astronomical methods cannot be improved significantly by present nucleocosmochronology.

In first attempts, the rate of element production was simply assumed to have decreased exponentially with time due to the decreasing density in the universe (Fowler 1973). Later, galactic evolution models were found to yield additional constraints, and were considered as well (Tinsley 1980, Clayton 1984). In all these studies, the history of element production had to be described by suited parameters, and it has been emphasised that the combined analysis of several long-lived radionuclides may

yield enough information for a reasonably good fit of these parameters, provided the respective half-lives were sufficiently different.

Studies of this type concentrated on the r-process chronometers ^{232}Th and $^{235,238}\text{U}$. Depending on the particular assumptions for the rate of element production and on the calculated r-process yields for the long-lived radionuclides, galactic ages between 10 and 20 Gyr were reported (Fowler 1978, Fowler and Meisl 1986, Thielemann and Truran 1986, Cowan *et al* 1987). This range is in reasonable agreement with, but no more accurate than, current estimates derived from the Hubble time (Sandage and Tammann 1984, Huchra 1987, Branch 1987) or from the age of globular clusters (Sandage 1982, VandenBerg 1983, 1985).

Beside these r-process chronometers, ^{176}Lu is the only long-lived isotope of pure s-process origin that seemed to be suited as a cosmic clock (Audouze *et al* 1972, Arnould 1973). However, quantitative studies revealed that this clock may be in question due to temperature effects (see § 7.4). The remaining long-lived species on the chart of nuclides, e.g. ^{40}K (Beer and Penzhorn 1987), ^{87}Rb (Beer and Walter 1984) and ^{187}Re (Yokoi *et al* 1983, Arnould *et al* 1984, Winters *et al* 1986b), are produced in at least two nucleosynthetic processes. For this reason they are difficult to interpret, apart from problems related to a likely enhancement of the stellar decay rates for the latter two isotopes (Takahashi and Yokoi 1987).

Recent progress in observational techniques meanwhile offers the exciting possibility of escaping the restriction to solar system material by direct determination of long-lived radionuclides in old stars. In this way, the timescale for nucleosynthesis can be directly related to that for stellar and galactic evolution. In a systematic study of ^{232}Th abundances in G-dwarf stars of different ages relative to the stable elements Ba, Nd and Eu (Butcher 1987, 1988), no evidence was found for an evolution of the thorium abundance with stellar age. These results are plotted in figure 28 together with results obtained by galactic evolution models (Clayton 1987, Mathews and Schramm 1988), which consider a gradually increasing abundance contribution from the s-process to an initial r-process yield. While both models are able to fit the observed Th/Nd ratios quite well, they fail to explain the more sensitive Eu/Ba ratios.

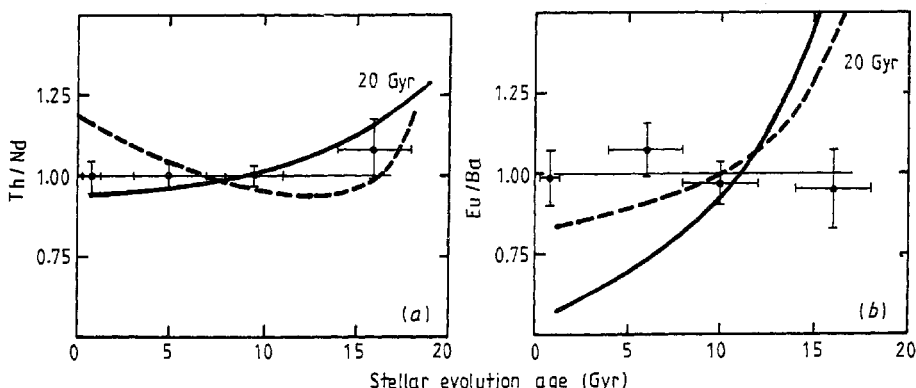


Figure 28. The abundance ratios (a) Th/Nd and (b) Eu/Ba as obtained for G-dwarfs of different ages (Butcher 1987, 1988) compared to results obtained with galactic evolution models (Clayton 1987, full curve; Mathews and Schramm 1988, broken curve) which postulate a gradually increasing contribution from the s-process to an initial r-process abundance. The good fits to the Th/Nd ratio for galactic ages of 20 and 15 Gyr are questioned by the fact that the Eu/Ba ratio cannot be reproduced.

It seems as if current ideas about galactic evolution are in conflict with Butcher's observations and as if this G-dwarf problem indicates that nucleosynthesis peaked at early epochs. This scenario fits to models concerning a quark-hadron phase transition in the big bang, which may have caused strong inhomogeneities in the proton-neutron distribution during primordial nucleosynthesis. Under such conditions even a big-bang r-process seems to be possible (Applegate and Hogan 1985, Alcock *et al* 1987, Malaney and Fowler 1989). On the other hand, this picture would have difficulty in explaining the galactic metallicity gradient. In any case, this fascinating chronometry is just starting and may produce new insights in the history of our galaxy as observational uncertainties are further reduced.

7.4. ^{176}Lu —cosmic clock or stellar thermometer?

The suited half-life of 36 Gy and the fact that it is shielded against the r-process (figure 29) makes ^{176}Lu a good candidate for studying the age of the s-process elements (Audouze *et al* 1972, Arnould 1973). The only difficulty seemed to be the proper treatment of the branching at ^{176}Lu as it is indicated in figure 29. This branching is due to the isomeric state at 125 ± 2 keV, which is significantly populated by neutron capture in ^{175}Lu , and which decays with a half-life of 3.68 h to ^{176}Hf . Because of the large difference in spin and K quantum number, electromagnetic transitions are highly forbidden by selection rules and the ground state and the isomer could be considered as independent of each other. Therefore, the s-process branching could be followed according to the relative population of ground state and isomer in the (n, γ) reaction.

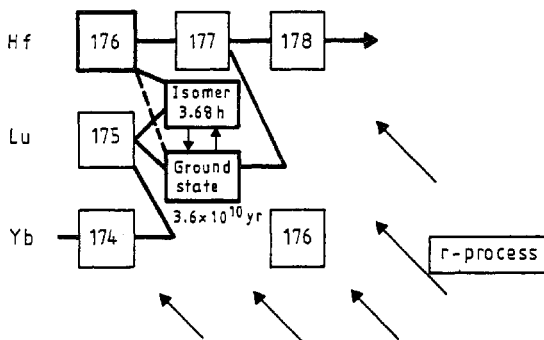


Figure 29. The s-process capture chain around ^{176}Lu .

Soon after the first quantitative study of ^{176}Lu as a cosmic clock (Beer and Käppeler 1980), it was realised that the decay of ^{176}Lu might be accelerated at high temperatures (Ward 1980, Beer *et al* 1981). Though direct transitions are forbidden, ground state and isomer could well be connected via transitions through higher lying states. This means that any quantitative treatment requires a detailed knowledge of the level scheme and the relevant transition rates. In 1980, Ward was left with two completely different families of excited states: those with high K quantum numbers related to the ground state and the others with small K connected with the isomer. The only possible links between these groups were K -forbidden transitions. By combination of estimated intra- and interband transition rates with the population probabilities of the excited states it was found that the levels at 239, 376 and 537 keV with $J^\pi = 3^-, 4^+$ provided

for the most efficient links between ground state and isomer. As a result, thermal equilibrium in the population of these states was expected to appear already above $T \sim 2 \times 10^8$ K, so that ^{176g}Lu is efficiently destroyed via isomer decay in the temperature range of the s-process. However, this result was considered to be rather uncertain because of the schematic estimates for transition rates and hindrance factors for K-forbidden transitions.

That the decay of ^{176}Lu was indeed thermally enhanced during the s-process was also inferred from an extensive analysis of the s-process path in the mass range $160 < A < 180$ (Beer *et al* 1984). If one just follows the neutron capture chain, the branching ratio at ^{176}Lu can be obtained from the ratio of the partial cross section to the isomer and the total (n, γ) cross section of ^{175}Lu , neglecting any thermally induced transitions. This simple solution yields branching ratios of 0.32 ± 0.05 , 0.17 ± 0.05 or almost zero, depending on the partial cross section adopted from literature (Beer and Käppeler 1980, Allen *et al* 1982, or Allen *et al* 1981, Stecher-Rasmussen *et al* 1988). In contrast, the complete analysis including s-only ^{176}Hf gives

$$0.39 < B_n^{\text{eff}} < 0.67$$

indicating that in fact more of the s-process flow bypassed ^{176}Hf . This means that at least some of the lutetium produced in the isomeric state was transformed to the long-lived ground state via thermally induced transitions. If the mechanism for these thermal effects could be described quantitatively, ^{176}Lu could possibly be used as a thermometer for the s-process. So far, only the extreme case of complete thermal equilibration between ground state and isomer can be treated (Beer *et al* 1984).

This problem of whether, to what extent and how the isomer and the ground state of ^{176}Lu are thermally connected, initiated a number of investigations. First, experimental evidence for an electromagnetic link between ground state and isomer was obtained by photoactivation of Lu samples in intense gamma-ray fields (Veres and Pavlicsek 1970, Norman and Kellogg 1985). In these measurements, a positive effect was found in irradiations with ^{60}Co ($E_\gamma = 1332, 1173$ keV), but not with ^{137}Cs ($E_\gamma = 662$ keV), a clear hint that excitation energies well above 500 keV were required. The quantitative interpretation of such measurements in terms of a stellar reaction rate (Norman and Kellogg 1985) is somewhat speculative, as neither the reaction mechanism nor the photon spectrum are well enough known to reliably infer the stellar photoactivation cross section. For example, figure 30 illustrates how critically the half-life of ^{176}Lu depends on the unknown energy of the mediating level (Norman and Kellogg 1985).

An improved theoretical approach was presented by Gardner *et al* (1988), who complemented the experimentally determined levels in ^{176}Lu by postulated states inferred from systematic trends in neighbouring nuclei. With this 'complete' level scheme, which extended up to 1.5 MeV, they obtained a strong temperature dependence of the ^{176}Lu half-life, but now using only *unhindered* transitions. Comparison with the estimates from photoactivation shows an even shorter half-life! If thermalisation is indeed provided by allowed transitions, there is a chance for the experimental assessment of level energies and branching ratios of the relevant interband transitions, e.g. from the 5^- band head found by Coulomb excitation (Elze 1984). Presently, a comprehensive set of experiments for the completion of the level scheme of ^{176}Lu is in progress (Klay *et al* 1988), using the high-resolution spectrometers GAMS and BILL at the high flux reactor of the Institut Laue-Langevin in Grenoble as well as additional information from (d, p)-reaction studies (Mayerhofer *et al* 1987).

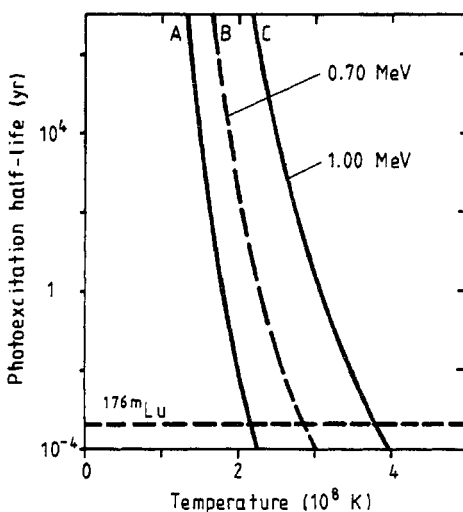


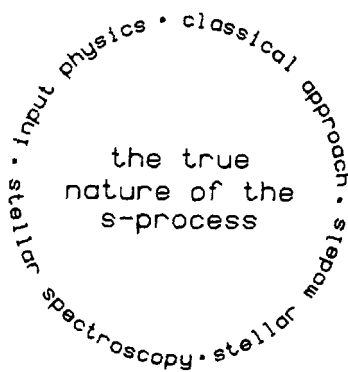
Figure 30. Estimates for the half-life of ^{176}Lu against photoactivation as a function of temperature based on experimental cross sections (curves B and C) (Norman and Kellogg 1985) and on a postulated level scheme (curve A) (Gardner *et al* 1988). The broken curve illustrates how sensitively the half-life depends on the energy of the activation level.

Annihilation of a positron with a K-shell electron has been proposed as another excitation mechanism for ^{176}Lu , that may populate mediating levels above 1 MeV. This effect was experimentally verified by Watanabe *et al* (1981), but the interpretation of Norman and Kellogg (1985) probably overestimated its influence in a stellar environment; a more conservative treatment indicates that the corresponding decay rate is lower than that due to photoexcitation (Käppeler 1988).

Though ^{176}Lu is likely not to be a useful chronometer for the s-process, the stellar fate of ^{176}Lu remains one of the fascinating problems of nuclear astrophysics—and there is a good chance that it may represent a sensitive stellar thermometer instead.

8. Summary

The quest for the s-process origin of the heavy elements stands for a lively field of research with numerous fascinating problems and many different aspects. The present status of this field is promising and rewarding in the sense that the overall picture seems fairly consistent, but that the many parts of the puzzle do not yet fit together. It appears hopeful that the aim of understanding the s-process within the next decade is in reach, and the rewarding aspect is that the present concept still allows or even demands substantial improvements and modifications. This mostly concerns the data base, i.e. the observed abundances and the relevant nuclear physics, which are the important input for the empirical approach via the classical s-process as well as for the stellar models. The results obtained from these models need definitely to be complemented with and checked against the s-process abundance patterns, which are directly obtained by spectroscopy of individual red giants. Our ultimate understanding of s-process nucleosynthesis therefore requires tightening of the circle indicated opposite:



Acknowledgments

We gratefully acknowledge the help of all colleagues who contributed to this work in many discussions, by critical comments on and amendments of the manuscript, and by allowing us to use their results prior to publication. In particular we thank J-P Arcoragi, R Gallino, H Holweger, H Palme, J T Wasson, K Yokoi, S Yorka, A Mengoni, G Reffo and N Grevesse. We also thank the editors for their patience during the delays in the preparation of this manuscript.

References

- Alaerts L, Lewis R S, Matsuda J-I and Anders E 1980 *Geochim. Cosmochim. Acta* **44** 189
Alcock C R, Mathews G J and Fuller G M 1987 *Astrophys. J.* **320** 439
Allen B J, Lowenthal G C, Boldeman J W and de Laeter J R 1982 *Neutron Capture Gamma Ray Spectroscopy and Related Topics 1981* (Inst. Phys. Conf. Ser. 62) p 573
Allen B J, Lowenthal G C and de Laeter J R 1981 *J. Phys. G: Nucl. Phys.* **7** 1271
Allen B J, Macklin R L and Gibbons J H 1971 *Adv. Nucl. Phys.* **4** 205
Almeida J and Käppeler F 1983 *Astrophys. J.* **265** 417
Anders E and Ebihara M 1982 *Geochim. Cosmochim. Acta* **46** 2363
Anders E and Grevesse N 1989 *Geochim. Cosmochim. Acta* **53** 197
Applegate J H and Hogan C 1985 *Phys. Rev. D* **30** 3037
Arnett W D and Thielemann F-K 1985 *Astrophys. J.* **295** 589
Arnould M 1973 *Astron. Astrophys.* **22** 311
— 1986 *Advances in Nuclear Astrophysics* ed. E Vangioni-Flam *et al* (Gif sur Yvette: Editions Frontières) p 113
Arnould M, Takahashi K and Yokoi K 1984 *Astron. Astrophys.* **137** 51
Audouze J, Fowler W A and Schramm D N 1972 *Nature Phys. Sci.* **238** 8
Bahcall J N 1961 *Phys. Rev.* **124** 495
Bao Z Y and Käppeler F 1987 *At. Data Nucl. Data Tables* **36** 411
Barden R 1985 *Diploma Thesis* Mainz University, FRG
Baschek B 1979 *Les Éléments et leurs Isotopes dans l'Univers* (Liège: University of Liège) p 327
Beer H 1985 *Kernforschungszentrum Karlsruhe internal report*
— 1986 *Advances in Nuclear Astrophysics* ed. E Vangioni-Flam *et al* (Gif sur Yvette: Editions Frontières) p 375
— 1988 *Origin and Distribution of the Elements* ed. G J Mathews (Singapore: World Scientific) p 505
Beer H and Käppeler F 1980 *Phys. Rev. C* **21** 534
— 1982 *Neutron Capture Gamma Ray Spectroscopy and Related Topics 1981* (Inst. Phys. Conf. Ser. 62) p 558
Beer H, Käppeler F and Arcoragi J-P 1989a *Proc. 5th Workshop on Nuclear Astrophysics* ed. W Hillebrandt and E Müller *Report MPA/PI MPZ für Physik und Astrophysik*, Munich

- Beer H, Käppeler F, Reffo G and Venturini G 1983 *Astrophys. Space Sci.* **97** 95
 Beer H, Käppeler F, Wissak K and Ward R A 1981 *Astrophys. J. Suppl.* **46** 295
 Beer H and Macklin R L 1982 *Phys. Rev. C* **26** 1404
 —— 1985 *Phys. Rev. C* **32** 738
 —— 1988 *Astrophys. J.* **331** 1047
 —— 1989 *Astrophys. J.* **339** 962
 Beer H and Penzhorn R-D 1987 *Astron. Astrophys.* **174** 323
 Beer H and Walter G 1984 *Astrophys. Space Sci.* **100** 243
 Beer H, Walter G and Käppeler F 1989b *Astron. Astrophys.* **211** 245
 —— 1989c in preparation
 Beer H, Walter G and Macklin R L 1985 *Capture Gamma-Ray Spectroscopy and Related Topics 1984* ed. S Raman (New York: AIP) p 778
 Beer H, Walter G, Macklin R L and Patchett P J 1984 *Phys. Rev. C* **30** 464
 Beer H and Ward R A 1981 *Astron. Astrophys.* **103** 189
 Begemann F 1980 *Rep. Prog. Phys.* **43** 1309
 Böhm-Vitense E, Nemec J and Proffitt C 1984 *Astrophys. J.* **278** 726
 Boothroyd A I and Sackmann I-J 1988 *Astrophys. J.* **328** 632, 641, 653, 671
 Bowman C D and Talbert W C 1985 *Neutron Capture Measurements on Radioactive Targets at the Proton Storage Ring, Los Alamos National Laboratory internal report*
 Branch D 1987 *Astrophys. J. Lett.* **320** L23
 Burbidge E M, Burbidge G R, Fowler W A and Hoyle F 1957 *Rev. Mod. Phys.* **29** 547
 Busso M and Gallino R 1985 *Astron. Astrophys.* **151** 205
 Butcher H R 1987 *Nature* **328** 127
 —— 1988 *The ESO Messenger* **51** 1
 Cameron A G W 1955 *Astrophys. J.* **121** 144
 —— 1973 *Space Sci. Rev.* **15** 129
 —— 1982 *Essays in Nuclear Astrophysics* ed. C A Barnes *et al* (Cambridge: Cambridge University Press) p 23
 Chrien R E 1975 *Nuclear Cross Sections and Technology* Vol. 1 ed. R A Schrack and C D Bowman (Washington DC: NBS) (Special Publication 425) p 139
 Clayton D D 1968 *Principles of Stellar Evolution and Nucleosynthesis* (New York: McGraw Hill)
 —— 1978 *Astrophys. J.* **224** 1007
 —— 1979 *Space Sci. Rev.* **24** 147
 —— 1983 *Astrophys. J. Lett.* **271** L101
 —— 1984 *Astrophys. J.* **285** 411
 —— 1987 *Nature* **329** 397
 Clayton D D, Fowler W A, Hull T E and Zimmerman B A 1961 *Ann. Phys.* **12** 331
 Clayton D D and Rassbach M E 1967 *Astrophys. J.* **148** 69
 Clayton D D and Ward R A 1974 *Astrophys. J.* **193** 397
 Conrad J H 1976 *PhD Thesis* University of Heidelberg
 Cosner K, Iben I Jr and Truran J W 1980 *Astrophys. J. Lett.* **238** L91
 Cosner K and Truran J W 1981 *Astrophys. Space Sci.* **78** 85
 Cowan J J, Thielemann F-K and Truran J W 1987 *Astrophys. J.* **323** 543
 Despain K H 1980 *Astrophys. J. Lett.* **236** L165
 Dominy J F and Wallerstein G 1986 *Astrophys. J.* **310** 371
 Elze Th W 1984 private communication
 Eschner W, Schmidt-Ott W-D, Gippert K L, Runte E, Beer H, Walter G, Kirchner R, Klepper O, Roeckl E and Schardt D 1984 *Z. Phys. A* **317** 281
 Fowler W A 1973 *Explosive Nucleosynthesis* ed. D N Schramm and W D Arnett (Austin: University of Texas)
 —— 1978 *Proc. 21st Welch Foundation Conf. on Chemical Research* ed. W D Milligan (Houston: Robert A Welch Foundation) p 61
 Fowler W A and Meisl C C 1986 *Cosmogonical Processes* ed. W D Arnett *et al* (Singapore: VNU) p 83
 Fuller G M, Fowler W A and Newman M J 1982 *Astrophys. J. Suppl.* **48** 279
 Gallino R 1989 *Evolution of Peculiar Red Giant Stars* ed. H R Johnson (Cambridge: Cambridge University Press) at press
 Gallino R, Busso M, Picchio G, Raiteri C M and Renzini A 1988 *Astrophys. J. Lett.* in press
 Gardner D G, Gardner M A and Hoff R W 1988 *Capture Gamma-Ray Spectroscopy 1987* (Inst. Phys. Conf. Ser. 88) p 315
 Goldschmidt V M 1937 *Skr. Nor. Vidensk.-Akad. Oslo I* no 4

- Grevesse N 1984 *Phys. Scr.* **T8** 49
— 1987 private communication
- Grevesse N and Meyer J-P 1985 *19th Int. Cosmic Ray Conf., La Jolla*
- Habs D, Stephens F S and Diamond R M 1979 *Lawrence Berkeley Laboratory LBL-8945*
- Harris M J 1981 *Astrophys. Space Sci.* **77** 357
- Hauser W and Feshbach H 1952 *Phys. Rev.* **78** 366
- Hodgson P E 1971 *Nuclear Reactions and Nuclear Structure* (Oxford: Clarendon Press)
- Hollowell D E and Iben I Jr 1988 *Astrophys. J. Lett.* **333** L25
- Holmes S E, Woosley S E, Fowler W A and Zimmerman B A 1976 *At. Data Nucl. Data Tables* **18** 306
- Holweger H 1979 *Les Éléments et leurs Isotopes dans l'Univers* (Liège: University of Liège) p 117
— 1984 update of figure 6 in Holweger (1979), private communication
- Howard W M, Mathews G J, Takahashi K and Ward R A 1986 *Astrophys. J.* **309** 633
- Huchra J P 1987 *13th Texas Symp. on Relativistic Astrophysics* ed. M P Ulmer (Singapore: World Scientific) p 1
- Huey J M and Kohman T P 1972 *Earth Planet. Sci. Lett.* **16** 401
- Iben I Jr *Astrophys. J.* 1975a **196** 525
— *Astrophys. J.* 1975b **196** 549
— *Astrophys. J.* 1976 **208** 165
— *Astrophys. J.* 1982 **260** 821
- Iben I Jr and Renzini A 1982 *Astrophys. J. Lett.* **259** L79
- Iben I Jr and Truran J W 1978 *Astrophys. J.* **220** 980
— 1983 *Ann. Rev. Astron. Astrophys.* **21** 271
- Käppeler F 1986a *Nucleosynthesis and its Implications on Nuclear and Particle Physics* ed. J Audouze and N Mathieu (Dordrecht: Reidel) p 253
— 1986b *Advances in Nuclear Astrophysics* ed. E Vangioni-Flam *et al* (Gif sur Yvette: Editions Frontières) p 355
— 1988 *Capture Gamma-Ray Spectroscopy 1987* (Inst. Phys. Conf. Ser. 88) p 297
— 1989 *Nuclear Science and Technology* ed. S Igarasi (Tokyo: Saikōn) p 1107
- Käppeler F, Bao Z Y, Reffo G and Wang S N 1989b *Astrophys. J.* submitted
- Käppeler F, Beer H, Wissak K, Clayton D D, Macklin R L and Ward R A 1982 *Astrophys. J.* **257** 821
- Käppeler F, Gallino R, Busso M, Picchio G and Raiteri C 1989a *Astrophys. J.* submitted
- Käppeler F, Naqvi A A and Al-Ohali M 1987 *Phys. Rev. C* **35** 936
- Käppeler F, Schatz G and Wissak K 1983 *Kernforschungszentrum Karlsruhe KFK-3472*
- Käppeler F, Walter G and Mathews G J 1985 *Astrophys. J.* **291** 319
- Kellogg S E and Norman E B 1986 *Phys. Rev. C* **34** 2248
- Klay N, Beer H, Börner H, Hoyler F, Käppeler F, Krusche B, Robinson S, Schatz G and Schreckenbach K 1988 *Kernforschungszentrum Karlsruhe Kfk-4405* p 7
- Klay N and Käppeler F 1988 *Phys. Rev. C* **38** 295
- Kopecky J 1982 *Neutron Capture Gamma-Ray Spectroscopy and Related Topics 1981* (Inst. Phys. Conf. Ser. 62) pp 423, 426
- Kratz K-L, Thielemann F-K, Hillebrandt W, Möller P, Harms V, Wöhr A and Truran J W 1988 *Capture Gamma-Ray Spectroscopy 1987* (Inst. Phys. Conf. Ser. 88) p 331
- Kwiatkowski M, Zimmermann P, Biémont E and Grevesse N 1984 *Astron. Astrophys.* **135** 59
- Lamb S A, Howard W M, Truran J W and Iben I Jr 1977 *Astrophys. J.* **217** 213
- Lambert D L 1989 *Evolution of Peculiar Red Giant Stars* ed. H R Johnson (Cambridge: Cambridge University Press) at press
- Laval M, Moszynski M, Allemand R, Cormoreche E, Guinet P, Odru R and Vacher J 1983 *Nucl. Instrum. Methods* **206** 169
- Lederer C M and Shirley V S 1978 *Table of Isotopes* (New York: Wiley)
- Lesko K T, Norman E B, Larimer R M, Bacelar J C and Beck E M 1989 *Phys. Rev. C* **39** 619
- Lesko K T, Norman E B, Moltz D M, Larimer R M, Crane S G and Kellogg S E 1986 *Phys. Rev. C* **34** 2256
- Lugmair G W, Shimamura T, Lewis R S and Anders E 1983a *Science* **222** 1015
— 1983b *Lunar Planet. Sci.* **14** 448
- Macklin R L 1982 *Nucl. Sci. Eng.* **81** 520
— 1985a *Nucl. Sci. Eng.* **89** 79
— 1985b *Astrophys. Space Sci.* **115** 71
- Macklin R L and Gibbons J H 1967 *Phys. Rev.* **159** 1007
- Malaney R A 1986 *Advances in Nuclear Astrophysics* ed. E Vangioni-Flam *et al* (Gif sur Yvette: Editions Frontières) p 407

- 1987 *Astrophys. J.* **321** 832
- Malaney R A and Fowler W A 1989 *Mon. Not. R. Astron. Soc.* **237** 67
- Malaney R A and Lambert D L 1988 *Mon. Not. R. Astron. Soc.* **235** 695
- Mathews G J and Käppeler F 1984 *Astrophys. J.* **286** 810
- Mathews G J and Schramm D N 1988 *Astrophys. J. Lett.* **324** L67
- Mathews G J, Takahashi K, Ward R A and Howard W M 1986 *Astrophys. J.* **302** 410
- Mathews G J and Ward R A 1985 *Rep. Prog. Phys.* **48** 1371
- Mayerhofer U, Hlawatsch G and von Egidy T 1987 private communication
- McClure R D 1984 *Astrophys. J.* **280** 231
- Merrill P W 1952 *Science* **115** 484
- Meyer J-P 1985 *Astrophys. J. Suppl.* **57** 173
- Mould J and Reid N 1987 *Astrophys. J.* **321** 156
- Moxon M C and Rae E R 1963 *Nucl. Instrum. Methods* **24** 445
- Newman M J 1973 *MSc Thesis* Rice University, Houston
- 1978 *Astrophys. J.* **219** 976
- Norman E B and Kellogg S 1985 *Capture Gamma-Ray Spectroscopy and Related Topics 1984* ed. S Raman (New York: AIP) p 753
- Ott U, Begemann F, Yang J and Epstein S 1988 *Nature* **332** 700
- Palme H 1985 data from MPI für Chemie, Abteilung Kosmochemie, Mainz, FRG, private communication
- Palme H, Suess H E and Zeh H D 1981 *Landolt-Börnstein New Series VI* vol. 2 ch. 3, 4
- Patchett P J 1983 *46th Annual Meeting of the Meteoritical Soc. (Mainz, FRG) September 5-9*
- Perrone F A and Clayton D D 1971 *Astrophys. Space Sci.* **11** 451
- Peters J G 1968 *Astrophys. J.* **154** 224
- Petrov Yu V and Slyakhter A I 1984 *Astrophys. J.* **278** 385
- 1988 *Astrophys. J.* **327** 294
- Picchio G, Busso M, Gallino R and Raiteri C M 1988 *Mass Outflow from Stars and Galactic Nuclei* ed. L Bianchi and R Gilmozzi (Dordrecht: Kluwer Academic.) p 279
- Prantzos N, Arnould M and Arcoragi J-P 1987 *Astrophys. J.* **315** 209
- Ratynski W and Käppeler F 1988 *Phys. Rev. C* **37** 595
- Ratzel U, Beer H and Käppeler F 1989 in preparation
- Rauch M 1987 *Diploma Thesis* University of Mainz, FRG
- Rayet M, Prantzos N and Arnould M 1988 *Origin and Distribution of the Elements* ed. G J Mathews (Singapore: World Scientific) p 625
- Reffo G 1980 *Parameter Systematics for Statistical Theory Calculations of Neutron Reaction Cross Sections IAEA-SMR-43* (Vienna: International Atomic Energy Agency) p 205
- Reffo G, Fabbri F, Wissak K and Käppeler F 1982 *Nucl. Sci. Eng.* **80** 630
- 1983 *Nucl. Sci. Eng.* **83** 401
- Ross J E and Aller L H 1976 *Science* **191** 1223
- Runte E, Schmidt-Ott W-D, Eschner W, Rosner I, Kirchner R, Klepper O and Rykaczewski K 1987 *Z. Phys. A* **328** 119
- Russell H N and Adams W S 1928 *Astrophys. J.* **68** 9
- Sandage A 1982 *Astrophys. J.* **252** 553
- Sandage A and Tamman G A 1984 *Nature* **307** 326
- Schatz G 1983 *Astron. Astrophys.* **122** 327
- Schwarzschild M and Härm R 1967 *Astrophys. J.* **150** 961
- Seeger P A, Fowler W A and Clayton D D 1965 *Astrophys. J. Suppl.* **11** 121
- Shaw P B and Clayton D D 1967 *Phys. Rev.* **160** 1193
- Shaw P B, Clayton D D and Michel F C 1965 *Phys. Rev.* **140** B1433
- Simpson J A 1983 *Ann. Rev. Nucl. Part. Sci.* **33** 323
- Smith V V 1988 *Origin and Distribution of the Elements* ed. G J Mathews (Singapore: World Scientific) p 535
- Smith V V and Lambert D L 1986 *Astrophys. J.* **311** 843
- 1988 *Astrophys. J.* in press
- Smith V V and Wallerstein G 1983 *Astrophys. J.* **273** 742
- Srinivasan B and Anders E 1978 *Science* **201** 51
- Stecher-Rasmussen F, Abrahams K, Kopecky J, Lindner J and Polak P 1988 *Capture Gamma-Ray Spectroscopy 1987* (Inst. Phys. Conf. Ser. 88) p 754
- Suess H E and Urey H C 1956 *Rev. Mod. Phys.* **28** 53
- Suess H E and Zeh H D 1973 *Astrophys. Space Sci.* **23** 173
- Takahashi K, Mathews G J, Ward R A and Becker S A 1986 *Nucleosynthesis and its Implications on Nuclear and Particle Physics* ed. J Audouze and N Mathieu (Dordrecht: Reidel) p 285

- Takahashi K and Yokoi K 1983 *Nucl. Phys. A* **404** 578
 —— 1987 *At. Data Nucl. Data Tables* **36** 375
- Thielemann F-K and Truran J W 1986 *Galaxy Distances and Deviations from Universal Expansion* ed. B F Madore and R B Tully (Dordrecht: Reidel) p 185
- Tinsley B A 1980 *Fund. Cosmic Phys.* **5** 411
- Tomkin J and Lambert D L 1983 *Astrophys. J.* **273** 722
- Toukan K A and Käppeler F 1989 *Astrophys. J.* at press
- Trautvetter H P *et al* 1986 *Z. Phys. A* **323** 1
- Trimble V 1975 *Rev. Mod. Phys.* **47** 877
- Truran J W and Iben I Jr 1977 *Astrophys. J.* **216** 797
- Twin P J 1983 *Proc. Int. Conf. on Nuclear Physics, Florence, Italy* (Bologna: Tipografia Compositori) p 527
- Ulrich R K 1973 *Explosive Nucleosynthesis* ed. D N Schramm and W D Arnett (Austin: University of Texas) p 139
- Unsöld A 1979 *Les Éléments et leurs Isotopes dans l'Univers* (Liège: University of Liège), p 7
- VandenBerg D A 1983 *Astrophys. J. Suppl.* **51** 29
 —— 1985 *Astrophys. J. Suppl.* **58** 711
- Veres A and Pavlicsek I 1970 *Acta Phys. Hung.* **28** 419
- Vogt E W 1969 *Advances in Nuclear Physics* vol. 1 ed. M Baranger and E Vogt (New York: Plenum) p 261
- Walter G and Beer H 1982 *Kernforschungszentrum Karlsruhe* KfK-3327
- Walter G, Beer H, Käppeler F and Penzhorn R-D 1986b *Astron. Astrophys.* **155** 247
- Walter G, Beer H, Käppeler F, Reffo G and Fabbri F 1986a *Astron. Astrophys.* **167** 186
- Ward R A 1977 *Astrophys. J.* **216** 540
 —— 1980 private communication
 —— 1981 *Astron. Astrophys.* **97** 154
- Ward R A and Beer H 1981 *Astron. Astrophys.* **103** 189
- Ward R A and Clayton D D 1982 unpublished
- Ward R A and Fowler W A 1980 *Astrophys. J.* **238** 266
- Ward R A and Newman M J 1978 *Astrophys. J.* **219** 195
- Ward R A, Newman M J and Clayton D D 1976 *Astrophys. J. Suppl.* **31** 33
- Wasserburg G J and Papanastassiou D A 1982 *Essays in Nuclear Astrophysics* ed. C A Barnes *et al* (Cambridge: Cambridge University Press) p 77
- Wasson J T 1985 *Meteorites—Their Record of Early Solar System History* (New York: Freeman)
- Watanabe Y, Mukoyama T and Katano R 1981 *Phys. Rev. C* **23** 695
- Weigert A 1966 *Z. Astrophys.* **64** 395
- Wiedenbeck M E and Greiner D E 1980 *Astrophys. J. Lett.* **239** L139
- Winters R R, Carlton R F, Harvey J A and Hill N W 1986b *Phys. Rev. C* **34** 840
- Winters R R, Käppeler F, Wissak K, Mengoni A and Reffo G 1986a *Astrophys. J.* **300** 41
- Winters R R and Macklin R L 1982 *Phys. Rev. C* **25** 208
- Wissak K and Käppeler F 1983 *Nucl. Sci. Eng.* **85** 251
 —— 1984 *Nucl. Instrum. Methods* **227** 91
- Wissak K, Käppeler F and Schatz G 1984 *Nucl. Instrum. Methods* **221** 385
- Wissak K, Käppeler F, Voß F and Guber K 1989 *IEEE Trans. Nucl. Sci., NS-36* 101
- Wood P R 1985 *Cool Stars with Excesses of Heavy Elements* ed. M Jaschek and P C Keenan (Dordrecht: Reidel) p 357
- Woosley S E, Fowler W A, Holmes J A and Zimmerman B A 1978 *At. Data Nucl. Data Tables* **22** 371
- Yokoi K and Takahashi K 1981 *Proc. 4th Int. Conf. on Nuclei Far from Stability (Helsingør) CERN rep 81-09* p 351
 —— 1983 *Nature* **305** 198
 —— 1985 *Kernforschungszentrum Karlsruhe* KfK-3849
- Yokoi K, Takahashi K and Arnould M 1983 *Astron. Astrophys.* **117** 65
 —— 1985 *Astron. Astrophys.* **145** 339
- Youssef N H and Khalil N M 1989 *Astron. Astrophys.* **208** 271
- Zook A C 1978 *Astrophys. J. Lett.* **221** L113